Fall 2017

Experimental study of natural convection heat transfer and gaseous dynamics from dual-channel circulation loop

Ibrahim Ahmed Said Abdallah

Department: Chemical and Biochemical Engineering

EXPERIMENTAL STUDY OF NATURAL CONVECTION HEAT TRANSFER AND GASEOUS DYNAMICS FROM DUAL-CHANNEL CIRCULATION LOOP

by

IBRAHIM AHMED SAID ABDALLAH

A DISSERTATION

Presented to the Faculty of the Graduate School of the

MISSOURI UNIVERSITY OF SCIENCE AND TECHNOLOGY

In Partial Fulfillment of the Requirements for the Degree

DOCTOR OF PHILOSOPHY

In

CHEMICAL ENGINEERING

2017

Approved by:
Muthanna Al-Dahhan, Advisor
Jee-Ching Wang
Xinhua Liang
Fateme Rezaei
Shoaib Usman

PUBLICATION DISSERTATION OPTION

This dissertation consists of the following four articles:

PAPER I pages 9-43. Investigation of natural convection heat transfer in a unique scaled-down dual-channel facility. It has been published in AIChE Journal.

PAPER II pages 44-86. Experimental investigation of the helium natural circulation heat transfer in two channels facility using varying riser channel heat fluxes. It has been submitted to the Journal of Experimental Thermal and Fluid Science (under review).

PAPER III pages 87-126. Experimental study of the effect of helium pressure on the natural convection heat transfer in a prismatic dual-channel circulation loop. It has been published in International Journal of Thermal Sciences.

PAPER IV pages 127-164. Axial dispersion and mixing of coolant gas within a separate-effect prismatic modular reactor. It has been submitted to the Nuclear Energy and Technology Journal (under review).

ABSTRACT

This research focuses on establishing a range of scaled separate and integral effects experiments for studying thermal-hydraulic behavior occurring within a component or region of the prismatic very high-temperature reactor (VHTR) such as plenum-to-plenum heat transfer and gaseous dynamics during natural circulation. Natural circulation of the coolant is the leading capability for VHTR to transport the decay heat from the core to the reactor vessel during accident scenarios. To address this need, a scaled-down facility is designed and developed with only two channels with upper and lower plena. The emphasis is placed on high-resolution and high-fidelity experimental data for local heat transfer and gaseous dispersion measurements utilizing sophisticated techniques under different operating conditions. These techniques are 1) non-invasive flush wall mounted heat transfer coefficient probe to measure reliably the heat flux and surface temperature along the flow channels, and by measuring simultaneously these two variables and the flowing fluid, the heat transfer coefficient can be obtained, 2) radial temperature sensor adjuster to measure radial temperature variations of the coolant along the flow channels, and 3) advanced gaseous tracer technique to accurately measure the residence time distribution (RTD) in an of flow systems by injecting pulse change gas tracer and then monitoring its concentration at the exit. The measured RTD is utilized to quantify the gas dispersion and identify the degree of mixing in the system. The obtained local heat transfer and gaseous dispersion data in this study will provide high spatial and temporal resolutions benchmarking data for validating heat transfer and gaseous dispersion computations and correlations that are integrated with CFD simulations.

ACKNOWLEDGMENTS

First and foremost, my praises and thanks are to ALLAH for his kindness and so many blessings in my life.

Throughout my stay here at Missouri University of Science and Technology, several people have supported me both academically and personally and inspired me. I express gratitude from the depth of my heart to my advisor, Professor Muthanna H. Al - Dahhan, who gave me an opportunity to conduct research under his supervision.
Dr. Al-Dahhan has continuously conveyed a passion for research work and excitement for teaching. I would also like to acknowledge Dr. Shoaib Usman for his contributions of time, great efforts to explain topics clearly and simply, encouragement and his patience. Without their guidance and persistent help, this dissertation would not have been possible.

I appreciatively would also like to thank my advisory committee members, Dr. Jee-Ching Wang, Dr. Xinhua Liang and Dr. Fateme Rezaei, for taking an interest in my work and examining my dissertation.

I express a deep sense of appreciation to my parents (Ahmed and Fahima), brother (Mohamed) and sisters (Fayza and Sara) for their support and encouragement throughout the years. Finally, thanks to my wife (Hager), and my daughter (Farida), who stood by my side during the ups and downs, for believing in me and for supporting my ideas and dreams. They were always the breath of fresh air that sailed me through my long Ph.D. Journey. My appreciation to my professors and colleagues at Alexandria University, Alexandria, EGYPT for supporting me.

TABLE OF CONTENTS

LIST OF ILLUSTRATIONS

Page

PAPER I

PAPER II

PAPER III

LIST OF TABLES

Page

1. INTRODUCTION

Investigations of natural circulation heat transfer and gaseous dynamics in different geometries and operating conditions have been the focus of the past and current research by several authors. Natural circulation has received great attention from researchers due to its presence in nature and engineering applications. In nuclear reactors, natural convection is considered the design criterion [1,2]. Also, natural circulation is one of the leading capabilities for Prismatic Very High-Temperature Nuclear Reactor (VHTR) after Loss of Flow Accidents (LOFA) [3]. The Prismatic Very-High-Temperature Reactor (VHTR) as a suitable candidate for the Next Generation Nuclear Plant (NGNP) intended not only to generate electricity but also to produce hydrogen, provide process heat, and for other potential ends. The prismatic Very-High-Temperature Reactor (VHTR) uses TRISO (Tri-isotropic) nuclear fuel particles coated in gas-solid spouted beds into pins (pellets) that are inserted in fixed fuel channels in a graphite block matrix. Additionally, these hexagonal graphite blocks include coolant channels to allow the passage of helium (coolant) from the upper plenum downward through the core to the lower plenum during normal operation. In the event of the failure of the gas circulator (LOFA), in the prismatic VHTR, the driving pressure drop force across the reactor core will decrease to zero, and the natural circulation will occur. Also, during LOFA scenario, the coolant flows direction is reversed. Hence, the central hot channels and lower plenum serve as up-comers (risers), while the upper plenum and outer cold channels serve as down-comers during intra-core natural circulation. Natural convection currents by coolant (working fluid) plume transport the decay heat from the reactor core to the outer vessel of the

reactor, and it prevents the core from meltdown and localized hot spots. There are many parameters affect the rate of natural convection heat transfer and gaseous dynamics, and any consideration of each in a representative geometry can enhance the knowledge about the phenomenon.

1.1 RESEARCH MOTIVATION

Most prismatic VHTR safety analyses and related natural circulation studies are conducted using standard computational fluid dynamics (CFD) codes combined with heat transfer computations such as CFD-STAR-CCM+, and CFD-Fluent and thermal hydraulic codes such as RELAP5-3D that can provide crucial details of heat transfer and gas dynamics data. There are extensive computational studies of natural circulation in the prismatic VHTR have been reported in the open literature [1,3-8]. However, the thermal hydraulic codes analyses involve approximations in the obtained results because of inexact nature of turbulence models that are used, assumptions used in the describing equation such as the Boussinesq approximation, and nature of discretization required. Despite there are many numerical and experimental studies available on natural convection heat transfer in the open literature [9-16], but these studies are carried out in simple geometries with limited measurement techniques and can not be extended to complex reactors. Also, there are some ongoing studies at Oregon State University (OSU) related to plenum-to-plenum natural circulation heat transfer during depressurized conduction cooldown (DCC) and pressurized conduction cooldown (PCC) accident scenarios [17-18]. These studies at Oregon State University are limited in ability to collect local high-resolution and high-fidelity data on heat transfer and gaseous dynamics because existing facilities have not implemented with newly available sophisticated

measurement techniques. This shows the lack of experimental studies on plenum-to-plenum natural circulation heat transfer and gaseous dynamics and dispersion during the loss of forced flow accident in the prismatic modular reactor. Particularly there are data gaps for local heat transfer and gaseous dynamics measurements using sophisticated noninvasive techniques. To fill these literature gaps, and to provide local experimental data on the natural circulation, a high temperature and pressure scaled-down dual-channel facility has been designed and developed in conjunction with sophisticated measurement techniques in a novel way and for the first time. This facility can perform separate and integral effects experiments under various operating conditions using different working fluids (air and helium) for studying thermal-hydraulic behavior occurring within a component or particular region of prismatic VHTR to provide crucial heat transfer and gaseous dynamics data.

1.2 RESEARCH OBJECTIVES

The current study aims to experimentally investigate the intensity of plenum-to-plenum natural circulation heat transfer and gaseous dynamics through the coolant flow channels under different intensities of natural circulation. The flow channels are equipped with a novel way sophisticated measurement techniques for the first time in this research. These measurement techniques measure simultaneously heat transfer coefficient from the coolant channels to the circulating gas and gas residence time distribution and dispersion along the flow channels. The general objectives of the current study can be summarized as follows:

1. Design and development a scaled-down dual-channel experimental setup that can be operated under high temperature and pressure.

2. Filling the gaps in the open literature and understanding of the natural circulation heat transfer and gaseous dynamics and dispersion in the prismatic VHTR under LOFA accident scenario using the sophisticated measurement techniques.
3. The measured local heat transfer and gas dynamics and dispersion data from this study will provide high crucial benchmarking data for verifying and validating thermal hydraulics codes and models for computations and correlations.

1.3 DESCRIPTION OF SOPHISTICATED MEASUREMENT TECHNIQUES

The advanced and sophisticated techniques that were implemented and utilized in a novel way and for the first time in this research for both separate-effects and integrated-effects measurements are as follows:

1.3.1 Radial Temperature Sensor Adjuster. A radial temperature sensor adjuster for T-thermocouple has been designed and developed in-house to measure radially the variation of helium temperatures along the flow channels (riser and downcomer) for different axial locations with a step size of 1 mm. This radial temperature adjuster is used to adjust the location of the T-thermocouple sensor (1.6 mm in diameter) along the flow channels. It is worth mentioning that the radial sensor adjuster is designed and constructed to withstand high temperature and pressure up to 300 ^{o}C and 1.034 x 10^{6} Pa respectively.

1.3.2 Noninvasive Flush Wall Mounted Heat Transfer Coefficient Probe. A new noninvasive heat transfer coefficient probe has been designed, developed, tested, and implemented as an integrated part of the channels. The probe consists of micro-foil heat flux sensor ($6.35x10^{-3}$ m x $1.78x10^{-2}$ m x $8x10^{-5}$ m) from RDF Corporation (model no.

27036-1) is a new fast-response sensor used to measure the heat flux and surface temperature in single and multiphase flow systems reliably. By measuring simultaneously the local instantaneous heat flux between the surface of the sensor and the flowing fluid, the surface temperature of the sensor, and the flowing gas temperature, heat transfer coefficient can be obtained.

It is worth mentioning that the sophisticated heat transfer coefficient probe has the capability to detect the direction of heat transfer between the surface of foil sensor and the flowing fluid. Negative heat flux signals mean that heat transfers from the flowing fluid to the surface of foil sensor while positive heat flux signals imply that heat transfers from the surface of foil sensor to the flowing fluid. The heat flux foil sensor is flush mounted on the inner surface of the flow channels using high-temperature glue. Hence, the micro-foil sensor is considered as non-invasive technique.

1.3.3 Gaseous Tracer (GT) Technique. The gaseous tracer (GT) is an advanced technique used to accurately measure the residence time distribution (RTD) in a complex flow structure of single and multiphase flow systems by injecting pulse change gas tracer and then monitoring its concentration at the exit. The measured RTD can be utilized to characterize and quantify the gas dispersion (which includes the contribution of both molecular diffusion and turbulent mixing) and identify the degree of mixing in the system. Also by applying axial dispersion model, the dispersion coefficient can be estimated in the flow channel. The technique has been well designed to account and de-convolute all the external mixing and dispersion. The GT technique consists of thermal conductivity detector (TCD), vacuum gas sampling pump, digital controller, signal

amplifier, analog/digital (AD) converter, data acquisition (DAQ) software and computer with data acquisition system.

1.4 DISSERTATION ORGANIZATION

The dissertation is structured in the following manner:

- Section 1. Introduction and motivation which provide a brief literature review relevant to the work done in this dissertation, the objectives of this study, and the implemented sophisticated measurement techniques.
- PAPER I. Investigation of natural convection heat transfer in a unique scaled-down dual-channel facility.
- PAPER II. Experimental investigation of the helium natural circulation heat transfer in two channels facility using varying riser channel heat fluxes.
- PAPER III. Experimental study of the effect of helium pressure on the natural convection heat transfer in a prismatic dual-channel circulation loop.
- PAPER IV. Axial dispersion and mixing of the coolant gas within a prismatic very high-temperature reactor.
- Section 2. Presents remarks and recommendations for future work on prismatic very high-temperature reactor (VHTR).

REFERENCES

1. Aldridge RJ. Scaling Study of the Depressurized Conduction Cooldown Event in the High Temperature Test Facility Using RELAP5-3D/ATHENA. Oregon State University: Department of Nuclear Engineering and Radiation Health Physics, Oregon State University; 2013.

2. Castañeda JA. Scaling analysis of the OSU high temperature test facility during a pressurized conduction cooldown event using RELAP5-3D: Nuclear Engineering, Oregon State University; 2014.

3. Tung Y-H, Ferng Y-M, Johnson RW, Chieng C-C. Study of natural circulation in a VHTR after a LOFA using different turbulence models. Nuclear Engineering and Design. 2013;263:206-217.

4. Haque H, Feltes W, Brinkman G. Thermal response of a modular high temperature reactor during passive cooldown under pressurized and depressurized conditions. Nucl Eng Des. 2006;236:475-484.
5. Simoneau JP, Champigny J, Mays B, Lommers L. Three-dimensional simulation of the coupled convective, conductive and radiative heat transfer during decay heat removal in an HTR. Nucl Eng Des. 2007;237:1923–1937.

6. Tung YH, Johnson, R.W.,. CFD Calculations of Natural Circulation in a HighTemperature Gas Reactor Following Pressurized Circulator Shutdown. ASME, IMECE, IMECE 2011-64259.; 2011.

7. Tung YH, Johnson, R.W., Chieng, C.C., Ferng, Y.M.,. Modeling Strategies toCompute Natural Circulation using CFD in a VHTR after a LOFA. ASME, IMECE, IMECE 2012-93007.; 2012.

8. Tung Y-H, Ferng Y-M, Johnson RW, Chieng C-C. Transient LOFA computations for a VHTR using one-twelfth core flow models. Nucl Eng Des. 2016;301:89-100.

9. Al-Arabi M, Khamis M, Abd-ul-Aziz M. Heat Transfer by Natural Convection from the Inside Surface of a Uniformly Heated Vertical Tube. Int J Heat and Mass Transfer. 1991;34:1019-1025.

10. Mohammed HA, Salaman YK. Heat transfer by natural convection from a uniformly heated vertical circular pipe with different entry restriction configuration. Energy Conversion and Management. 2007;48:2244-2253.

11. Salman YK, Mohammed HA. Free convection heat transfer with different sections lengths placed at the exit of vertical circular tube subjected to a constant heat flux. Al-Khwarizmi Engineering Journal. 2007;3(3):31-52.
12. Mohammed HA, Salman YK. Laminar air flow free convection heat transfer inside a vertical circular pipe with different inlet configuration. Thermal Science. 2007;11(1):43-63.

13. M. Misale PG, J.C. Passos, G. Ghisi de Bitencourt. Experiments in a single-phase natural circulation mini-loop. Experimental Thermal and Fluid Science. 2007;31:1111-1120.

14. P.K. Vijayan MS, D. Saha, Steady state and stability characteristics of single-phase natural circulation in a rectangular loop with different heater and cooler orientations. Experimental Thermal and Fluid Science. 2007;31:925–945.

15. Misale M. Overview on single-phase natural circulation loops. Proc. of the Intl. Conf. on Advances In Mechanical And Automation Engineering – MAE 2014; 2014.

16. Mustafa Z. Ghani YKS. Natural convection heat transfer in inclined open annulus passage heated from two sides. International Journal of mechanical engineering and technology. 2014;5(11):76-91.

17. Aldridge RJ. Scaling Study of the Depressurized Conduction Cooldown Event in the High Temperature Test Facility Using RELAP5-3D/ATHENA. Oregon State University: Department of Nuclear Engineering and Radiation Health Physics, Oregon State University; 2013.

18. Castañeda JA. Scaling analysis of the OSU high temperature test facility during a pressurized conduction cooldown event using RELAP5-3D: Nuclear Engineering, Oregon State University; 2014.

PAPER

I. INVESTIGATION OF NATURAL CONVECTION HEAT TRANSFER IN A UNIQUE SCALED-DOWN DUAL-CHANNEL FACILITY

Ibrahim A. Said [1], Mahmoud M. Taha [1], Shoaib Usman [2], Brian G. Woods[3], Muthanna H. Al-Dahhan [1,2]*

[1] Chemical and Biochemical Engineering Department, Missouri University of Science and Technology, Rolla, MO, 65409, USA

[2] Mining and Nuclear Engineering Department, Missouri University of Science and Technology, Rolla, MO, 65409-0170, USA

[3] Nuclear Engineering Department, Oregon State University, Corvallis, OR, 97331, USA

* *Corresponding author: aldahhanm@mst.edu*

Abstract

Multiphase Reactors Engineering and Applications Laboratory (mReal) has designed and constructed a scaled-down dual-channel facility to investigate plenum-to-plenum natural circulation heat transfer through two channels for coolant flow that would be encountered during a loss of flow accident in the prismatic modular reactor (PMR). Heat transfer characterization of the current facility has been investigated under different upper plenum and cooled channel outer surface temperatures using sophisticated flush mounted heat transfer sensors**.** Results show a reduction in the values of local heat transfer coefficient and Nusselt number along the heated channel with increasing outer surface temperatures. One significant observation was the heat transfer reversal close to heated channel exit, where the heat flows from gas to the channel wall. This flow

reversal is attributed to recirculation at the heated channel exit to the upper plenum. The average heat transfer results, when compared with previous literature, showed a similar qualitative trend.

Keywords: dual-channel facility, natural circulation, prismatic modular reactor (PMR), heat transfer characterization

Introduction

The very high-temperature nuclear reactors (VHTRs) are considered one of the promising next generation nuclear plants (NGNPs) designs due to their high efficiency, inherent safety features, and a variety of applications [1]. The prismatic modular reactor (PMR) is one of the candidates for VHTRs. The PMR design concept uses TRISO (Tri-isotropic) nuclear fuel particles coated in gas-solid spouted beds into pins (pellets) that are inserted in fixed fuel channels in a graphite block matrix. Additionally, these hexagonal graphite blocks include coolant channels to allow the passage of helium from the upper plenum downward through the core to the lower plenum during normal operation. The nuclear reactor core consists of an annular ring of graphite blocks with fuel and coolant channels around reflector in the center with an outer ring of reflector blocks. In the case of loss of flow accidents (LOFA), the normal gas flow is interrupted as the coolant circulation system is lost. However, the coolant channels provide potential paths for gas flow through natural circulation. Efficient decay heat removal by natural circulation is desirable to achieve passive safety, which is a characteristic feature of PMR design. Several computational studies have been conducted for heat transfer in prismatic VHTRs during postulated accident scenarios. Tung et al. [2] investigated potential natural circulation using computational fluid dynamics (CFD) with different turbulence and laminar models. Because of the geometrical symmetry in VHTRs, Travis et al. [3] performed a CFD study for only 1/6 core while Tung et al. [4] used a 1/12 core sector to model natural circulation loops and investigated the effect of the distributed heat generation on natural circulation strength. Haque et al. [5] analyzed the thermal response of prismatic VHTRs numerically using thermal hydraulics code THERMIX under a

pressurized conduction cooldown (PCC) scenario and depressurized conduction cooldown (DCC) scenario. These studies revealed that natural convection is effective in preventing a core meltdown. However, there is a lack of benchmarking data to validate these computational results. Limited numbers of experimental studies on plenum-to-plenum natural circulation thermal hydraulics phenomena have been reported in the open literature. For example, there is an ongoing study on plenum-to-plenum natural circulation heat transfer during PCC and DCC accident scenarios at Oregon State University's high-temperature test facility (OSU-HTTF) [6]. However, the facility is not equipped for some separate effect experiments for local flow and heat transfer measurements. Therefore, there is a need for establishing a range of scaled separate and integral effects experiments for studying thermal-hydraulic behavior occurring within a component or particular region of VHTRs such as plenum-to-plenum heat transfer during natural circulation. To address this need, a scaled-down facility is designed and constructed at Multiphase Reactors Engineering and Applications Laboratory (mReal) with only two channels with upper and lower plena. The emphasis is placed on high resolution and high fidelity data for local heat transfer measurements utilizing sophisticated techniques. An advanced fast response flush mounted heat transfer sensors together with a series of thermocouples have been implemented for the first time in this study. This study focuses on the effect of upper plenum and cooled channel temperatures on the intensity of the natural circulation heat transfer. The data collected from this facility will provide crucial benchmark data to validate codes such as; RELAP5-3D, CFD-STAR-CCM+, CFD-Fluent, etc.

Experimental work

Multiphase Reactors Engineering and Applications Laboratory (mReal) at Missouri S&T has designed, developed, and tested a scaled-down dual-channel facility with reference to the OSU-HTTF[7,8]. The HTTF scaling down criteria provides a good similarity to the reference prismatic block modular high-temperature gas-cooled reactor (MHTGR). mReal has adopted the same scaling criteria for developing the current facility with reference to HTTF[7,8]. The current setup is 1 m in height with channel grid plate diameter of 0.305 m. This layout mimics seven graphite blocks of the PMR; one central block surrounded by six identical blocks as shown in Fig. 1(a). Each graphite block would have one channel for the nuclear fuel surrounded by six coolant channels. A physical picture of the current scaled-down facility is shown in Fig. 1(b) which consists of two channels; one heated channel for upward flow in the center block and the other cooled channel for downward flow in the outer edge of the outer block (Fig. 1(a)). The outlet from the heated channel mixes in the upper plenum and returns through the cooled channel to the lower plenum (Fig. 1(c)). The air was used in the current study as a working fluid to perform natural flow conditions at operating pressure of 413.685 kPa. Table 1 shows the dimensions of the current setup with respect to Oregon State's HTTF. The inside diameter of the two channels is kept constant at 0.016 m. The current facility is made of an alloy of stainless steel with a thermal conductivity of 16.2 W/m.K to handle high pressure up to 1034.21 kPa and temperature up to 533.15 K. The upper plenum of the current facility is designed and developed with an external cooling jacket using chilled water, which surrounds the whole upper plenum to control the temperature of the outer surface as shown in Fig. 1(d). Also, a helical coil heat exchanger of 1 m length is

used around the downward channel (cooled channel) to maintain the outside surface temperature of the cooled channel at the desired value. A 3.5 mm diameter high thermal conductivity copper tube with a wall thickness of 0.85 mm is used for the helical coil heat exchanger on the cooled channel. Also, a high temperature and thermally conductive silicone paste (OT-201-16, Omega Engineering, INC.) is added between the helical coil and outer surface of the cooled channel to improve heat transfer. A high capacity chiller (Applied Thermal Control Ltd, K4 chiller) is used to provide the chilled water at 275.8 kPa. The chiller is equipped with temperature and pressure controllers. Chilled water comes from the chiller and goes upward (counter-current) with respect to the air flow inside the cooled channel. The cooling jacket at the upper plenum is also connected with the chiller to control the outer surface temperature of the upper plenum. Thus, the temperatures of the outer surfaces for the cooled channel and the upper plenum are kept constant at desired values during all experiments. The temperatures of the outer surface of the upper plenum and cooled channel are the main variable for this study. An electrical heater of 2.438 m length and a 0.0254 m width is wrapped continuously around the heated channel to form a uniform heating source. The electrical heater is connected with a variable voltage regulator with a span of 0-130 volts with a digital power reader (0.2% accuracy) to control and monitor the magnitude of power supplied to the heated channel. The outer surface of the heater is properly insulated by 0.05 m thickness ceramic fiber blanket (thermal conductivity of 0.07 W/m.K) to minimize the heat loss from the heater to the surrounding environment and to increase the heat input to the system. Also, the lower and upper plena and the cooled channel are also thermally insulated by a ceramic fiber blanket as shown in Fig. 1(b). For the heat transfer investigations, advanced

integrated fast response heat transfer technique has been developed which consists of flush mounted heat transfer foil sensors (6.35 mm x 17.78 mm x 0.08 mm) on the inner wall of the channels (Fig. 2 and 3(a)) and a series of T-thermocouple (1.6 mm in diameter) that are mounted along the channel's axis at the front of heat transfer foil sensors to measure the air temperature at the centerline. The foil sensor can simultaneously measure the local heat flux and surface temperature by a thermocouple built into the surface of the foil sensor. mReal laboratory and others[9,10] have used such flush mounted heat transfer techniques to characterize the heat transfer coefficients in cold multiphase flow systems with an additional cartridge heater. The heated channel is the source of heat in the current study. Therefore, additional cartridge heater is not needed in this work. The heat transfer technique in the current study (Fig. 2) is implemented in a novel way within this facility to allow heat transfer investigations at different axial locations along the channels. Six axial positions along the heated channel (Z/L= 0.044, 0.279, 0.409, 0.591, 0.773, 0.956 (end effect)) and three axial positions along the cooled channel (Z/L= 0.044, 0.5, 0.956) are used in the current study to collect the experimental data. These positions are used to collect data after reaching steady state conditions. A small number of axial positions for the cooled channel is due to low variation in the channel based on our preliminary computational study carried out during the design of the facility [11]. The heated and cooled channels are divided into small sections. There is a connecting block for data collection at ends of each section along the heated and cooled channels as shown in Fig. 2 and 3(a). Foil sensor flush mounted with high-temperature glue at the inner surface is shown in Fig. 3(a). The T-thermocouple is placed in front of the foil sensor (B in Fig. 3(a)) at the centerline of the channel to

measure the centerline temperatures at the axial locations. It is worth mentioning that the foil sensor is capable of detecting the direction of the heat transfer. Positive signal means that heat transfers from the inner wall of the channel to the adjacent fluid, while negative signal means that heat transfers from the adjacent fluid to the inner wall of the channel. In the current work, a heat flow reversal is observed at Z/L =0.956 in the heated channel. This end effect heat flow reversal is attributed to axial conduction from the upper plenum inside the solid wall of the heated channel (conjugate heat transfer). This negative heat transfer is excluded from the calculation of heat transfer coefficient. The local bulk temperature of air in the heated channel is determined by fitting a straight line interpolation between the measured inlet and outlet bulk air temperature since the isoflux boundary condition is applied[12,13]. A highly accurate system (Fig. 3(b)) is designed and implemented to radially adjust the locations of T-thermocouple. This development allowed us to measure the radial temperature of the air at the inlet and outlet of the heated channel. In this study, the inlet and outlet (Z/L=0.779) bulk air temperatures are measured by averaging 8 radial values with a step of 1/16 of channel diameter. Outlet location is selected lower than the last sensor location (Z/L=0.956) due to the heat flow reversal and the end effect. Available literature for an open channel without plenum also reported heat flow reversal at the outlet of the heated channel[14,15]. By simultaneously measuring the local instantaneous heat flux (q_i) through the heated foil sensor, its surface temperature (T_s) by a thermocouple at the foil surface, and the local bulk air temperature (T_b), the instantaneous heat transfer coefficient (h_i) and local time-averaged heat transfer coefficients (h_{avg}) can be determined from the following equations [9,10]:

$$h_i = \frac{q_i}{(T_{s,i} - T_{b,i})} \qquad (1)$$

$$h_{avg} = \frac{1}{N} \sum_{i=1}^{i=N} h_i \quad (2)$$

where N is the number of the collected data points, which is selected to be 2000 to achieve stable values. The signals from the heat flux and thermocouples are sampled simultaneously at 50 Hz for 40 s. The sampling frequency is selected based on preliminary experiments with various frequencies that showed no difference in the time-averaged heat transfer coefficients. In the current work, we are interested in estimating the heat transfer coefficient along the heated channel.

Experimental procedure

The system is pressurized to the desired pressure before starting the experiments using an external air compressor. All experiments for this study are carried out at 413.685 kPa. Once the pressure inside the facility reached the desired pressure of 413.685 kPa, the air supply was turned off, and the electrical heater was adjusted to the desired power. The total power supplied, Q_t, from the electrical heater to the outer surface of the heated channel is calculated as follows:

$$Q_t = V\,I \quad (3)$$

The total power supplied could be divided through the following equation:

$$Q_t = Q_{conv.} + Q_{rad.} + Q_{cond.} \quad (4)$$

The radiation heat transfer, $Q_{rad.}$, from the heated channel is ignored in this study due to the small value of $Q_{rad.}$. The conduction heat transfer, $Q_{cond.}$, can be calculated from the following equation:

$$Q_{cond.} = K_s A \frac{\Delta T}{\Delta X} = \frac{\Delta T}{(\frac{\Delta X}{K_s A})} = \frac{\Delta T}{R_{th}} . \quad (5)$$

The conduction heat losses ($Q_{cond.}/Q_t$) from the heated channel to the environment was found to be 18% of the total input wattage to the heated channel. The wall heat flux (q_w) is calculated by subtracting the 18% conduction losses from the total power and then dividing the remaining power by the area of the heated channel ($\pi D_o L$). The constant heat flux to fluid in the heated channel was 2.046×10^3 W/m^2 for all experiments performed for this study. After adjusting the desired heat flux (2.046×10^3 W/m^2) to the heated channel, the chiller is turned on and the chilled water is allowed to flow continuously through the heat exchanger around the cooled channel and the cooling jacket of the upper plenum. The effect of the outer surface temperatures of the upper plenum and cooled channel on the intensity of natural circulation is investigated using four outer surface temperatures (278.15 K, 288.15 K, 298.15 K, and 308.15 K). This range of temperatures is restricted due to the capability of the current chiller. After adjusting the desired outer surface temperatures and the power supplied to the heated channel, the system is allowed to reach steady state. The steady-state condition was confirmed when the temperature readings were not varying by more than 0.5 K within 30 minutes, and the local heat transfer coefficient was not changing by more than 0.8 W/m^2.K within 30 minutes. Once the steady-state conditions were established, the measurements of the heat transfer were taken and recorded. Local instantaneous and time-averaged heat transfer coefficients (h_i and h_{avg}) are determined using Eq.(1) and (2).

Results and Discussion

The results of the current work are presented using various parameters which are defined in this section. The average free convection heat transfer coefficients in tubes can be represented in the following form for a variety of circumstances [16]:

$$\mathrm{Nu} = \mathrm{m}\,(\mathrm{Gr}\,\mathrm{Pr})^{\mathrm{n}}. \tag{6}$$

The Rayleigh number (Ra) is the product of Grashof and Prandtl numbers (Gr and Pr), so Eq. (6) can be rewritten as:

$$\mathrm{Nu} = \mathrm{m}\,(\mathrm{Ra})^{\mathrm{n}}. \tag{7}$$

Hence, the physical properties of air ($i.e., \rho, \beta, K, \mu, \upsilon, c_p$) are determined at the film temperature (T_f) which is calculated from the following equation [16]:

$$T_f = \frac{T_{S,i} + T_{b,i}}{2}. \tag{8}$$

Then, the local Nusselt numbers (Nu) at different axial locations are calculated as:

$$\mathrm{Nu} = \frac{h_{avg}\, l}{k}. \tag{9}$$

Afterward, the average heat transfer coefficient ($\overline{h_L}$) and the average Nusselt Number ($\overline{Nu_L}$) along the heated channel can be calculated as:

$$\overline{h_L} = \frac{1}{L}\int_{L=0}^{L=0.773} h_{avg}\; d(L) \tag{10}$$

$$\overline{Nu_L} = \frac{\overline{h}_L\, l}{k}. \tag{11}$$

The average values of other parameters such as the Grashof number (Gr) and Prandtl number (Pr) can be calculated based on the axial average inner surface temperature ($\overline{T}_S$), the axial average bulk temperature ($\overline{T}_b$), and the average mean film temperature ($\overline{T}_f$) as follows:

$$\overline{T}_S = \frac{1}{L}\int_{L=0}^{L=0.773} T_s \, d(L) \tag{12}$$

$$\overline{T}_b = \frac{1}{L}\int_{L=0}^{L=0.773} T_b \, d(L) \tag{13}$$

$$\overline{T}_f = \frac{\overline{T}_S + \overline{T}_b}{2} \tag{14}$$

$$Gr = \frac{g\,\beta\,(\overline{T}_S - \overline{T}_b)l^3}{\upsilon^2}. \tag{15}$$

The volumetric expansion coefficient of air (β) is calculated as:

$$\beta = \frac{1}{\overline{T}_f}. \tag{16}$$

The Prandtl number is calculated as:

$$Pr = \frac{\mu\, c_p}{k}. \tag{17}$$

Finally, the average Rayleigh number (Ra) is calculated as:

$$Ra = Gr\ Pr. \tag{18}$$

Centerline and inner surface temperatures variations along the heated channel

Fig. 4 shows centerline air temperature (Fig. 4(a)) and the inner surface temperature (Fig. 4(b)). Both graphs exhibit the same trend for all conditions. With

increasing the upper plenum and cooled channel temperatures the air centerline and channel wall temperatures are also increasing for all different axial positions. The air temperature at the centerline and inner surface temperature along the heated channel are increased by 21 % and 12 % respectively with increasing the outer surface temperatures of the upper plenum and cooled channel from 278.15 K to 308.15 K. In general, the distribution of both temperatures shows that the temperature is increased from the heated channel leading edge (Z/L=0.044) to a certain axial position (Z/L=0.773). Beyond this axial position, a reduction in both temperatures is observed. As noted for Z/L =0.956 there is a decrease in both air and surface temperatures as compared to the next lower axial location (Z/L=0.773). The temperature increase from the inlet to Z/L=0.773 is due to the continuous uniform heating applied to the channel. But temperature reduction in the last portion of the channel is indicating towards possible heat flow reversal. This heat flow reversal at the outlet of the channel is reported in the open literature[14,15] for an open channel without a plenum. It is worth mentioning that at Z/L=0.956 (end effect) the heat transfers from the adjacent air to the inner wall of the heated channel is observed by the negative signal of heat flux from the foil sensor, while the other locations have positive signals. This reversal in the direction of heat transfer at the end effect (Z/L=0.956) is attributed to downward axial conduction inside the solid wall of the heated channel (conjugate heat transfer between the upper plenum and top section of the heated channel). So, a reduction in the temperatures is observed at Z/L=0.956 (end effect) for the heated channel. Also, end heat losses at the top section of the heated channel have a significant effect on the temperature reduction. The back-mixing is evidence of the complex thermal fluids interactions in VHTRs. The literature also reports that the axial conduction along

the heated channel and laminarization (buoyancy induced acceleration) have strong effects on centerline and wall temperatures [17-20]. The complexity of VHTRs and interaction between mixing phenomena in the two plena and natural circulation in the core could cause back-mixing and intensive recirculation of cooled air plumes from the upper plenum into the top section of the heated channel that would lead to a reduction in both temperatures (T_s and T_c) at the top portion of the heated channel (Z/L=0.956). From these results, it is concluded that the outer surface temperatures of the upper plenum and cooled channel have a significant effect on the air temperature at the centerline and the inner surface temperature of the upward flow channel in the natural circulation conditions of PMR.

Centerline and inner surface temperatures variations along the cooled channel

The distribution of inner surface temperature (T_s) and air temperature at the centerline (T_c) for cooled channel under various cooling conditions exhibits a general decreasing trend from the top inlet (Z/L=0.956) to bottom exit (Z/L=0.044), as shown in Fig. 5. However, for high cooling rate (lower chiller temperatures of 278.15 and 288.15 K) the end effects are observed even for the cooled channel. The obtained results along the cooled channels indicated that there is a small local temperature difference between T_s and T_c, which is less than 2 K along the cooled channel for all conditions. This finding emphasizes that the majority of the thermal energy carried by air coming up from the heated channel is absorbed in the upper plenum. By increasing the outer surface temperatures of the upper plenum and cooled channel from 278.15 K to 308.15 K, the

temperatures of the air and channel inner surface along the cooled channel (downward flow) increase.

Heat transfer coefficient and Nusselt number variations along the heated channel

The heat transfer coefficient (h_i) is a quantitative characteristic of convective heat transfer between the bulk fluid temperature and inner surface temperature of the heated channel. It is usually used to calculate the dimensionless group Nusselt number as shown in Eq. (9) and (11). The local heat transfer coefficient and local Nusselt number are decreased by 23% and 25% respectively with increasing the outer surface temperatures of the upper plenum and cooled channel from 278.15 K to 308.15 K as shown in Fig. 6. It worth mentioning that the direction of heat transfer is observed to be from the inner wall of the heated channel to the adjacent air from Z/L=0.044 to Z/L= 0.773, but at the position of Z/L=0.956 (end effect) there is a reversal in the direction of heat transfer. The heat transfers from the adjacent air layer to the inner wall at Z/L =0.956. This reversal in the direction of heat transfer could be attributed to the downward axial cooling conduction inside the solid wall of the heated channel from the upper plenum and co-circulation at the top section of the heated channel as reported in the literature[14,15]. Therefore, we have excluded the value of heat transfer coefficient at this position (Z/L =0.956) in calculating the average heat transfer coefficient. These negative values are also not included in the heat transfer coefficient and Nusselt number plots. Therefore, additional investigations are needed in conjunction with computational fluid dynamics to identify the thermal boundary layer and heat reversal at the top portion of the channel. Also, it is observed from the distribution of local Nusselt number, and heat transfer

coefficient for a certain condition that the heat transfer coefficient and Nusselt number initially decrease from the leading entrance of the heated channel to a certain axial position (Z/L) equals 0.409. This reduction is attributed to the building up of hydrodynamic and thermal boundary layers of the air. Beyond this axial position (Z/L=0.409), the local Nusselt number and heat transfer coefficient values tend to increase up to Z/L =0.591. This enhancement in the Nusselt number and heat transfer coefficient could be attributed to the possibility of transition to turbulence and a secondary flow effect of upward flow along the sides of the channel and downward flow near the channel centerline due to radial temperature and viscosity differences that lead to a higher heat transfer coefficient which is discussed by Mohammed and Salman [13]. Also, it is observed that there is a reduction in the value of heat transfer coefficient and Nusselt number after Z/L =0.591, which could be attributed to an extension of the end effect but without a reversal in the direction of heat transfer.

Test of the heat transfer results with the available correlations from literature

There are many correlations available in the literature to predict the heat transfer data in natural convection. The correlations related to natural convection induced by a constant wall heat flux have been selected and used in this study, as summarized in Table 2 [21,22]. The selected correlations for testing the heat transfer data collected in this study were based on a wide range of experimental data. The comparison between the current experimental data in terms of average Nusselt number and the selected correlations is shown in Fig. 7. One can observe the qualitative similarity between the experimental data and the selected correlations, but the present experimental results are always higher than

the predictions from Miyamoto et al. [21] and Aydin and Guessous [22] correlations. The deviation between experimental and predicted results is presented in terms of the average absolute relative error (AARE) that is calculated from the following equation:

$$\mathrm{AARE} = \frac{1}{N}\sum_{i=1}^{i=N}\frac{Nu_{predicted,i} - Nu_{experimental,i}}{Nu_{experimental,i}}. \quad (19)$$

The AARE between the experimental results and the Miyamoto et al. [21] and Aydin and Guessous [22] correlations are 21 % and 20% respectively. From the comparison, it is clear that the upper and lower plena have a significant effect on the heat transfer and natural circulation phenomenon leading to end effects. These end effects produce heat flow reversal which may have implications for PMR design and safety analysis.

Conclusions

A high temperature and pressure scaled-down dual-channel facility at Multiphase Reactors Engineering and Applications Laboratory (mReal) at Missouri S&T has been designed and developed to experimentally investigate natural circulation that would be encountered during an accident scenario of pressurized conduction cooldown (PCC) in a prismatic modular reactor (PMR). The current facility consists of two channels for coolant flow and an upper plenum and a lower plenum. In the current study, the effect of the outer surface temperatures of the upper plenum and cooled channel (downward flow) on the intensity of natural circulation is investigated using advanced fast response flush mounted foil sensors in conjunction with a series of thermocouples. Four different outer surface temperatures of the upper plenum and cooled channel (278.15, 288.15, 298.15,

and 308.15 K) are examined at a high pressure of 413.685 kPa using air as working fluid. The specific conclusions of the current study are summarized as follows:

- The majority of heat removal occurs by heat transfer through the upper plenum.
- Due to conjugate heat transfer and re-circulation at the top section of the heated channel, there is a drop of both centerline air temperature, and the channel wall temperature is observed.
- Measurements also reveal a reversal of heat flow close to the heat channel outlet, where the heat started to flow into the channel wall rather than from the wall to the air.
- Inner channel surface temperature and air temperature at the centerline are influenced by the outer surface temperatures of the upper plenum and cooled channel along the circulation loop. The air temperature at the centerline and inner surface temperature along the heated channel (upward flow) are increased by 21% and 12 % respectively with increasing the outer surface temperatures from 278.15 K to 308.15 K.
- The local heat transfer coefficient and local Nusselt number are decreased by 23 % and 25 % respectively with increasing the outer surface temperatures of the upper plenum and cooled channel from 278.15 K to 308.15 K.
- Experimental results of the convective heat transfer are compared with literature correlation[21,22] and are found within 20% and 21% respectively.

The obtained benchmark data will be used to validate commercial CFD codes that can be reliably used to predict flow behavior inside such systems.

Acknowledgment

The authors acknowledge the financial support provided by the U.S. Department of Energy-Nuclear Energy Research Initiative (DOE-NERI) Project (NEUP 13-4953 (DENE0000744)) for the 4th generation nuclear energy, which made this work possible.

Notation

C_p	heat capacity of air (J/ kg.K)
D_o	outer diameter of the heated channel (m)
g	acceleration gravity (m/s^2)
Gr	Grashof number, dimensionless, $\frac{g\beta(\bar{T}_s-\bar{T}_b)l^3}{\upsilon^2}$
Gr*	modified Grashof number, dimensionless, Ra_L^*/Pr
h_{avg}	time-averaged local heat transfer coefficient (W/m^2.K)
h_i	local instantaneous heat transfer coefficient (W/m^2.K)
$\overline{h_L}$	average heat transfer coefficient (W/m^2.K)
I	total current applied (Amps)
K_s	thermal conductivity of the insulation material (W/m.K)
k	thermal conductivity of air (W/m.K)
L	length of the heated channel (m)
l	characteristic length (m)
m	coefficient of correlation
n	coefficient of correlation
N	number of data points

Nu	Nusselt number, dimensionless, $\frac{h_{avg}\, l}{k}$
$\overline{Nu_L}$	average Nusselt Number, dimensionless, $\frac{\bar{h}_L\, l}{k}$
$Nu_{predicted,i}$	predicted Nusselt number from empirical correlation, dimensionless
$Nu_{experimental,i}$	experimental Nusselt number, dimensionless
Pr	Prandtl number, dimensionless, $\frac{\mu\, c_p}{k}$
q_i	local instantaneous heat flux (W/m^2)
q_w	imposed wall heat flux (W/m^2)
Q_t	total power supplied (W)
Q_{conv}	convection heat transfer from the heated channel surface (W)
Q_{rad}	radiation heat transfer from the heated channel surface (W)
Q_{cond}	axial conduction heat transfer through the heated channel (heat losses) (W)
R_{th}	thermal resistance (K/W)
Ra	Rayleigh number, dimensionless, Gr Pr
Ra_L^*	modified Rayleigh number, dimensionless, $\frac{g\,\beta\, q_w\, l^4}{\upsilon\,\alpha\, k}$
T_s	channel inner Surface Temperature (K)
T_b	bulk air temperature (K)
T_c	air temperature at the centerline (K)
T_f	air film temperature (K)
$\bar{T}_f$	average mean film temperature (K)
$\bar{T}_s$	average value of channel inner surface temperature(K)
$\bar{T}_b$	average value of bulk temperature (K)

ΔT	temperature difference across the insulation material (K)
V	total voltage applied (Volts)
Δx	thickness of insulation (m)
Z/L	dimensionless axial position

Greek Letters

α	thermal diffusivity (m^2/s)
β	volumetric expansion coefficient of air (1/K)
μ	dynamic viscosity of the air (kg.m/s)
υ	kinematic viscosity of air (m^2/s)
ρ	density of air (kg/m^3)

References

1. Lee JH, Yoon SJ, Kim ES, Park GC. CFD analysis and assessment for cross-flow phenomena in VHTR prismatic core. Heat Transfer Engineering. 2014;35(11-12):1152-1160.

2. Tung YH, Ferng YM, Johnson RW, Chieng CC. Study of natural circulation in a VHTR after a LOFA using different turbulence models. Nuclear Engineering and Design. 2013;263:206-217.

3. Travis BW, El-Genk MS. Thermal-hydraulics analyses for 1/6 prismatic VHTR core and fuel element with and without bypass flow. Energy Conversion and Management. 2013;67:325-341.

4. Tung YH, Johnson RW, Ferng YM, Chieng CC. Modeling strategies to compute natural circulation using CFD in a VHTR after a LOFA. Nuclear Engineering and Design. 2014;275:80-90.

5. Haque H, Feltes W, Brinkmann G. Thermal response of a modular high temperature reactor during passive cooldown under pressurized and depressurized conditions. Nuclear Engineering and Design. 2006;236(5-6):475-484.

6. Schultz RR, Bayless PD, Johnson RW, McCreery GE, Taitano W, Wolf JR. Studies Related to the Oregon State University High Temperature Test Facility: Scaling, the Validation Matrix, and Similarities to the Modular High Temperature Gas-Cooled Reactor. Idaho National Lab 2010.

7. Castañeda JA. Scaling analysis of the OSU high temperature test facility during a pressurized conduction cooldown event using RELAP5-3D: Nuclear Engineering, Oregon State University; 2014.

8. King BM. Natural Circulation Scaling of a Pressurized Conduction Cooldown Event in the Upper Plenum of the Modular High Temperature Gas Reactor: Nuclear Engineering, Oregon State University; 2012.

9. Abdulmohsin RS, Al-Dahhan MH. Characteristics of convective heat transport in packed pebble-bed reactor, Nuclear Engineering and design., 2015;284:143-152.

10. Pisters K, Prakash A. Investigation of Axial and Radial Variations of Heat Transfer Coefficient in Bubbling Fluidized Bed with Fast Response Probe. powder technology. 2011;207:224-231.

11. Kao MT, Jain P, Usman S, et al. Investigation of Plenum-to-Plenum Heat Transfer and Gas Dynamics under Natural Circulation in a Scaled-Down Dual Channel Module Mimicking Prismatic VHTR core using CFD. ANS-NURTH-16; 2015; Chicago, USA.

12. Ozisik MN. Basic Heat Transfer. McGraw-Hill, Boston; 1977.

13. Mohammed HA, Salman YK. Laminar air flow free convective heat transfer inside a vertical circular pipe with different inlet configurations. Thermal Science. 2007;11(1):43-63.

14. Kihm KD, Kim JH, Azevedo LS. Onset of flow reversal and penetration lengths of natural convective flow between isothermal vertical walls. J Heat Transf. 1995;117:776-779.

15. Sanvicente E, Giroux-Julien S, Menezo C, Bouia H. Transitional natural convection flow and heat transfer in an open channel. International Journal of Thermal Sciences. 2013;63:87-104.

16. Bergman TL, Incropera FP, Lavine AS. Fundamentals of heat and mass transfer. John Wiley & Sons; 2011.

17. Ede A. Natural convection on free vertical surfaces. MERL Report Heat 141Mechanical Engineering Laboratory, East Kilbride, Glasgow. 1956.

18. Kageyama M, Izumi R. Natural heat convection in a vertical circular tube. Bulletin of the JSME. 1970;13:382- 394.

19. Davis LP, Perona JJ. Development of free convection flow of a gas in a heated vertical open tube. International Journal of Heat and Mass Transfer. 1971;14(7):889-903.

20. Dyer J. The development of laminar natural-convective flow in a vertical uniform heat flux duct. International Journal of Heat and Mass Transfer. 1975;18(12):1455-1465.

21. Miyamoto M, Kajino H, Kurima J, Takanami I. Development of turbulence characteristics in a vertical free convection boundary layer. in: Proceedings of the 7th International Heat Transfer Conference; 1982.

22. Aydin O, Guessous L. Fundamental correlations for laminar and turbulent free convection from a uniformly heated vertical plate. International Journal of Heat and Mass Transfer. 2001;44:4605-4611.

List of Tables

List of Figures

Table 1. Dimensions of the current facility with reference to OSU-HTTF.

Parameter	Current facility	OSU-HTTF
Tube diameter (m)	0.016	0.016
Coolant channel length inside block (m)	1	2
Core diameter (m)	0.3	1.2
Upper plenum height (m)	0.239	0.956
Outer vessel diameter (m)	0.381	1.524
Number of channels	Two channels (one upward flow and other downward flow)	516 coolant channel 210 Heater Rod Six inner gap channel 36 outer gap channel

Table 2. Correlations from literature.

Investigators	Empirical correlation	Conditions
Miyamoto et al.[21]	$\overline{Nu_L}$ =0.104 $Ra_L^{*0.25}$	$(1.5 \times 10^{13} \leq Gr^* \leq 1.7 \times 10^{4})$, air
Aydin and Guessous[22]	$\overline{Nu_L} = 0.219 \left(\frac{Ra_L^* Pr}{0.191+Pr}\right)^{1/4}$	Apply to all fluids.

(a)

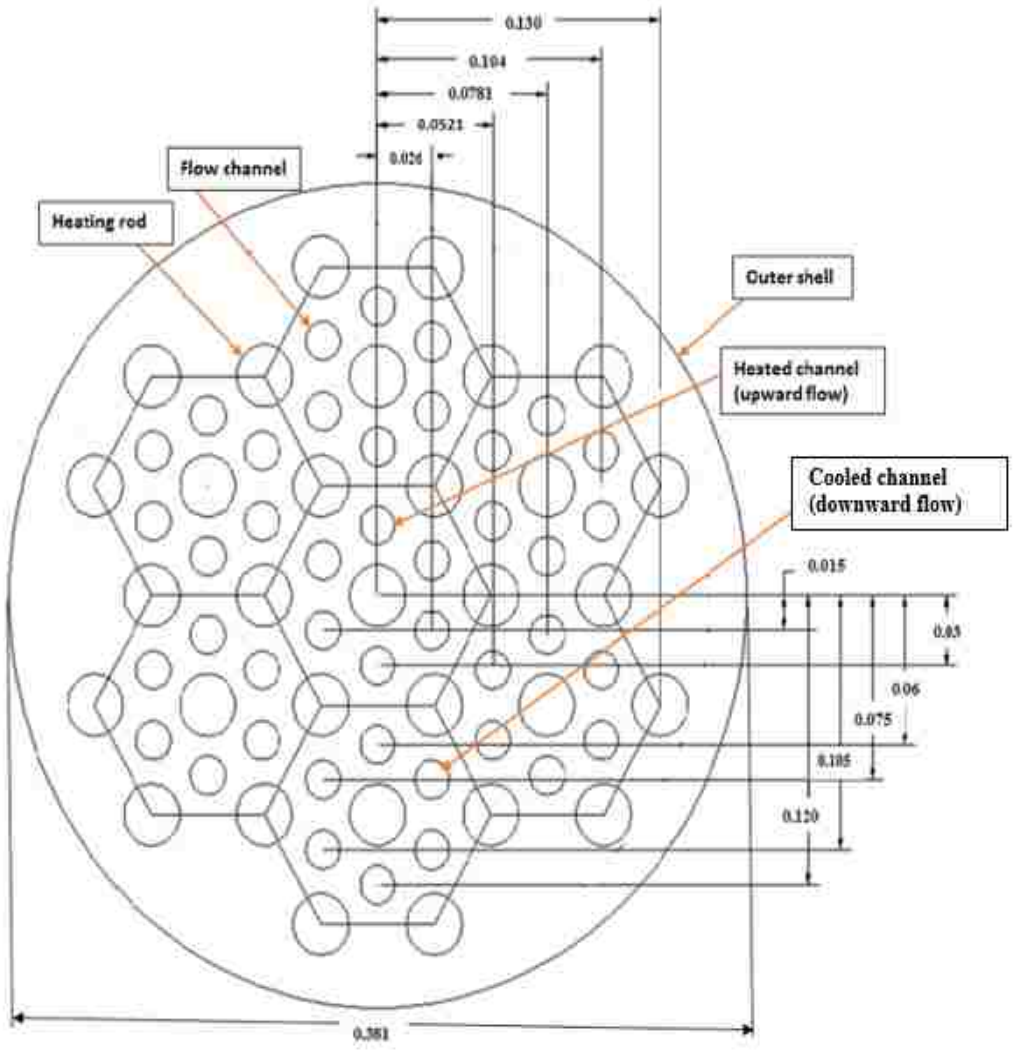

Fig. 1. (a) schematic diagram of top view of the seven blocks, (b) physical picture of the current facility, (c) position of the channels at the lower plenum, and (d) insulated upper plenum with cooling jacket (all dimensions in SI units, m)

(b)

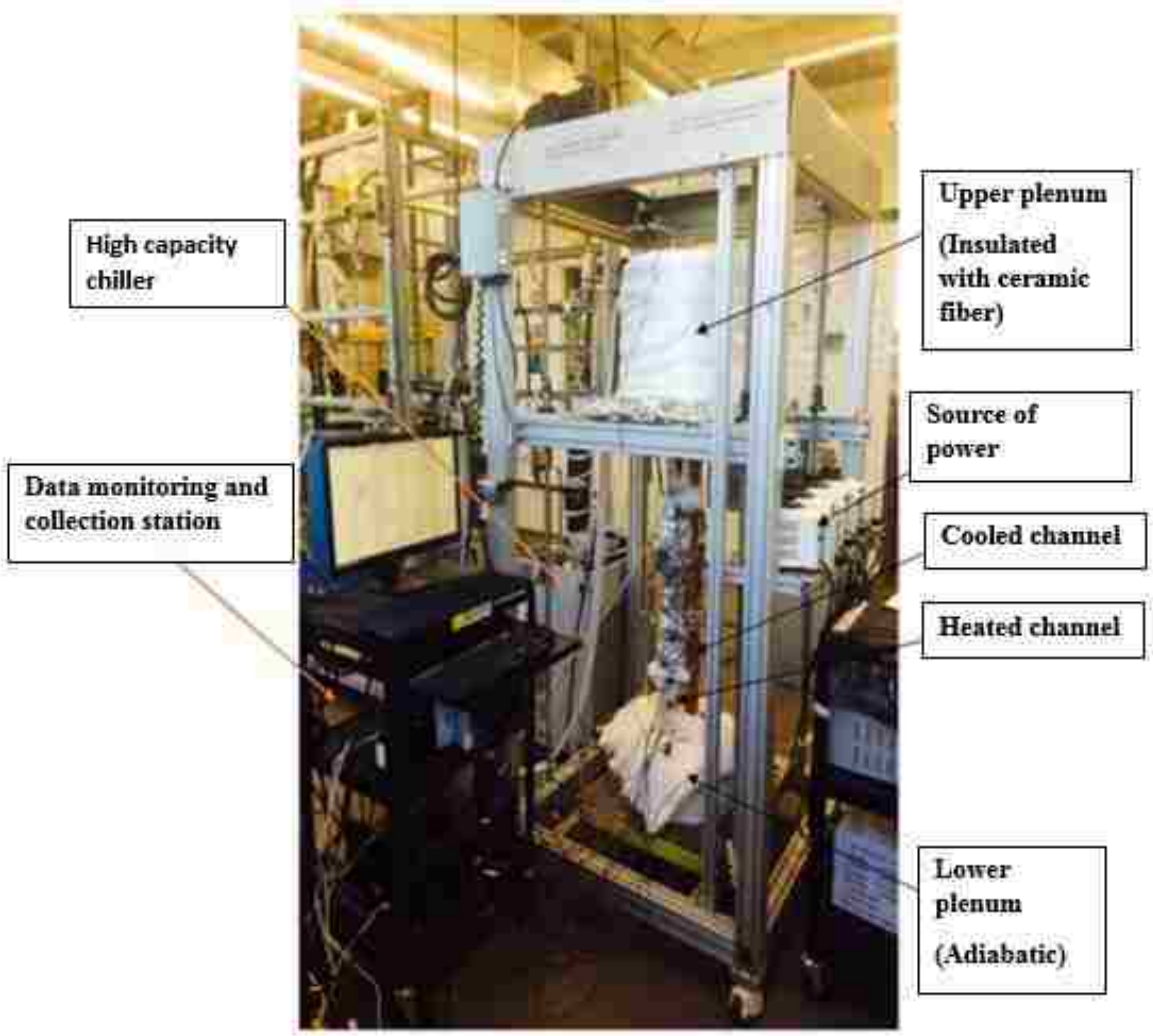

Fig. 1. (a) schematic diagram of top view of the seven blocks, (b) physical picture of the current facility, (c) position of the channels at the lower plenum, and (d) insulated upper plenum with cooling jacket (all dimensions in SI units, m) (cont.)

(c)

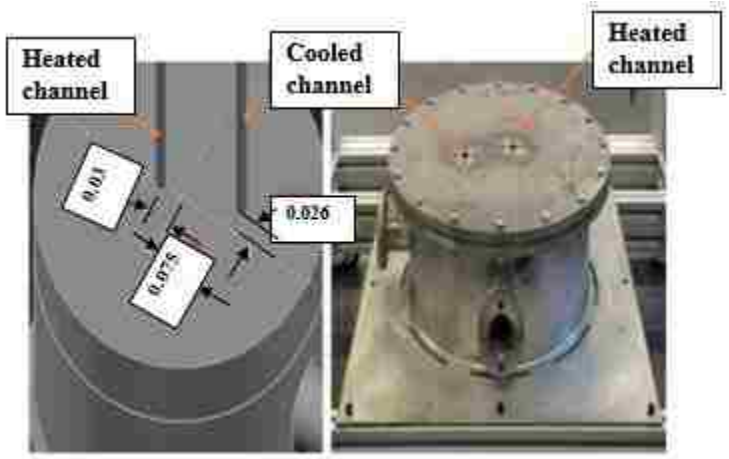

(d)

Fig. 1. (a) schematic diagram of top view of the seven blocks, (b) physical picture of the current facility, (c) position of the channels at the lower plenum, and (d) insulated upper plenum with cooling jacket (all dimensions in SI units, m) (cont.)

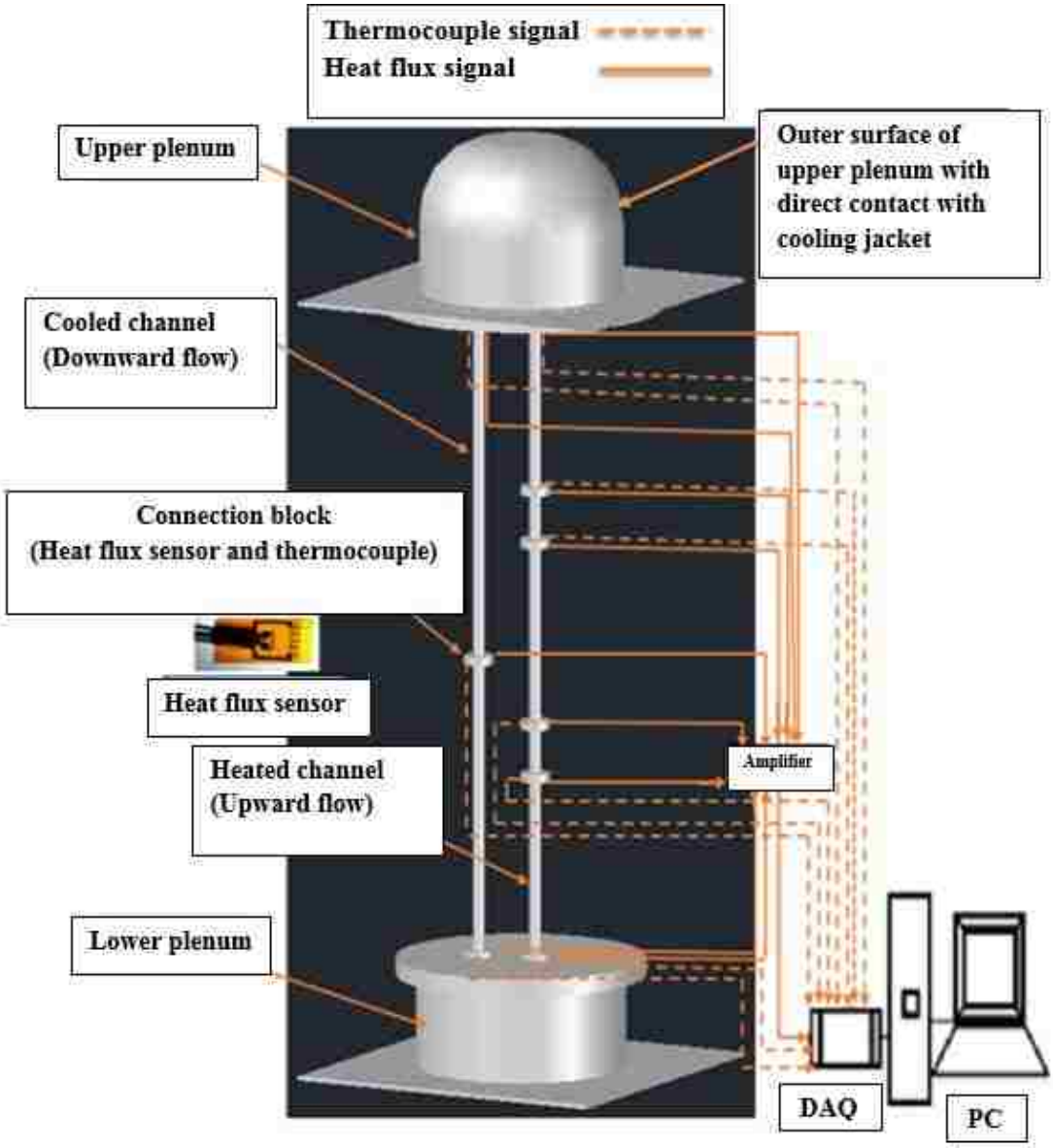

Fig. 2. Schematic diagram of the experimental setup with the heat transfer technique

(a)

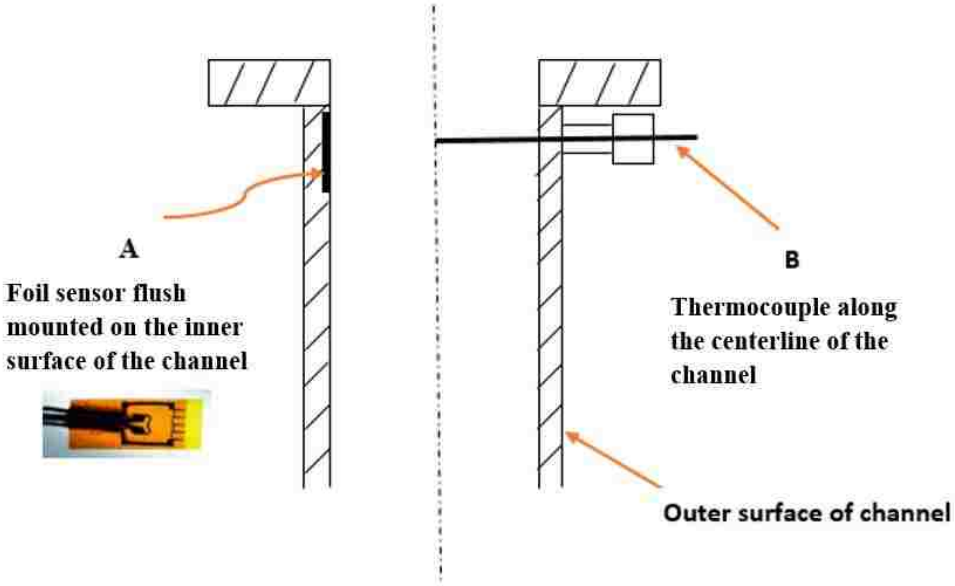

(b)

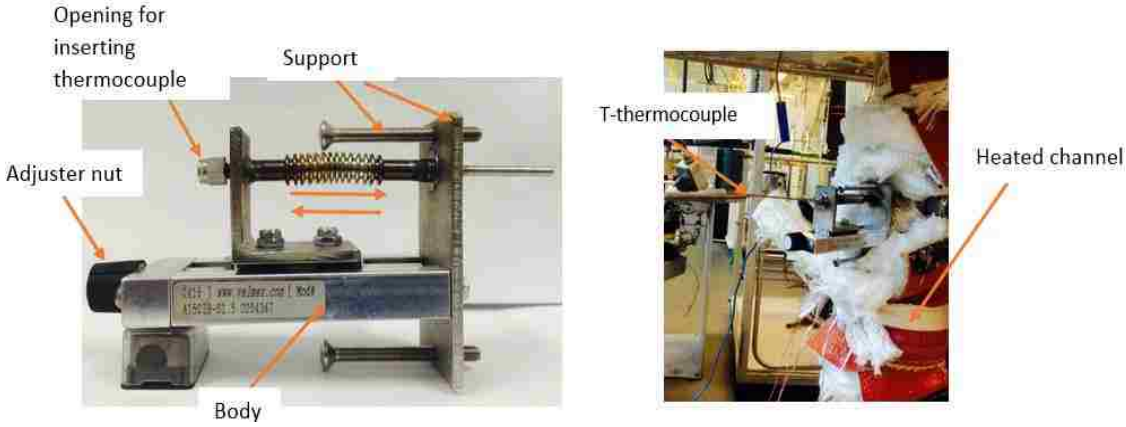

Fig. 3. (a) the connection block for data collection along the channels and (b) the radial adjuster

(a)

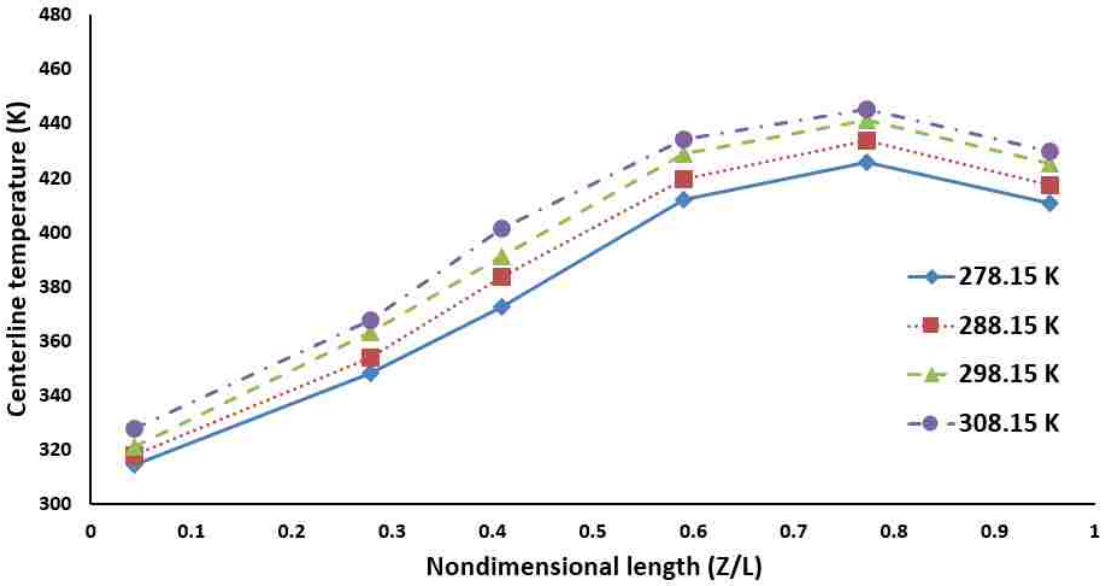

(b)

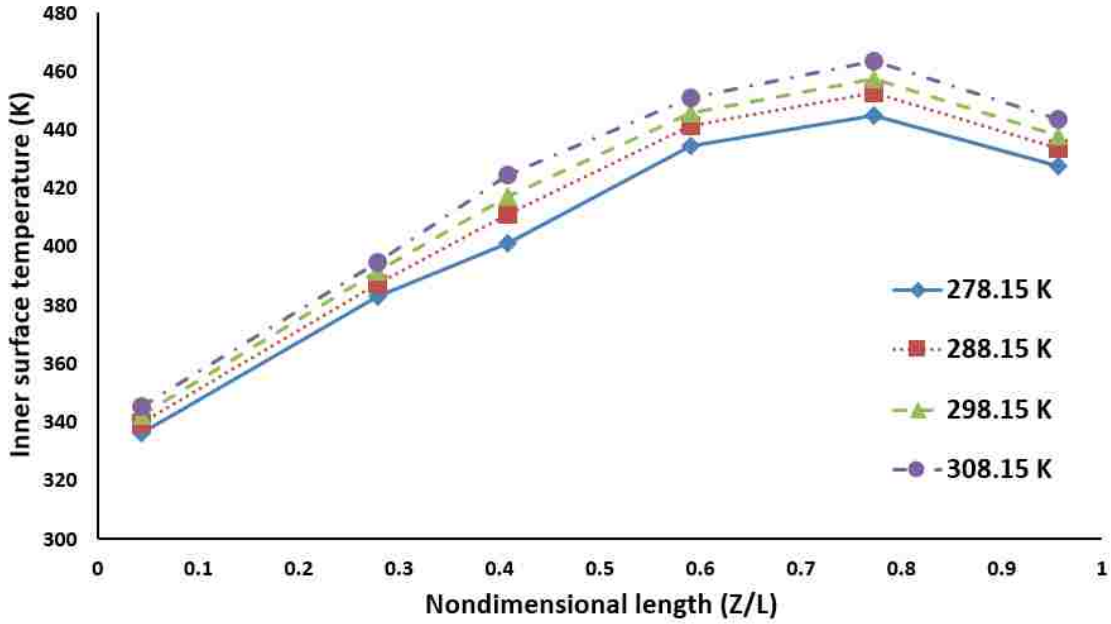

Fig. 4. Axial temperature distribution along the heated channel: (a) air temperature at the centerline and (b) inner surface temperature

(a)

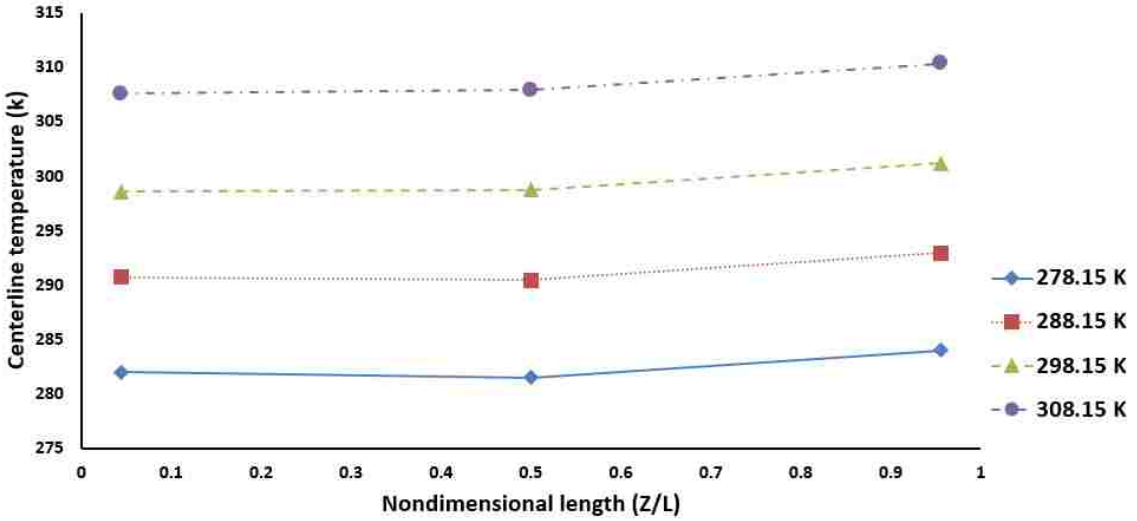

(b)

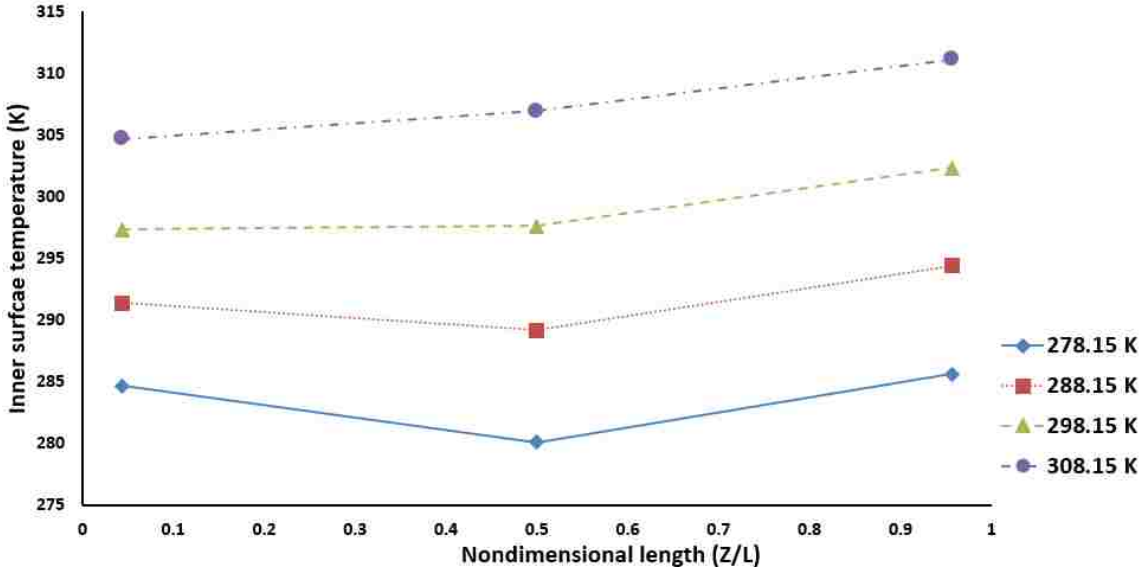

Fig. 5. Axial temperature distribution along the cooled channel: (a) air temperature at the centerline and (b) inner surface temperature

(a)

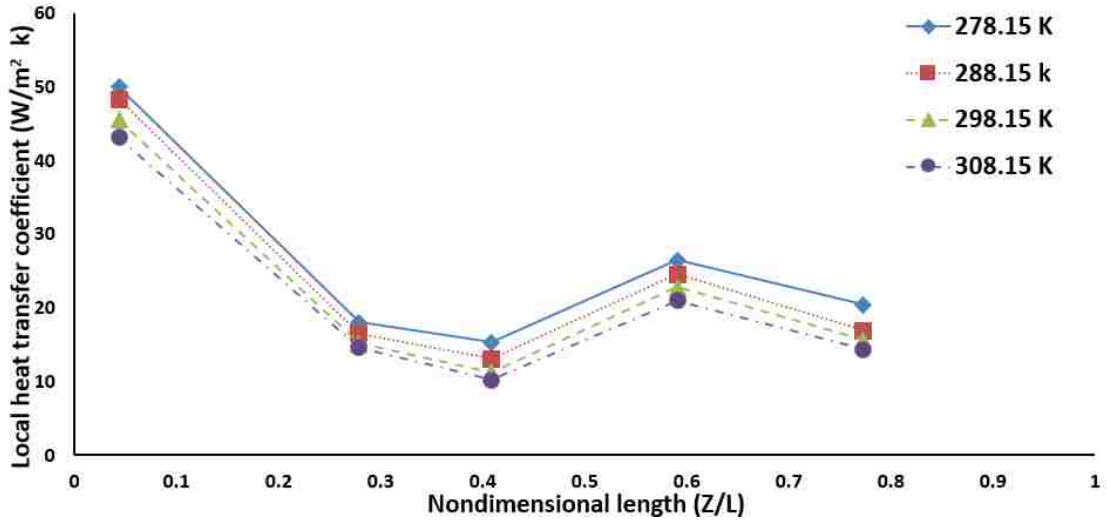

(b)

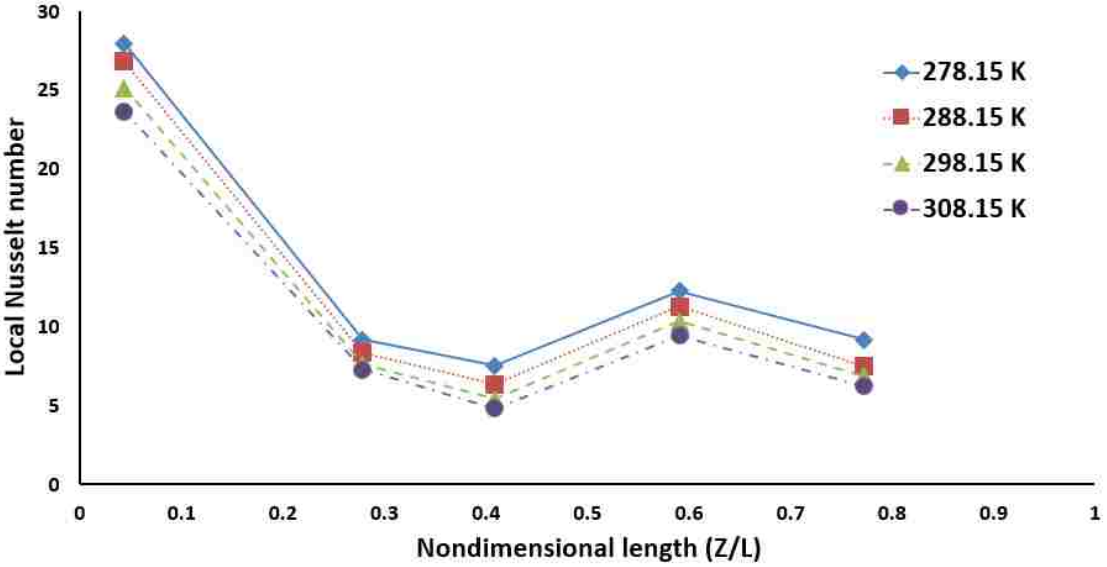

Fig. 6. (a) axial distribution of local heat transfer coefficient along the heated channel and(b) axial distribution of local Nusselt number along the heated channel

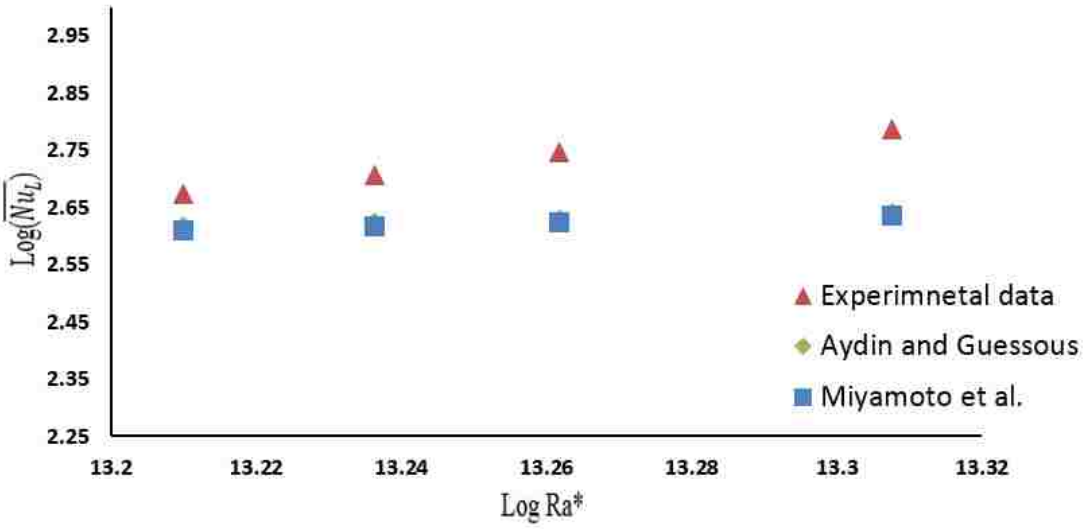

Fig. 7. Comparison of experimental results with available correlations in the literature.

II. EXPERIMENTAL INVESTIGATION OF THE HELIUM NATURAL CIRCULATION HEAT TRANSFER IN TWO CHANNELS FACILITY USING VARYING RISER CHANNEL HEAT FLUXES

Ibrahim A. Said [1,3], Mahmoud M. Taha [1,3], S. Usman [2] *, M. H. Al-Dahhan [1,2]

[1] Multiphase Reactors Engineering and Applications Laboratory (mReal), Chemical and Biochemical Engineering Department, Missouri University of Science and Technology, Rolla, MO, 65409, USA

[2] Mining and Nuclear Engineering Department, Missouri University of Science and Technology, Rolla, MO, 65409-0170, USA

[3] Chemical Engineering Department, Faculty of Engineering, Alexandria University, Alexandria, Egypt

** Corresponding author: usmans@mst.edu*

Abstract

Natural circulation is considered an important passive safety aspect of the prismatic block gas cooled reactor during accident scenarios. Experimental investigations for helium natural circulation heat transfer in a scaled down separate-effects dual-channel facility have been performed at Multiphase Reactors Engineering and Applications Laboratory (mReal). The current facility consists of two channels (riser and downcomer) for coolant flow between upper and lower plena. In the present study, the riser channel is heated uniformly using an electric heater, and the downcomer channel is cooled uniformly using a heat exchanger with chilled water to initiate natural circulation. The intensity of natural circulation heat transfer along the riser and downcomer channels is investigated at different levels of constant heat fluxes ranging from 860 W/m^2 to 2293

W/m^2 at 413.7 kPa using sophisticated a noninvasive heat transfer probe. The heat transfer data in terms of the local heat transfer coefficient, the local wall surface, and helium temperatures are collected at different axial and radial locations. Also, the local Nusselt numbers are estimated along the two channels. Results confirm that the heat transfer coefficient and Nusselt number values increase as the heat fluxes increase due to increased convection currents. Average riser wall surface temperature increased by 84% when heat fluxes increase from 860 W/m^2 to 2293 W/m^2. Also, small variations in the temperatures of the wall surface and helium are observed along the downcomer channel due to the large volume of the upper plenum. A reversal in the direction of heat transfer close to the outlet of the riser channel (Z/L = 0.956) is observed, as well as a reduction in the wall surface temperature due to co-circulation. The heat transfer reversal being reported here is very significant and would have profound effects on the overall design of the natural circulation systems. The radial temperature distributions along the riser channel showed a unique peaking in the center close to the exit (Z/L = 0.956). Also, the local radial variation of density, dynamic viscosity, and thermal conductivity as dimensionless values with respect to bulk values are measured along the riser channel. Results showed that the deviation of local values from the bulk values increases with increasing the magnitude of heat flux to the riser channel. The average heat transfer results in terms of Rayleigh number and Nusselt number, when compared with previous literature correlations, showed a similar qualitative trend.

Keywords: natural circulation; prismatic block gas cooled reactor; noninvasive heat transfer probe; heat transfer coefficient and Nusselt number

Introduction

High-temperature gas-cooled reactor (HTGR) or very high-temperature reactor (VHTR) is considered one of the candidates for the next generation nuclear plants (NGNPs) due to their advantages over other new reactor designs. One of the very high-temperature reactor advantages is their capability to passively remove decay heat from the reactor through natural circulation and convection from the reactor core during accident scenarios. Natural circulation of the coolant and high thermal conductivity of graphite (moderator) are the leading capabilities for VHTR to transport the decay heat from the core to the reactor vessel. Natural circulation is expected to occur under pressurized conduction cooldown (PCC) and depressurized conduction cooldown (DCC) scenarios in VHTR [1,2]. There are some studies performed on the fluid flow and heat transfer in the VHTR under the natural circulation in VHTR using computational fluid dynamics (CFD) calculations[3-5]. These studies reveal that natural circulation is an effective safety system, and it prevents the core from meltdown and localized hot spots after the loss of flow accidents (LOFA). Valentin et al. [6] at City College of New York examined natural circulation in a simplified graphite-fuel matrix using COMSOL Multiphysics code. They investigated the effect of geometry, operational conditions, and fluid properties on the passive cooling systems. There is an ongoing study at Oregon State University's high-temperature test facility (OSU-HTTF) related to plenum-to-plenum natural circulation heat transfer during PCC and DCC accident scenarios [1,2,7]. These studies are limited in the ability to measure local high-resolution and high-fidelity heat transfer coefficient and heat transfer rate because the used facilities are not equipped with newly available sophisticated measurement techniques. Haque et al. [8] investigated the PCC and DCC accident scenarios using thermal hydraulic code called THERMIC.

Also, Simone et al. [9] employed CFD code to examine combined convective, conductive, and radiative heat transfer during decay heat removal in VHTR. The discussed literature survey shows the lack of experimental studies on plenum-to-plenum natural circulation heat transfer during the loss of forced flow accident scenario in the prismatic modular reactor. Particularly there are data and knowledge gaps for local heat transfer coefficient measurements using sophisticated noninvasive techniques. To fill these literature gaps and to provide local experimental data on the natural circulation, a high temperature and pressure dual-channel facility has been used in this study. The facility is designed, developed, and implemented by Multiphase Reactors Engineering and Applications Laboratory (mReal)[10] research team at Missouri S&T. This facility can perform separate and integral-effects experiments for studying thermal-hydraulic behavior occurring within a component or particular region of VHTR. The facility is equipped with sophisticated measurement techniques that are integrated in a novel way to experimentally investigate the intensity of natural circulation between the two plena through the flow channels. In this study, a noninvasive fast-response flush-mounted heat transfer probe with high response time and high sensitivity that measures heat flux and surface temperature has been developed. A radial temperature measurement adjuster using T-thermocouple (1.6 mm in diameter) has also been developed and machined in-house to measure the radial helium temperature variations along the flow channels. Heat transfer data in terms of the heat transfer coefficients, Nusslet numbers, and axial and radial temperatures are measured across the flow channels with the considerations of the thermal boundary conditions of isoflux (constant axial heat flux conditions), ranging from 860 to 2293 W/m^2, for the riser channel. The experiments have been performed at high

operating pressure, 413.7 kPa, using helium as a working fluid, for constant outer surface temperatures of the upper plenum and downcomer channel. We performed all the experiments at 413.7 kPa for safety considerations, and we also have an ongoing separate effect study on the operating pressure effect. Hence, a mid-value pressure of 413.7 kPa is selected here. The obtained local heat transfer data in this study will provide high spatial and temporal resolutions benchmarking data for validating heat transfer computations and correlations that are integrated with CFD simulations.

Experimental work

Multiphase Reactors Engineering and Applications Laboratory (mReal) at Missouri S&T has designed, developed, and implemented a unique small scale dual-channel facility[10]. This facility which was used in this work is shown in Figure 1. The dual-channel facility is made of stainless steel alloy and consists of two vertical channels (riser and downcomer) and two plena connected with two stainless steel flanges. The inside diameter of the channels is 1.6 mm, while the height of the channels and the channel spacing (measured from the axis of the two channels) are 1 m and 105 mm, respectively. The height of the channel represents five scaled-down blocks[10]. A flexible tape-type electrical heater (2.4 m in length and 254 mm in width) is wound uniformly around the riser channel. A variable voltage regulator with a span of 0-130 volts and a digital power reader is connected to the electrical heater to control the power supplied to the riser channel. A heat exchanger using chilled water (length 1 m) of copper tube is used around the downcomer channel to control the outer surface temperature of the downcomer channel to the desired value. Furthermore, the heat exchanger around the downcomer channel is used to make a cooling by chilled water for the helium inside the

downcomer and simulate the downward flow. Also, the outer surface of the upper plenum is equipped with a cooling jacket using chilled water to maintain the outer surface of the upper plenum at the desired temperature. A chiller (Applied Thermal Control Ltd, K4 chiller) was used in the current study to provide the chilled water at the desired temperature for the cooling jacket and heat exchanger. The chilled water flows countercurrent with respect to the helium flow inside the downcomer channel. The cooling jacket at the upper plenum is also connected with the chiller to maintain the outer surface temperature of the upper plenum at the desired value. Since the difference between the inlet and outlet chilled temperatures of the cooling jacket and heat exchanger always turned out to be less than 1 ^{o}C, the constant wall temperature can be assumed as the thermal boundary condition for the downcomer channel and upper plenum. Thus, the temperatures of the outer surfaces for the downcomer channel and upper plenum are kept constant at 5 ^{o}C. This temperature of 5 ^{o}C for outer surface temperatures for the upper plenum and downcomer channel, is selected due to the higher rate of heat transfer coefficients along the riser channel, which is based on our experimental study carried out and related to the effect of the outer surface temperatures of the downcomer channel and upper plenum on the intensity of natural circulation[10]. The entire lower plenum is insulated using a ceramic fiber blanket to establish adiabatic conditions. To minimize the heat exchange between the experimental facility and the environment, every part of the system was also carefully insulated using a thick ceramic fiber blanket (0.05 m in thickness). More details regarding the experimental facility and cooling and heating systems can be found elsewhere[10]. A radial adjuster for helium radial temperature measurements has been developed and machined in-house to radially adjust the location

of the T-thermocouples (1.6 mm in diameter) along the flow channels (Figure 2). This in-house development of a radial adjuster allowed us to measure the radial temperatures of helium at different axial locations along the flow channels. Six axial positions along the riser channel (Z/L= 0.044, 0.279, 0.409, 0.591, 0.773, 0.956 (end effect)) and three axial positions along the downcomer channel (Z/L= 0.044, 0.5, 0.956) have been used in the present study to perform the measurements of the heat transfer coefficients and the flowing helium radial temperatures. The local instantaneous heat fluxes and surface temperatures along the riser and downcomer channels are measured using a noninvasive heat transfer probe of micro-foil heat flux sensor ($6.35x10^{-3}$ m x 0.01778 m x $8x10^{-5}$ m) from RDF Corporation (model no. 27036-1). The micro-foil heat flux sensor was flush-mounted on the inner surface of the flow channels (Figure 3) to make the measurements noninvasive. The micro-foil sensor has both the heat flux and thermocouple sensors. Thus, the micro-foil sensor can simultaneously measure the local instantaneous heat flux between the foil sensor and the flowing fluid and the local instantaneous inner surface wall temperature of the sensor. In our laboratory (mReal), we have used such flush mounted heat transfer technique to characterize the heat transfer coefficient and consequently Nusselt number in cold flow multiphase systems [11,12]. The measured signals of the heat flux, in the range of microvolts, need to be amplified prior to being sent to the data acquisition system. Hence, an amplifier with model number JH4300-AC from JH Technology has been used in the current study. Figure 4 shows the sequence of the signal collection from the micro-foil heat flux sensor to the data acquisition system. After amplification, the heat flux signals together with the signals of the thermocouples were sampled at 50 Hz sampling rate for 40 seconds. It is worth mentioning that the micro-foil

sensor is capable of detecting the direction of the heat transfer between the wall surface and flowing helium. The positive signal of heat flux means that heat transfers from the inner surface of the channel to the flowing fluid, while a negative signal means that heat transfers from the flowing fluid to the inner surface of the channel. In the downcomer channel, negative signals of heat fluxes are observed for all experimental conditions. These negative signals confirm that helium flows downward through the downcomer channel. Positive signals of heat flux are observed along the riser channel from Z/L = 0.044 to Z/L = 0.773, but negative heat flux signals close to the exit (end effect) of the riser channel (Z/L =0.956) are observed for all experiments. These negative heat flux signals confirm that there is a reversal in the direction of heat transfer from the flowing helium to the inner surface of the riser channel. Hence, we have excluded the heat flux signals at Z/L =0.956 from the measurements of heat transfer coefficient and consequently the Nusselt number for the riser channel[10]. More details regarding the end effects are discussed in the results and discussion section. The local instantaneous heat transfer coefficient (h_i) and the local time-averaged heat transfer coefficient (h_{avg}) could be estimated from Equations 1 and 2 by measuring the local heat flux (q_i) by the heat flux sensor and the difference between wall surface temperature ($T_{s,i}$) measured by the heat flux sensor and the characteristic fluid temperature ($T_{b,i}$) measured by the T-thermocouple using the radial adjuster [10,12]:

$$h_i = \frac{q_i}{(T_{s,i} - T_{b,i})} \qquad (1)$$

$$h_{avg} = \frac{1}{N} \sum_{i=1}^{i=N} h_i \quad (2)$$

Where *N* is the number of the data points over 40 seconds for 50 Hz sampling rate, which is selected to be 2000 to achieve a high stable value of heat transfer coefficient over all the experiments. The characteristic fluid temperature ($T_{b,i}$) for the riser channel is measured at each axial location by averaging eight radial values ($T_{f\,i,j}$) with a step 1/16 of the channel inside diameter (1 mm step size) as follows:

$$T_{b,i} = \frac{1}{8} \sum_{j=1}^{j=8} T_{f\,i,j} \quad (3)$$

In the downcomer channel, the characteristic fluid temperature is the helium temperature at the centerline due to slight variation in the radial measured temperatures. T-thermocouples (1.6 mm in diameter) are used to measure the helium temperature at the centerline of the downcomer channel. A series of experiments were performed using helium as a working fluid at a high temperature and operating pressure of 413.7 kPa (selected due to safety reasons and in light of other ongoing research), in which the outer surface temperatures of the upper plenum and downcomer channel are kept constant at 5 ^{o}C during all experiments. Six values of the supplied constant heat fluxes (isoflux) to the riser channel have been used ranging from 860 to 2293 W/m^2. Each experiment was performed from the rest state at uniform helium and wall temperatures distribution (within ± 0.3 ^{o}C), starting with the simultaneous dissipation of electrical power in the heated section (riser) and circulation of the chilled water in the heat exchanger around the heat sink (downcomer) and cooling jacket around the upper plenum. The steady-state conditions were established for each experiment when the readings become stable for all thermocouples signals (± 0.5K) and heat transfer coefficient signals (±0.8 W/m^2 K),

which were usually achieved after approximately 3-4 hours. A National Instrument SCXI module data acquisition system and a personal computer were used for the data collection and reduction (Figure 5). The data acquisition was performed through the LabVIEW software.

Results and discussion

End effects

Heat flow reversal is observed at the outlet of the riser channel (Z/L = 0.956) under conditions (high pressure and temperature) that are not identified or systematically reported in the open literature. Barnes[13] predicted that heat is transported from the gas to the wall (heat flow reversal) in the exit region of the test section. Figure 6 shows the negative signals of the heat flux at Z/L = 0.956 for all different experimental conditions. It is worth mentioning that the remaining signals of the heat flux from Z/L = 0.044 to Z/L = 0.773 give positive values. Also, the radial distributions of helium temperature close to the exit (Z/L = 0.956) showed a central peaking for all experiments (Figure 7). This central peaking is evidence of the heat flow reversal from the adjacent flowing fluid to the inner wall, which is consistent with the negative signals for the heat fluxes. Therefore, this reversed flow should also induce separation of the ascending boundary layer flow as well flow oscillations as reported in literature [13]. The heat flow reversal can take its origin from several parameters: axial cooling conduction through the solid wall of the riser channel (conjugate heat transfer) and the presence of the upper plenum as an adiabatic extension with large expansion ratio at the outlet [14,15].The upper plenum as adiabatic extension acts as a shroud with respect to the helium plumes coming from the riser

channel. This phenomenon has to be investigated further, especially regarding the expansion ratio between the riser channel and upper plenum.

Axial distribution of wall surface temperatures along the riser channel

Figure 8 exhibits very similar wall surface temperature patterns at different applied constant heat fluxes ranging from 860 to 2293 W/m^2. In all experimental conditions, the maximum surface temperature is not attained at the exit section of the riser channel due to the end effects, which are discussed previously. Also, one can remark that the surface temperature gradually increases with the channel length until Z/L = 0.773, beyond which it begins to decrease. This behavior can be explained if Figure 9 is considered. At the leading edge of the riser channel, point (A), the thickness of the boundary layer is too small; then, it gradually increases until the point (B). From point (A) to the point (B), the helium inside the riser channel is heated by convection currents from the inner surface while it flows through the riser channel. This makes the helium temperature increases with the axial distance (Z/L) until the point (B), where the maximum temperature is attained. Beyond point (B), one would expect a straight line relation between the surface wall temperature and the channel length (BC) with the case being that of constant heat flux (isoflux). A reduction in the wall surface temperatures, as represented by (ABD) is observed due to the end effects. In fact, an inflow of denser helium from the upper plenum cools the thermal helium plumes coming out from the riser channel, and it can penetrate the riser channel. As shown in Figure 8, for any given axial position, the surface temperature increases with the increase of the heat fluxes from 860 W/m^2 to 2293 W/m^2 because the natural convection is the dominating factor in the heat

transfer process. The average riser wall surface temperature increased by 84 % for heat fluxes increase, from 860 W/m^2 to 2293 W/m^2.

Radial distribution of helium temperatures along the riser channel

Figures 10-15 show the radial distribution of helium temperatures along the riser channel from the entrance (Z/L = 0.044) to the exit (Z/L = 0.956) for different applied constant heat fluxes. For all experimental conditions, the radial temperatures exhibit a very similar trend. Three interesting distinguished radial profiles emerge from these figures as follows: 1) developing profile from Z/L = 0.044 to Z/L = 0.591, 2) flattened profile at Z/L = 0.773, and 3) reversed profile close to the exit (Z/L = 0.956). At the top section of the riser channel, the flow is slow and unable to remove large amounts of heat compared to higher flow. Hence, the helium bulk temperature will increase to a value approximately equaling the wall surface temperature, as shown in the flattened profiles for Z/L = 0.773. After Z/L = 0.773, the gas is unable to remove additional heat, and the direction of the heat is reversed. This phenomenon has significant effects on the dynamic performance in terms of buoyancy force. Also, at this condition, the buoyancy force has no more contribution to the increased fluid velocity. Figure 16 shows the effects of the axial surface wall temperature on the helium radial temperature profiles along the channel.

Radial variation of the physical properties along the riser channel

The radial variations of density, dynamic viscosity, thermal conductivity, and heat capacity in the terms describing the transfer of momentum, mass, and heat are the primary cause of the changes in the distribution of temperature, heat transfer coefficient,

and velocity profiles. Figures 17-19 show the experimental density, thermal conductivity, and dynamic viscosity radial profiles as dimensionless values for helium plotted as a physical property at local radial temperature divided by the bulk value. The bulk values for the physical properties along the riser channel are estimated at the operating pressure and characteristic fluid temperature ($T_{b,i} = \frac{1}{8}\sum_{j=1}^{j=8} T_{f\,i,j}$), while the local values (eight values with a step size of 1 mm from the inner wall) are estimated at the operating pressure and the measured local radial temperature ($T_{f\,i,j}$) using the radial adjuster for T-thermocouple. The helium properties used in the current study are based on a report from Petersen[16]. Figures 17-19 are presented for selected levels of applied constant heat fluxes to the riser channel (860, 1433, and 2293 W/m^2) for three different axial locations: the inlet (Z/L = 0.044), close to the middle (Z/L = 0.409), and at the exit (Z/L = 0.956). It is clear from Figures 17-19 that the deviation of properties from the bulk values increases for any given axial location with increasing the magnitude of heat fluxes. Also, one can remark that the variation of the dynamic viscosity is very similar to the thermal conductivity for all cases.

Axial distribution of the local heat transfer coefficient (h_{avg}) and Nusselt number ($Nu_D = \frac{h_{avg} D}{k}$) along the riser channel

The evolution of the local heat transfer coefficient and local Nusselt number (Nu_D) along the height of the riser channel is presented in Figures 20 and 21 for different constant heat fluxes ranging from 860 to 2293 W/m^2 with similar approximate trends. In the inlet section (Z/L = 0.044), the cold helium is drawn into the lower end of the riser

channel, causing a high heat transfer coefficient and consequently high Nusselt number. Between Z/L= 0.044 and Z/L = 0.409, a decrease in the local heat transfer coefficient and Nusslet number can be observed for low values of constant heat flux (860, 1146, 1433, and 1720 W/m^2), while for higher constant heat fluxes (2006 and 2293 W/m^2), the local heat transfer coefficient and Nusslet number decrease from Z/L = 0.044 to Z/L= 0.279 due to higher convection currents. This reduction in the local heat transfer coefficient and the Nusselt number could be attributed to growing of the boundary layers by rising helium. After Z/L = 0.409 for lower values of heat flux or Z/L = 0.279 for higher values of heat flux, an increase in the local heat transfer coefficient and Nusslet number is observed until Z/L= 0.591. This enhancement in the local heat transfer coefficient and Nusslet number is due to the laminarization effect in the wall region (buoyancy effect) and due to upstream axial conduction in the solid walls, preheating the helium in the hydrodynamics developing section. Also, a transition to turbulence could be happening in this region. Beyond Z/L = 0.591, one would expect the increase in local heat transfer coefficient and local Nusselt number to continue with the case being that of constant wall heat flux, but a reduction in the values of the local heat transfer coefficient and the Nusselt number is observed. This could be attributed to an extension of the end effects of the riser channel. Also, Tung et al.[3] reported that at the interface between the upward flow channel and the upper plenum, the axial velocity decreases quickly as the working fluid expands into the upper plenum. Hence, a reduction in the values of heat transfer coefficients is observed at the top section of the riser channel. Figures 20 and 21 also confirm that the local heat transfer coefficient and Nusslet number increase as the heat

flux increases due to increasing natural convection currents, which improve the heat transfer process.

Comparison of the natural convection Nusselt numbers along the riser channel with the previous work

To the authors' knowledge, there are no available correlations regarding natural convection heat transfer for the current geometry of the riser channel with upper and lower plena (end effects) that may be compared with the heat transfer coefficient obtained in this work. The only available correlations that can be compared with this work are established for natural convection heat transfer in a vertical isoflux circular tube without plena at atmospheric pressure using air[17,18]. Table 1 summarizes the selected and used correlations for comparison. The selected correlations are based on a wide range of experimental data that were used to develop these correlations. The comparison of heat transfer coefficient obtained in this work in terms of the average Nusselt number ($Nu_L = \frac{h_{avg}\, L}{k}$) and Rayleigh number ($Ra_L = Gr_L$ Pr) is shown in Figure 22. All the physical properties of the helium in Nu_L and Ra_L have been evaluated at the average mean film temperature ($\overline{T}_{film} = \frac{\overline{T}_s + \overline{T}_b}{2}$) [19,20]. One can remark that the average experimental Nusselt numbers (Nu_L) showed a similar qualitative trend. Also, from the comparison, it is clear that the average experimental Nusselt numbers (Nu_L) are higher than that calculated by the literature correlations[17,18]. This confirms that simple geometry without upper and lower plena, as well as higher pressure, has a significant quantitative

effect on the results of convective heat transfer. This finding is consistent with the open literature about the role of restrictions at the ends of heated sections on the obtained heat transfer coefficients and consequently, Nusselt numbers [18,21,22] in which the restriction configurations at the ends of the heated section have a significant effect on the heat transfer results.

Axial distribution of wall centerline's helium and inner wall surface temperatures along the downcomer channel

Figures 23 and 24 show the centerline's helium temperature (Figure 23) and the inner wall surface temperature (Figure 24). Both figures exhibit general decreasing rate for all experimental conditions from the inlet (Z/L = 0.956) to the outlet (Z/L = 0.044). One can remark that the end effects are observed at the outlet of the downcomer channel in terms of an increase in both temperatures. This end effect, at the end of the downcomer channel, may be attributed to the conductive heat transfer between two channels close to the exit of the downcomer as well as co-circulation. Hence, a dip in both temperatures is observed at Z/L = 0.5. With increasing the applied heat fluxes for the riser channel, the centerline's helium and channel wall temperatures also increase for all axial positions (Z/L = 0.044, 0.5, 0.956). The helium temperature at the centerline and inner wall surface temperature along with the downcomer channel increase by 16 % and 14 %, respectively, with increasing the magnitude of applied constant heat fluxes to the riser channel from 860 W/m^2 to 2293 W/m^2. It is worth mentioning that small local temperature differences are observed between the both temperatures, which are less than 2 ^oC for all experimental conditions. These small local temperature differences mean that the majority of heat

carried by helium plumes from the riser channel is absorbed within the upper plenum. This finding is also reported by Said et al.[10] along the downcomer channel. Therefore, in this study, we did not measure the radial variation of helium temperatures along the downcomer channel.

Axial distribution of the local heat transfer coefficient (h_{avg}) and Nusslet number ($Nu_D = \frac{h_{avg} D}{k}$) along the downcomer channel

Figures 25 and 26 show an axial distribution for the local heat transfer coefficient and Nusslet number along with the downcomer channel with a decreasing trend from the inlet (Z/L = 0.956) to the outlet (Z/L = 0.044) for all experimental conditions. It worth mentioning that the direction of heat transfer is observed to be from to helium flow to the inner wall of the downcomer channel. This finding emphasizes that the helium flows downward through the downcomer channel. Also, it is observed from Figures 25 and 26 for a given condition that the local heat transfer coefficients and Nusselt number decrease from the leading entrance of the downcomer channel to the outlet. This decreasing rate of local heat transfer coefficients and the Nusselt number is evidence of the descending flow in the downcomer channel.

Remarks

A high pressure and temperature natural circulation heat transfer experiments have been carried out at Multiphase Reactors Engineering and Applications Laboratory (mReal). A dual-channel facility with two channels for coolant flow and two plena has been used to measure crucial local heat transfer data in terms of axial and radial temperatures, heat transfer coefficients, and Nusslet numbers along the flow channels using helium as a working fluid. Experiments are carried out at 413.7 kPa using a sophisticated noninvasive heat transfer probe in conjunction with a radial temperature measurement adjuster for T-thermocouple, which has been designed and developed in-house to measure the radial helium temperatures radially. The intensity of natural convection across the two channels (riser and downcomer) has been investigated by varying the supplied constant heat fluxes to the riser channels. Six values of constant heat fluxes are used in the current study (860, 1146, 1433, 1720, 2006, and 2293 W/m^2), while the outer surface temperatures of the upper plenum and downcomer channel are kept at 5 ^oC. The main findings of the current study can be summarized as follows:

- The upper plenum as adiabatic extension acts as a shroud for the helium flow coming from the riser channel. Hence, a reduction in the wall surface temperature is observed close to the exit of the riser channel
- A reversal in the direction of heat transfer is observed close to the exit of the riser channel with a central peaking for helium radial temperatures.
- The radial temperature measurements of helium for the riser channel revealed three interesting distinguished radial profiles: 1) developing profile from Z/L =

0.044 to Z/L = 0.591, 2) flattened profile at Z/L = 0.773, and 3) reversed profile close to the exit (Z/L = 0.956).

- Radial variations of density, dynamic viscosity, and thermal conductivity as dimensionless values with respect to the bulk values are experimentally measured for the riser channel. The experimental results showed that the deviation of these properties from the bulk values increases with increasing the magnitude of heat fluxes applied to the riser channel.
- Local time-averaged Nusslet values decrease initially from the leading edge of the riser channel to a certain axial position (Z/ L = 0.409 for small values of constant heat fluxes and Z/L= 0.279 for high values). Then, they gradually increase to Z/L = 0.591 with a sharp drop after Z/L = 0.591 due to end effects.
- A qualitative agreement is obtained between the current experimental heat transfer results and literature correlations in terms of average Nusselt numbers. Also, the average Nusselt numbers for this work were greater than the predicted values from the literature correlations. This could be attributed to the role of upper and lower plena as adiabatic extensions at the ends of the riser channel, which was missing in the literature.
- Experimental measurements reveal a decreasing rate for values of a local Nusselt number from the inlet of the downcomer channel (Z/L = 0.956) to the outlet (Z/L = 0.044).
- Small local temperature differences between the centerline’s helium temperature and wall surface temperature are observed along the downcomer channel. This

finding emphasizes that the majority of heat carried by the helium from the riser channel is absorbed in the upper plenum.

- The obtained benchmark results can be used to validate the heat transfer computations in conjunction with CFD simulations.
- This study has advanced the knowledge and understanding of the natural circulation phenomenon in nuclear systems using a representative setup.

Acknowledgment

The authors acknowledge the financial support provided by the U.S. Department of Energy-Nuclear Energy Research Initiative (DOE-NERI) Project (NEUP 13-4953 (DENE0000744)) for the 4th generation nuclear energy, which made this work possible.

Notation

C_p	heat capacity of helium (J/ kg.K)
D	diameter of the riser channel (m)
g	acceleration gravity (m/s^2)
Gr_L	Grashof number, dimensionless, $\frac{g\beta(\bar{T}_s-\bar{T}_b)L^3}{\upsilon^2}$
h_{avg}	time-averaged local heat transfer coefficient (W/m^2.K)
h_i	local instantaneous heat transfer coefficient (W/m^2.K)
k	thermal conductivity of helium (W/m.K)
L	length of the riser channel (m)
N	number of data points

Nu_D	Nusselt number, dimensionless, $\frac{h_{avg} D}{k}$
Nu_L	Nusselt number, dimensionless, $\frac{h_{avg} L}{k}$
Pr	Prandtl number, dimensionless, $\frac{\mu c_p}{k}$
q_i	local instantaneous heat flux (W/m^2)
Ra_L	Rayleigh number, dimensionless, Gr_L Pr
T_s	channel inner Surface Temperature (K)
T_b	characteristic helium temperature (K)
T_f	radial temperature (K)
$\overline{T}_{film}$	average mean film temperature (K), $\frac{\overline{T}_S + \overline{T}_b}{2}$
$\overline{T}_S$	average value of channel inner surface temperature(K)
$\overline{T}_b$	average value of chracteritic helium temperature (K)
Z/L	dimensionless axial position

Greek Letters

α	thermal diffusivity (m^2/s)
β	volumetric expansion coefficient of helium (1/K)
μ	dynamic viscosity of the helium (kg.m/s)
υ	kinematic viscosity of helium (m^2/s)
ρ	density of helium (kg/m^3)

References

1. Aldridge RJ. Scaling Study of the Depressurized Conduction Cooldown Event in the High Temperature Test Facility Using RELAP5-3D/ATHENA. Oregon State University: Department of Nuclear Engineering and Radiation Health Physics, Oregon State University; 2013.

2. Castañeda JA. Scaling analysis of the OSU high temperature test facility during a pressurized conduction cooldown event using RELAP5-3D: Nuclear Engineering, Oregon State University; 2014.

3. Tung Y-H, Ferng Y-M, Johnson RW, Chieng C-C. Study of natural circulation in a VHTR after a LOFA using different turbulence models. Nuclear Engineering and Design. 2013;263:206-217.

4. Tung YH, Johnson RW, Ferng YM, Chieng CC. Modeling strategies to compute natural circulation using CFD in a VHTR after a LOFA. Nuclear Eng Design. 2014;275:80-90.

5. Tung Y-H, Ferng Y-M, Johnson RW, Chieng C-C. Transient LOFA computations for a VHTR using one-twelfth core flow models. Nucl Eng Des. 2016;301:89-100.

6. Valentin FI, Bindra H, Kawaji M. Natural circulation in HTGR type system with coolant channels in a simplified graphite-fuel matrix. Proc. of ANS Winter Meeting and Technology EXPO; 2013; Washington, D.C, Nov 10-14.

7. Schultz RR, Bayless PD, Johnson RW, McCreery GE, Taitano W, Wolf JR. Studies Related to the Oregon State University High Temperature Test Facility: Scaling, the Validation Matrix, and Similarities to the Modular High Temperature Gas-Cooled Reactor. Idaho National Lab 2010.

8. Haque H, Feltes W, Brinkman G. Thermal response of a modular high temperature reactor during passive cooldown under pressurized and depressurized conditions. Nucl Eng Des. 2006;236:475-484.

9. Simoneau JP, Champigny J, Mays B, Lommers L. Three-dimensional simulation of the coupled convective, conductive and radiative heat transfer during decay heat removal in an HTR. Nucl Eng Des. 2007;237:1923–1937.

10. Said IA, Taha MM, Usman S, Wood BG, Al-Dahhan MH. Investigation of natural convection heat transfer in a unique scaled-down dual-channel facility. AIChE Journal. 2017;63(1):387-396.

11. Kagumba MOO. Heat transfer and bubble dynamics in bubble and slurry bubble columns with internals for fischer-tropsch synthesis of clean alternative fuels and chemicals. Missouri University of Science and Technology: Chemical and Biochemical Engineering Department, Missouri University of Science and Technology; 2013.

12. Abdulmohsin RS, Al-Dahhan MH. Characteristics of convective heat transport in packed pebble-bed reactor, Nuclear Engineering and design, 2015;284:143-152.

13. Barnes JF. An experimental investigation on heat transfer from the inside surface of a hot smooth tube to air, helium, and carbon dioxide. Ministry of Aviation;1961.

14. Auletta A, Manca O. heat and fluid flow resulting from the chimney effect in asymmetrically heated vertical channel with adiabatic extension. Int J Thermal Sci. 2002;41:1101 – 1111.

15. Manca O, Musto M, Naso V. Experimental analysis of asymmetrically heated vertical channel with an asymmetric chimney. J Heat Transf 2005;127:888-896.

16. Petersen H. The Properties of Helium: Density, Specific Heats, Viscosity, and Thermal Conductivity at Pressure from 1 to 100 bars from Room Temperature to 1800 K. Danish Atomic Energy Commission Research Establishment Riso Report No. 224;1970.

17. Cengel YA. Heat transfer a practical approach. Mc-Graw Hill Company; 2004.

18. Mohammed HA, Salaman YK. Heat transfer by natural convection from a uniformly heated vertical circular pipe with different entry restriction configuration. Energy Conversion and Management. 2007;48:2244-2253.

19. Incropera FP, Dewitt DP. Fundamentals of heat and mass transfer. 5 th ed. New York, USA: John Wiley & Sons Inc.; 2003.

20. Holman JP. Heat Transfer. 10th ed: McGraw-Hill; 2010.

21. Salman YK, Mohammed HA. The effect of restriction shape on laminar natural convection heat transfer in a vertical circular tube. Al-Khwarizmi Engineering Journal. 2005;1:83-100.

22. Mohammed HA, Salman YK. Laminar air flow free convection heat transfer inside a vertical circular pipe with different inlet configuration. Thermal Science. 2007;11(1):43-63.

List of Tables

List of Figures

Table 1. The available literature correlations

Author	Correlation	Conditions of correlation
Yunus [17]	$Nu_L = 0.59\ Ra_L^{0.25}$	• A vertical tube open at both ends without restriction. • Isoflux thermal configuration. • Air (atmospheric pressure).
Mohamed and Salman [18]	$Nu_L = 1.248\ Ra_L^{0.23}$	• A vertical tube opens at both ends with tube restriction at the entry. • Isoflux thermal configuration. • Air (atmospheric pressure).

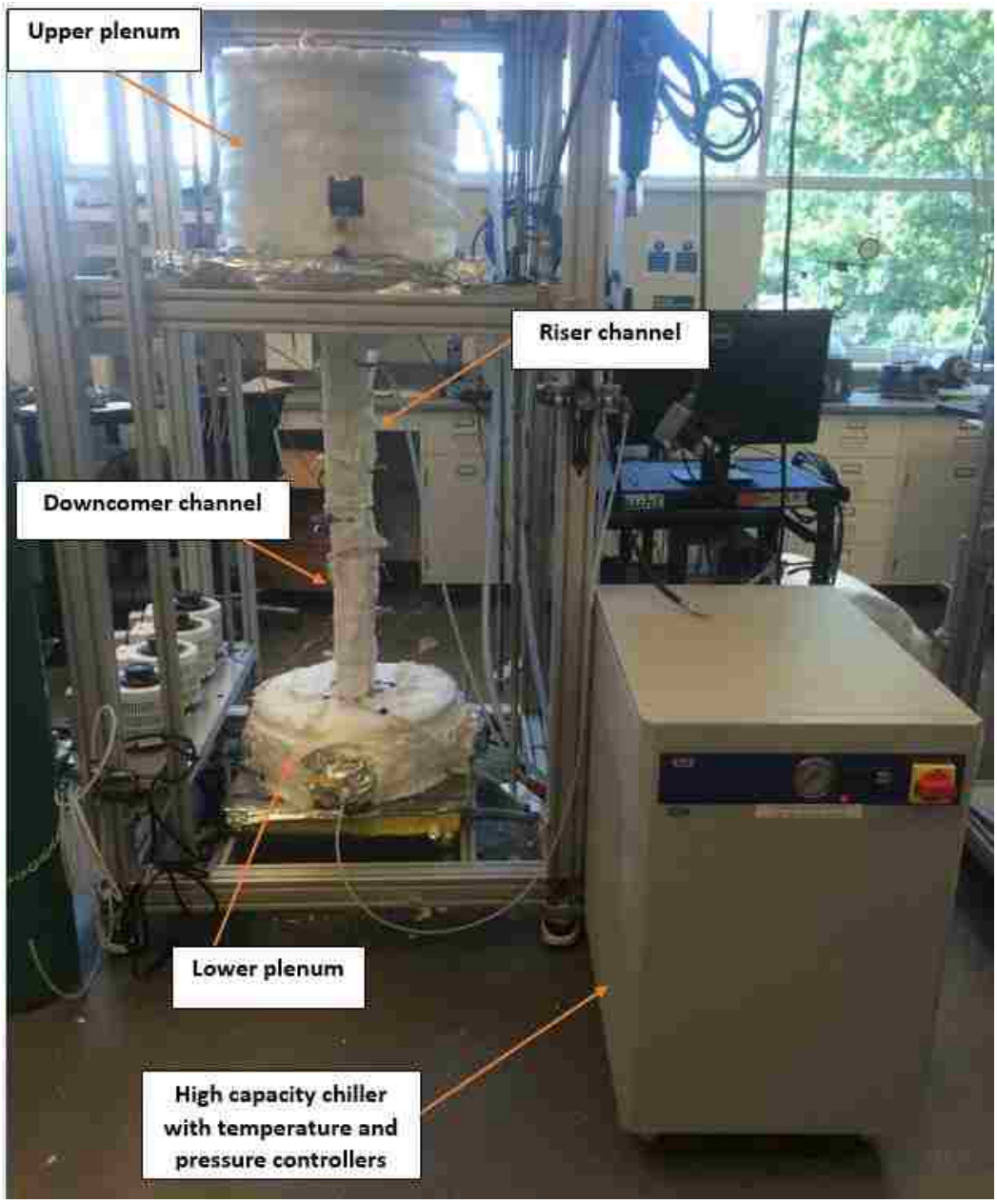

Fig. 1. Physical picture of the mReal dual-channel natural circulation loop.

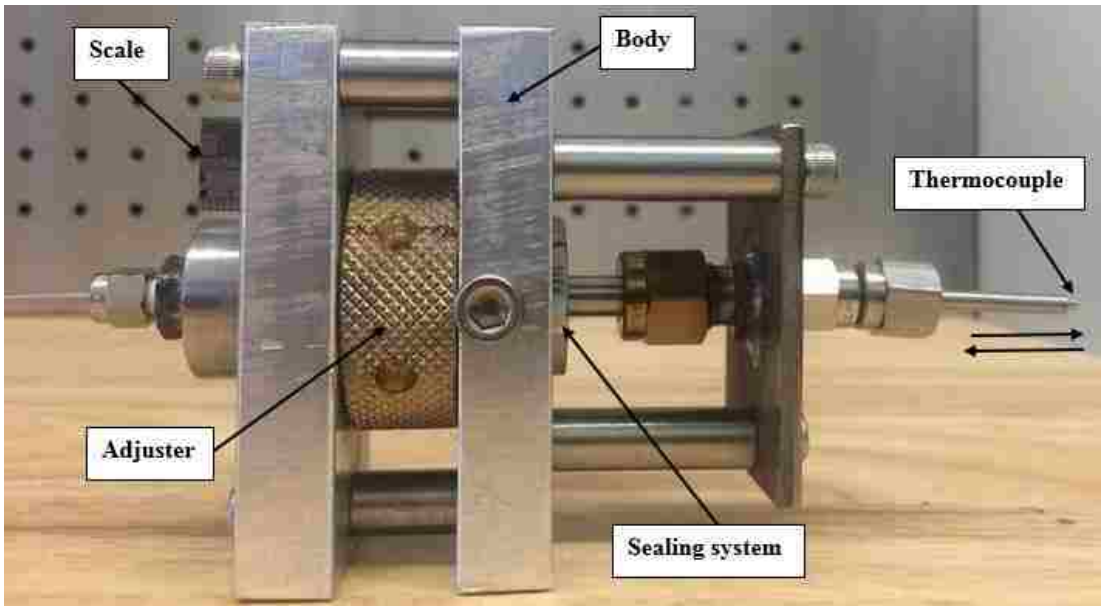

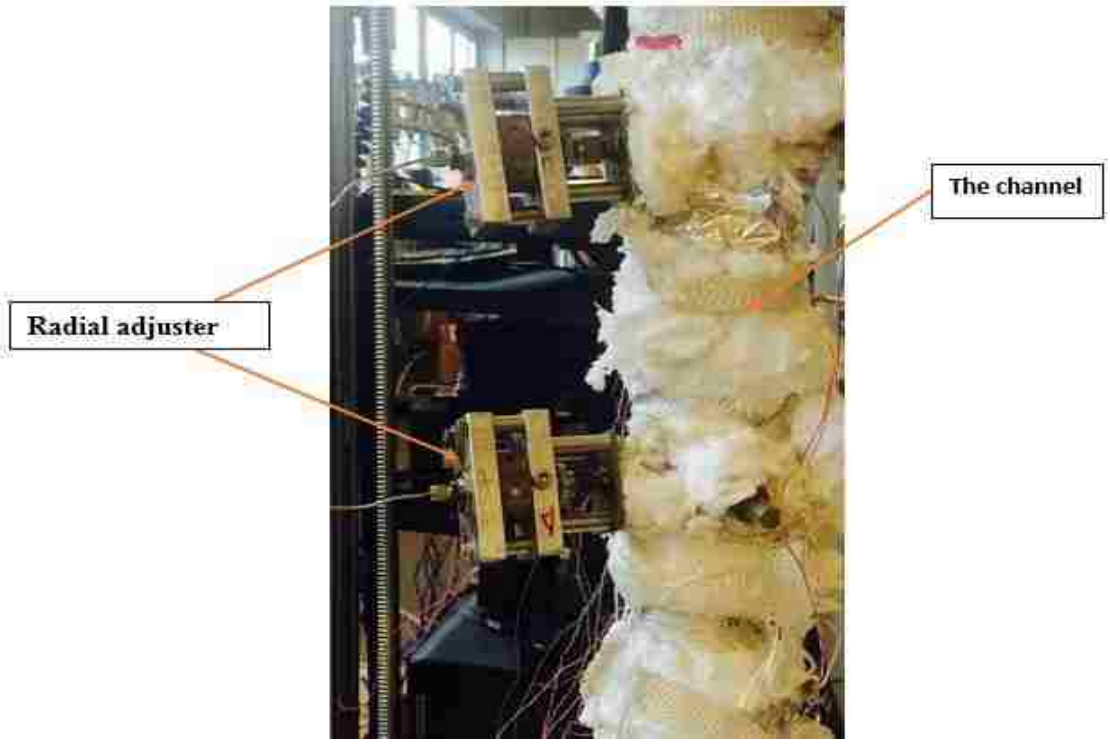

Fig. 2. Physical picture for the radial adjuster for the temperature measurement using T-thermocouple.

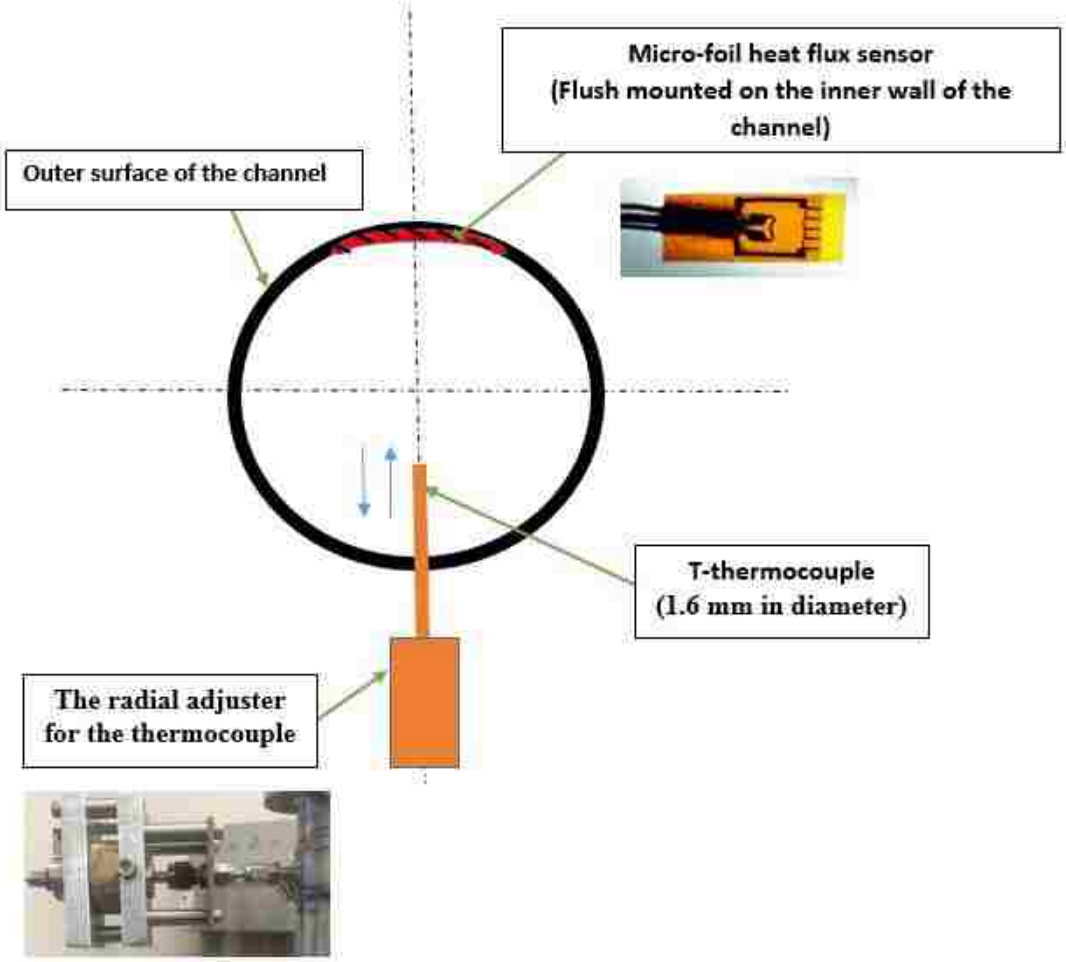

Fig.3. Schematic diagram for the mounting of the measurement techniques (cross-sectional view) of the radial temperature adjuster for T-thermocouple and heat transfer probe.

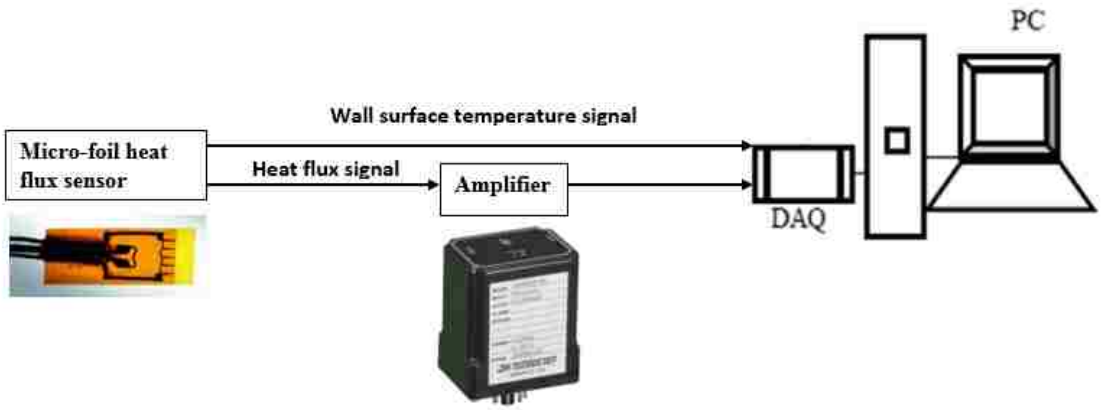

Fig. 4. The sequence of the signals collection from the micro-foil heat flux sensor to the data acquisition system.

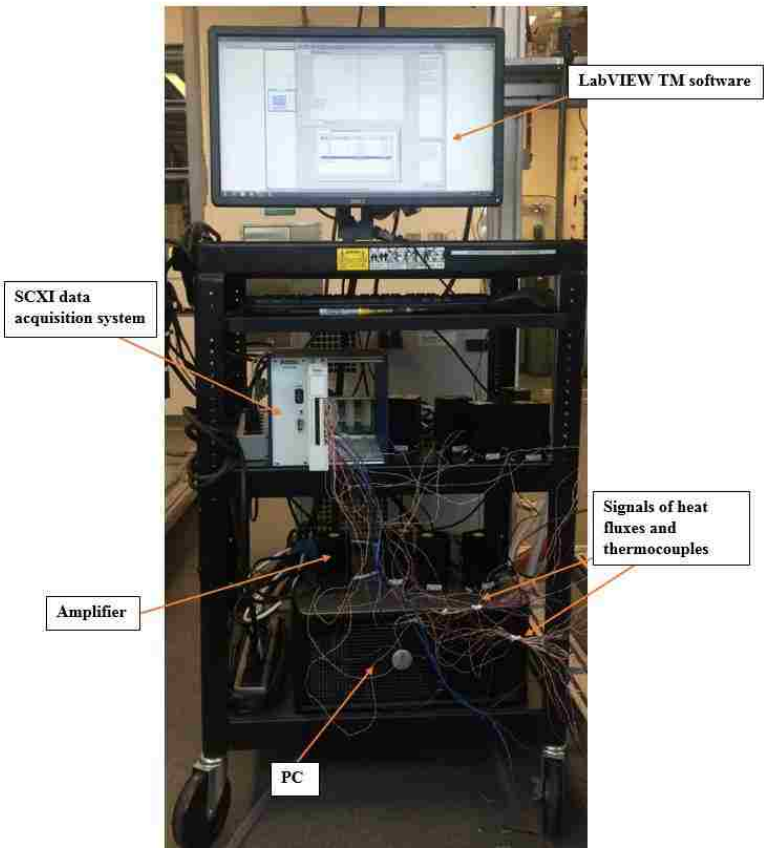

Fig. 5. Data acquisition system and the monitoring station.

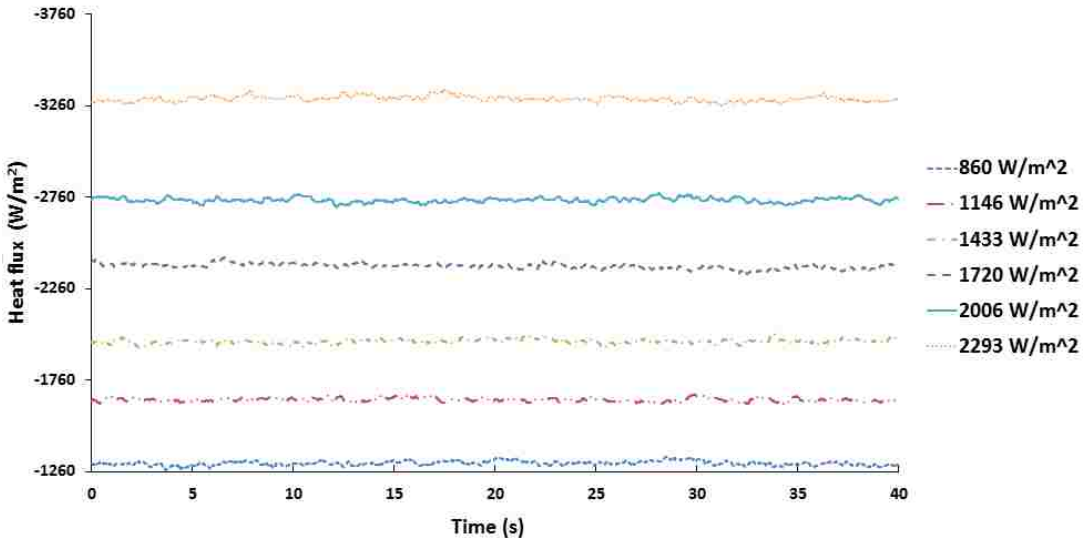

Fig. 6. Distribution of the heat fluxes close to the exit of the riser channel (Z/L = 0.956).

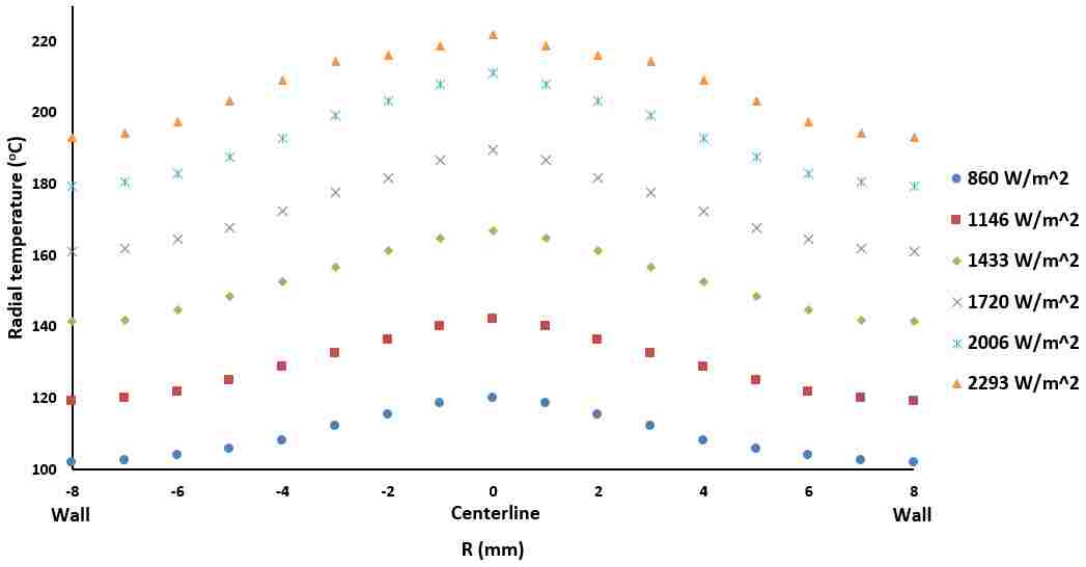

Fig. 7. Radial distribution of helium temperature close to the exit of the riser channel (Z/L = 0.956).

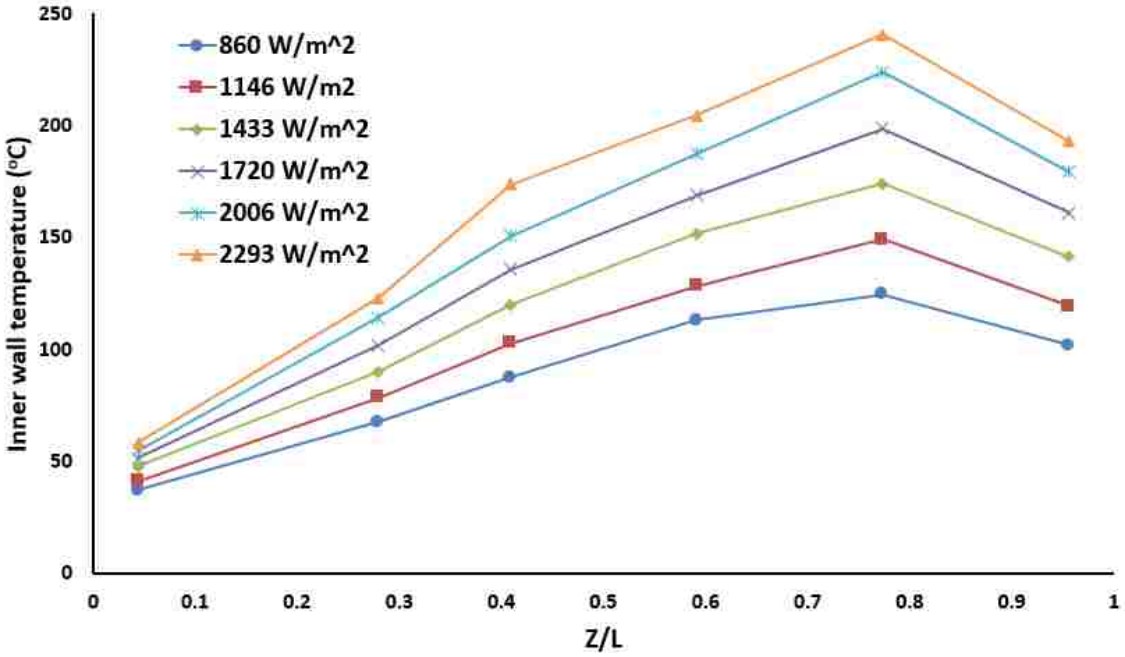

Fig. 8. Axial distribution of the inner wall surface temperature along the riser channel.

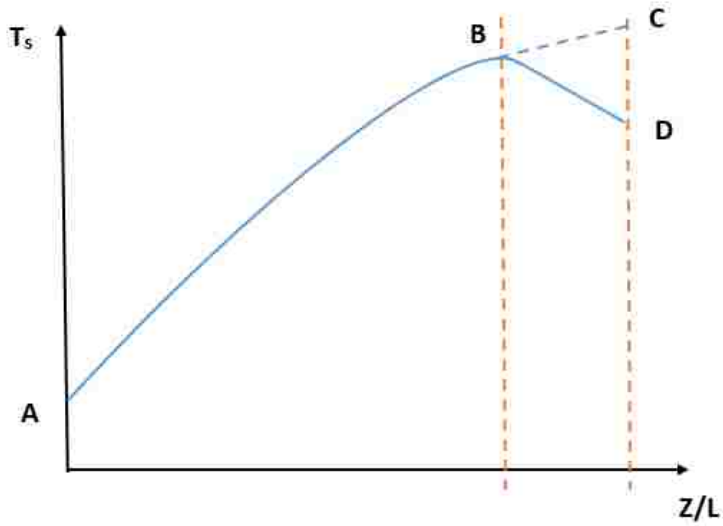

Fig. 9. Variation of the inner surface temperature versus the axial distance along the riser channel.

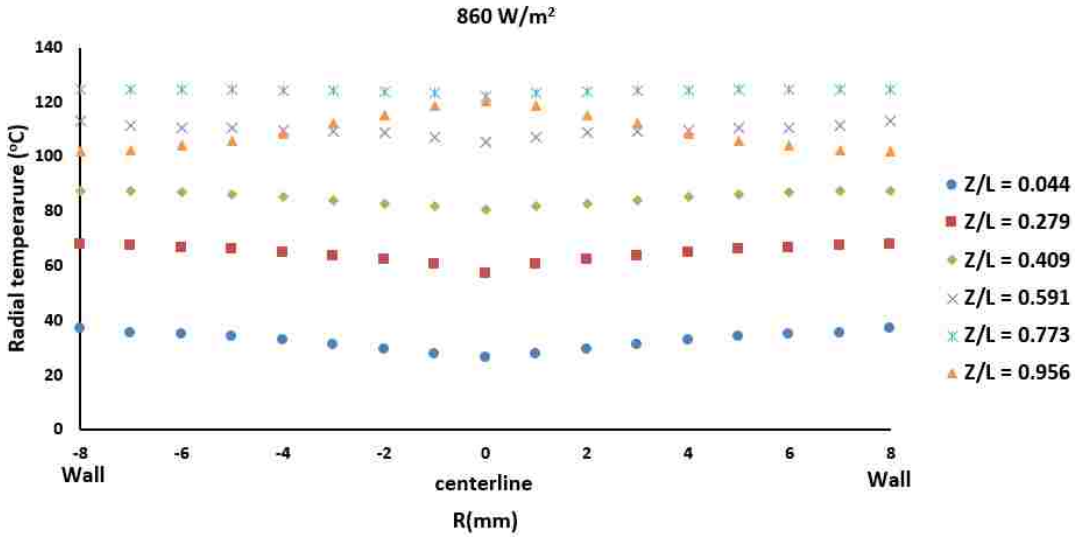

Fig. 10. Radial temperature distribution for helium at 860 W/m^2 along the riser channel.

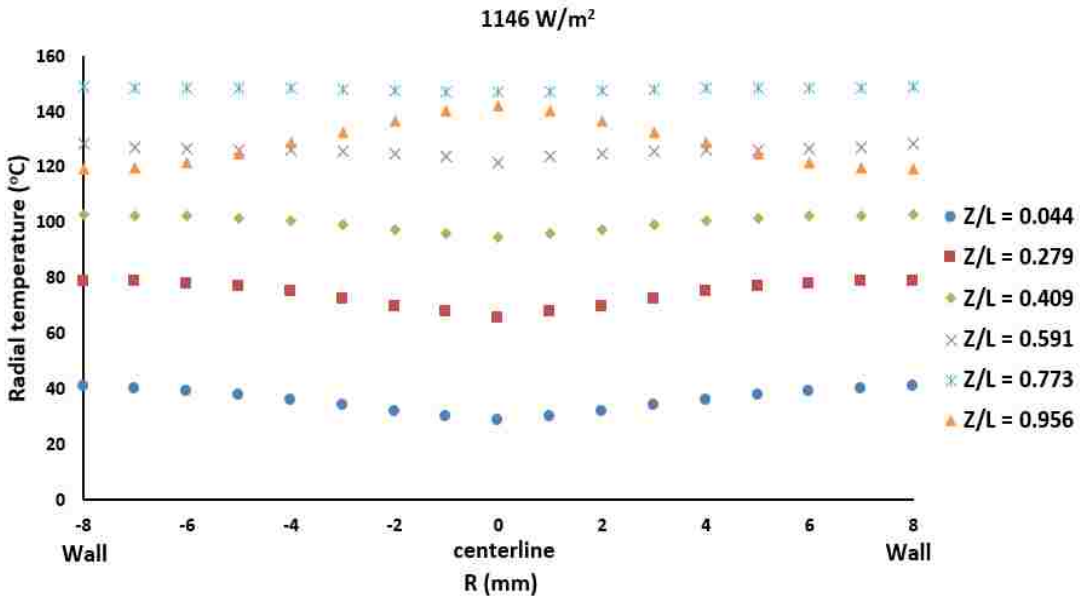

Fig. 11. Radial temperature distribution for helium at 1146 W/m^2 along the riser channel.

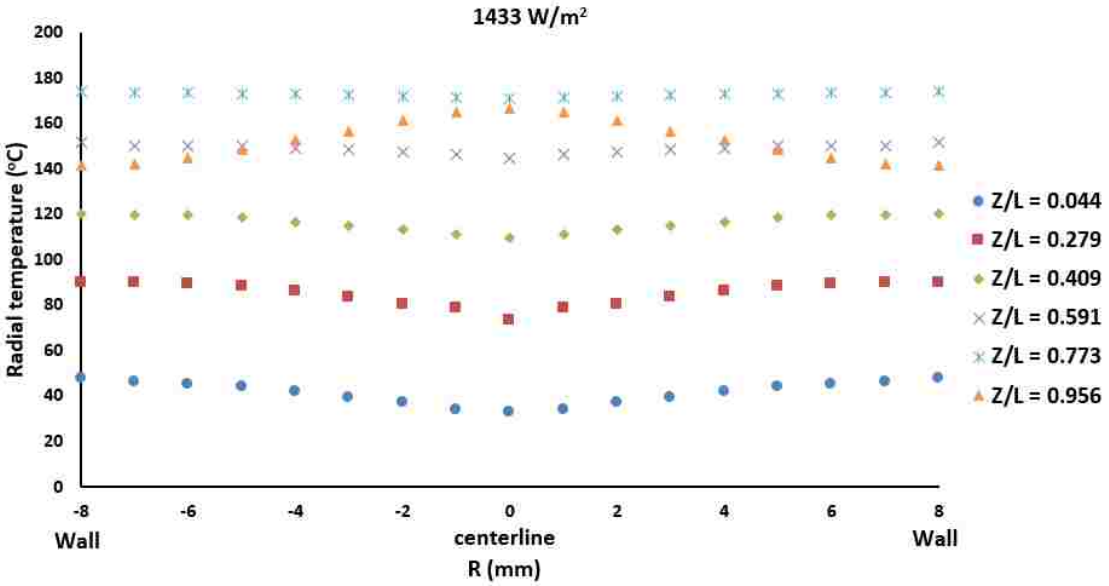

Fig. 12. Radial temperature distribution for helium at 1433 W/m^2 along the riser channel.

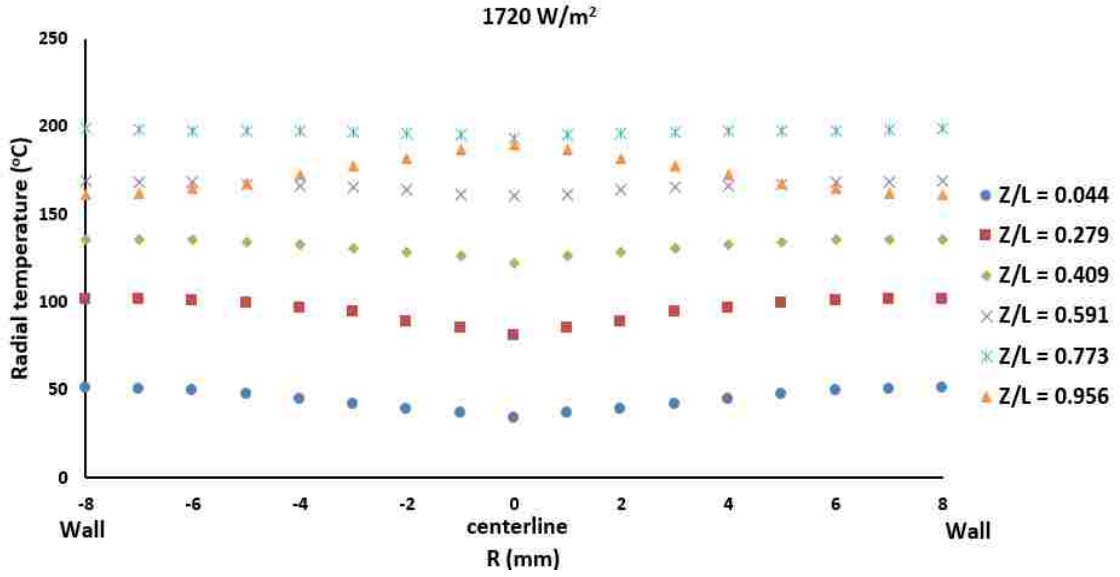

Fig. 13. Radial temperature distribution for helium at 1720 W/m^2 along the riser channel.

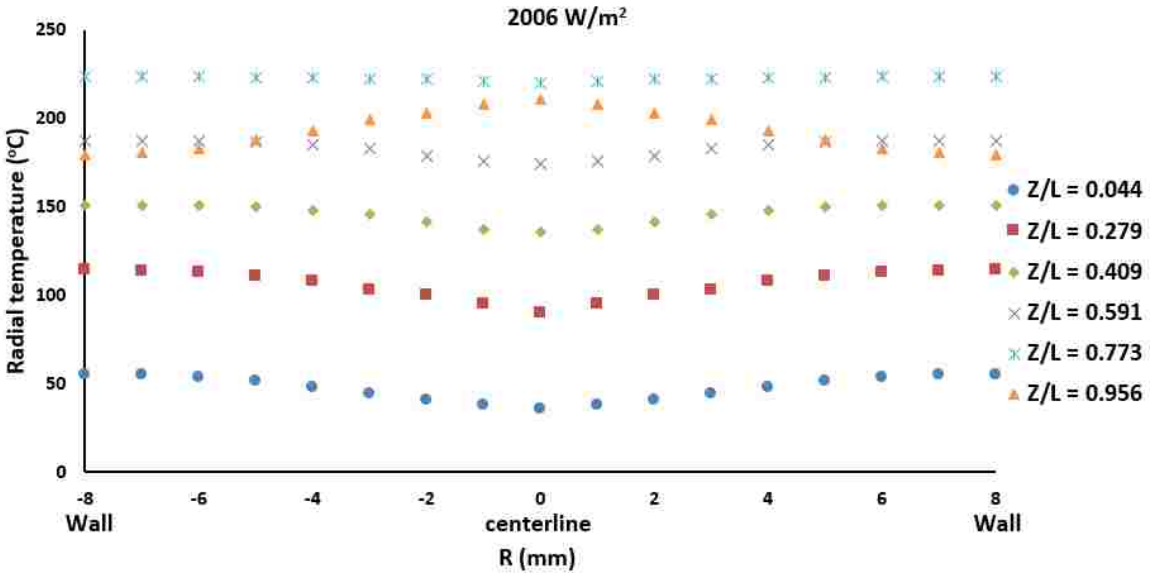

Fig. 14. Radial temperature distribution for helium at 2006 W/m^2 along the riser channel.

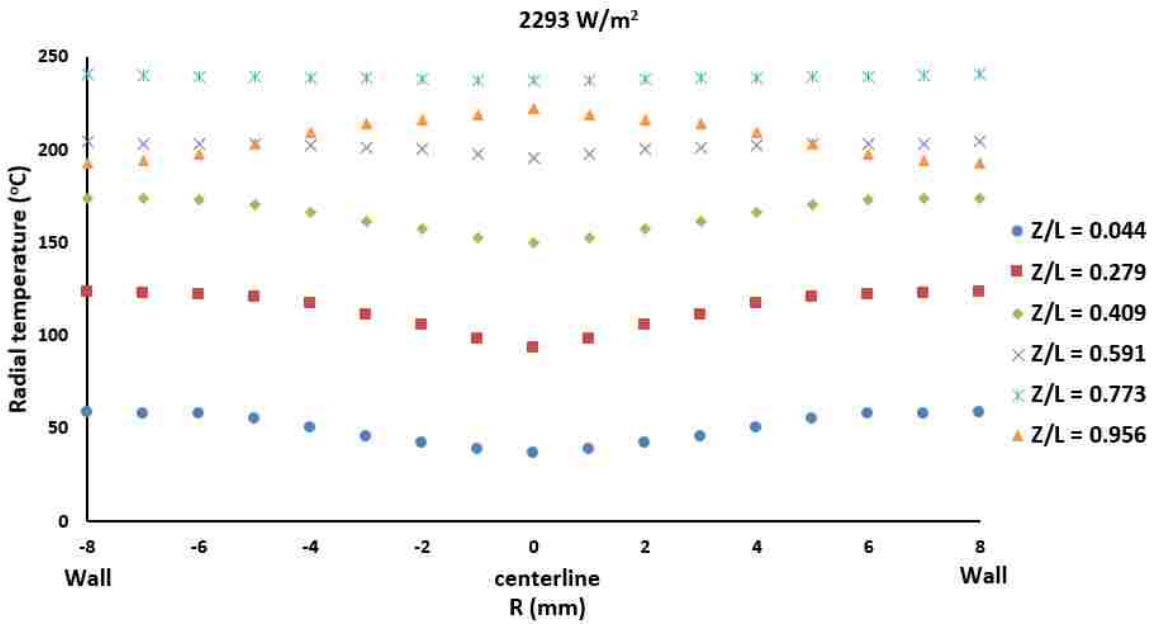

Fig. 15. Radial temperature distribution for helium at 2293 W/m^2 along the riser channel

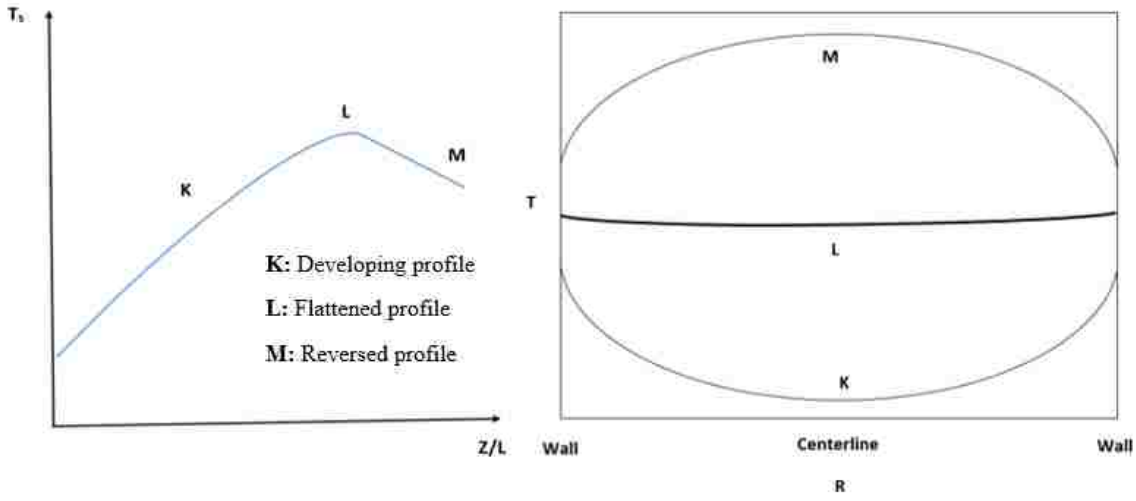

Fig. 16. Effects of the axial inner wall surface temperature on the helium radial temperature profiles along the riser channel.

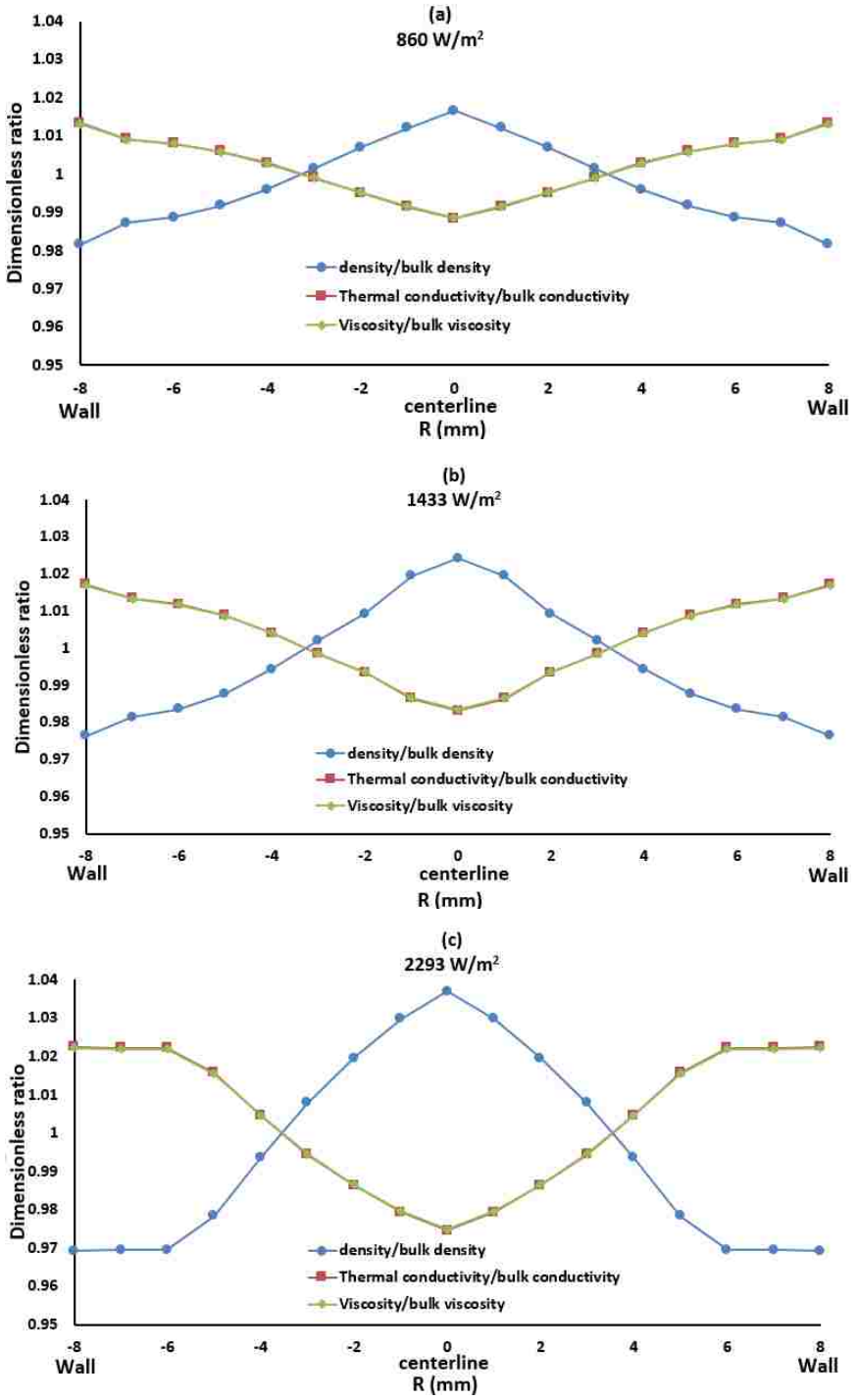

Fig. 17. Radial distribution of the physical properties at Z/L = 0.044 for different heat fluxes: (a) 860 W/m^2, (b) 1433 W/m^2, and (c) 2293 W/m^2 along the riser channel.

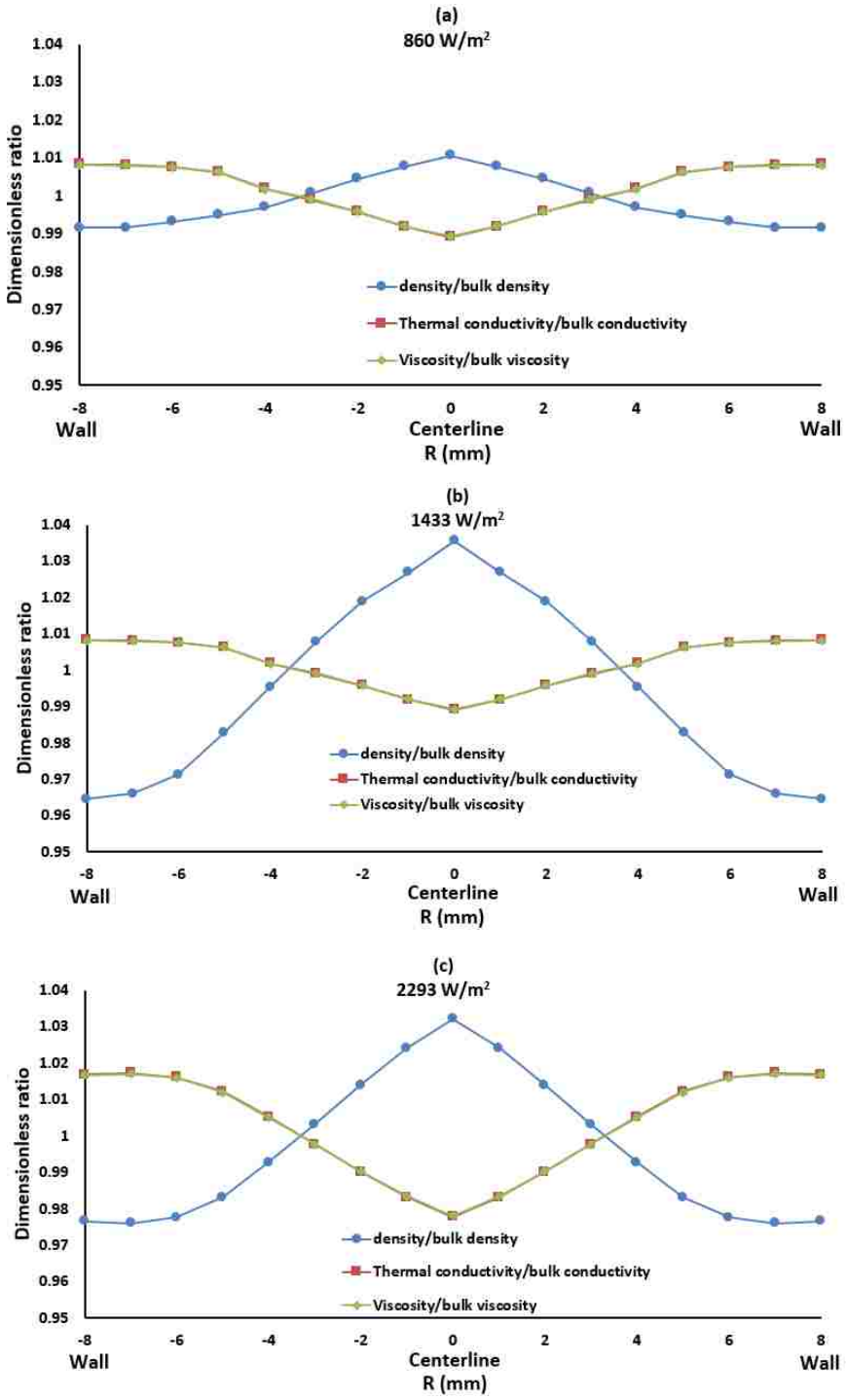

Fig. 18. Radial distribution of the physical properties at Z/L = 0.409 for different heat fluxes: (a) 860 W/m^2, (b) 1433 W/m^2, and (c) 2293 W/m^2 along the riser channel.

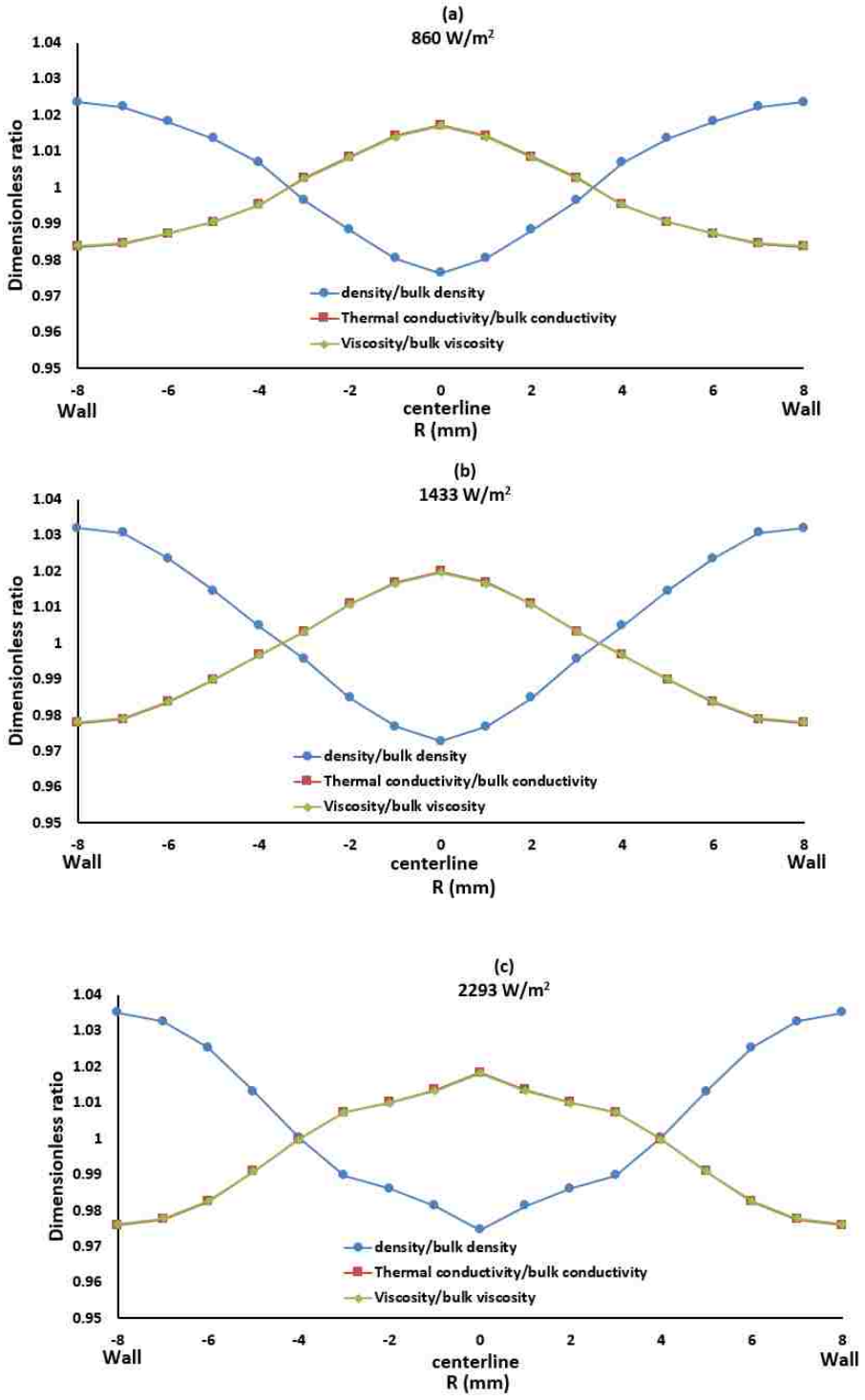

Fig. 19. Radial distribution of the physical properties at Z/L = 0.956 for different heat fluxes: (a) 860 W/m^2, (b) 1433 W/m^2, and (c) 2293 W/m^2 along the riser channel.

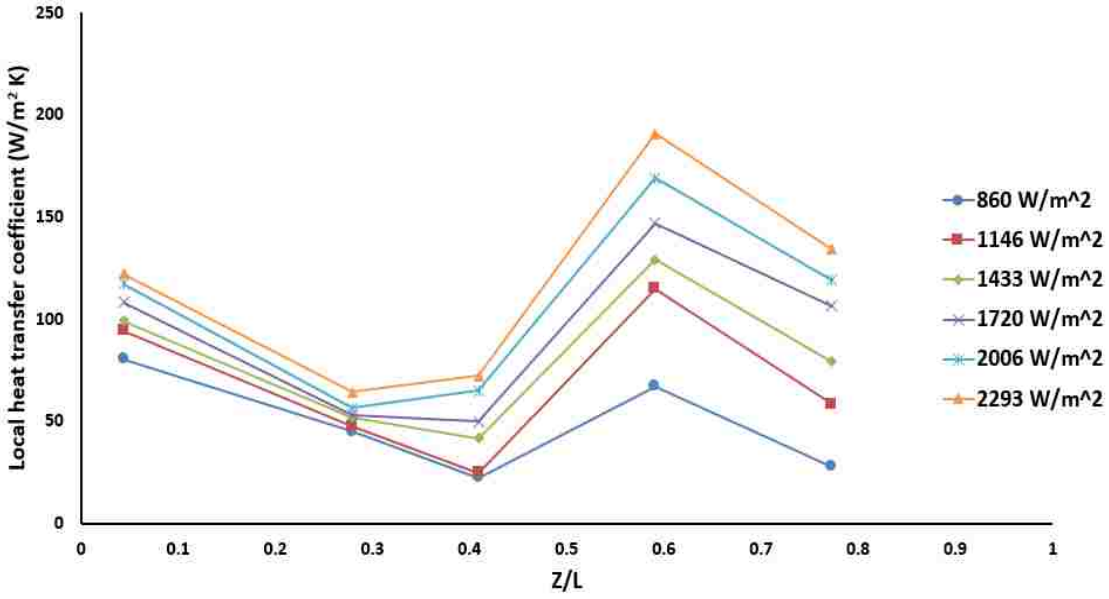

Fig. 20. Axial distribution of the local heat transfer coefficient for the riser channel.

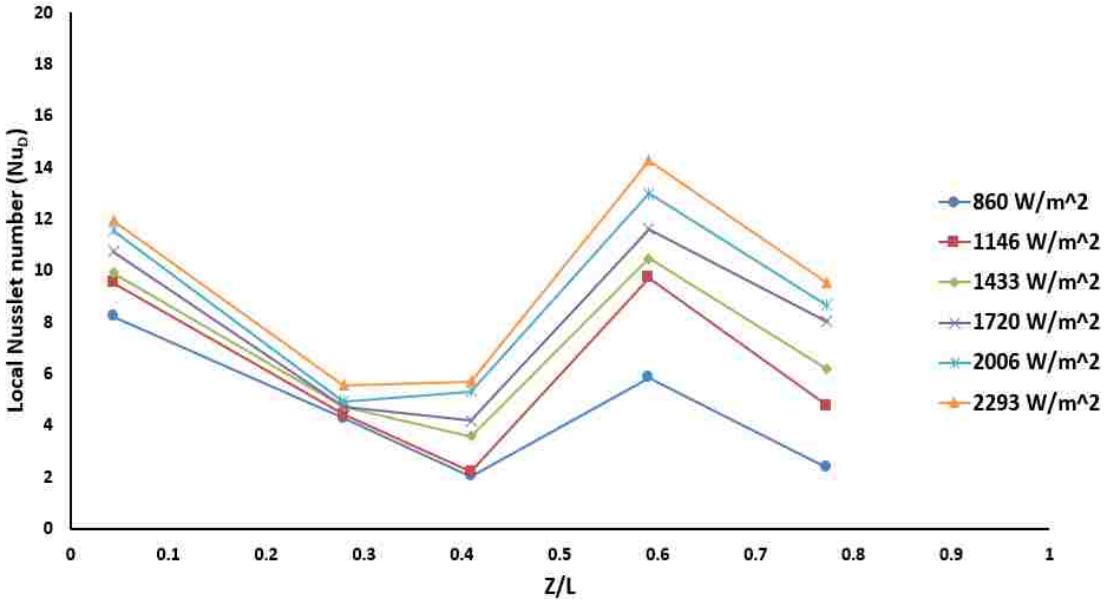

Fig. 21. Axial distribution of the local Nusselt number for the riser channel.

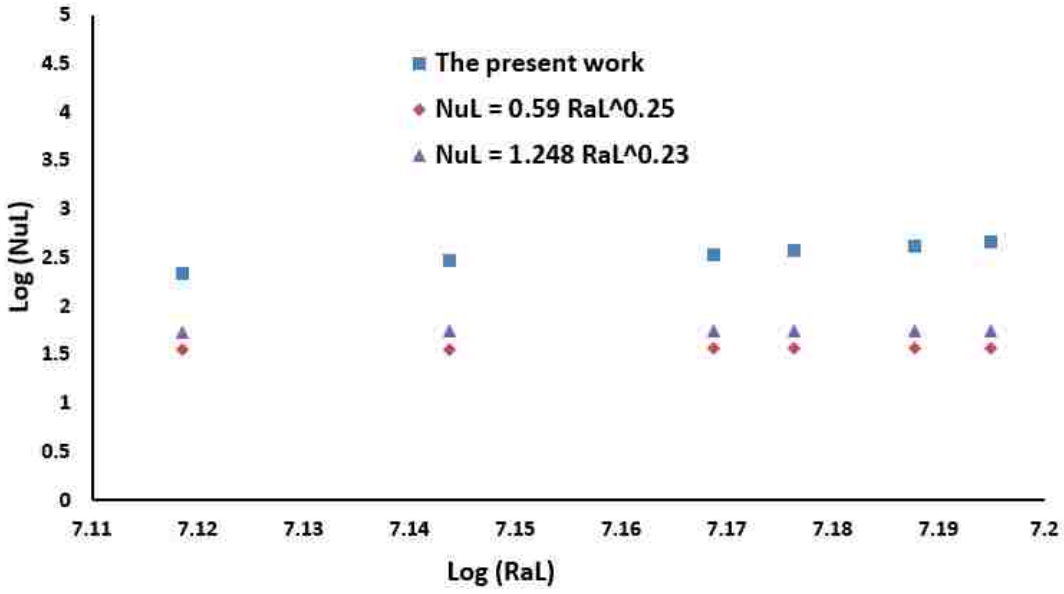

Fig. 22. Comparison of the present work in terms of Nu_L and Ra_L with the literature correlations.

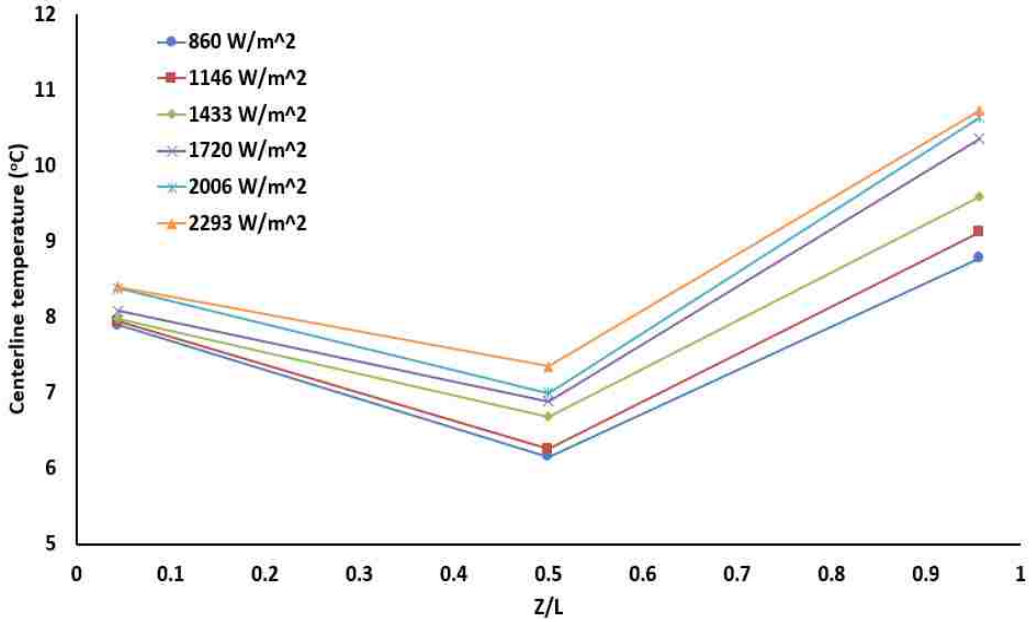

Fig. 23. Axial distribution of the centerline's helium temperature along the downcomer channel.

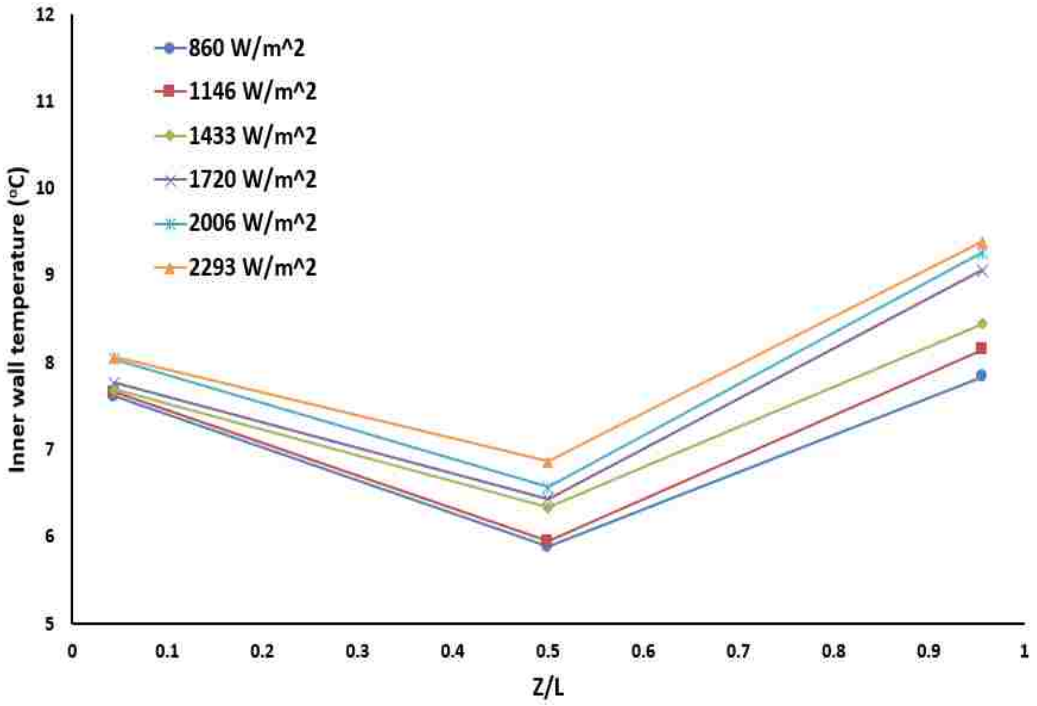

Fig. 24. Axial distribution of the inner wall surface temperature along the downcomer channel.

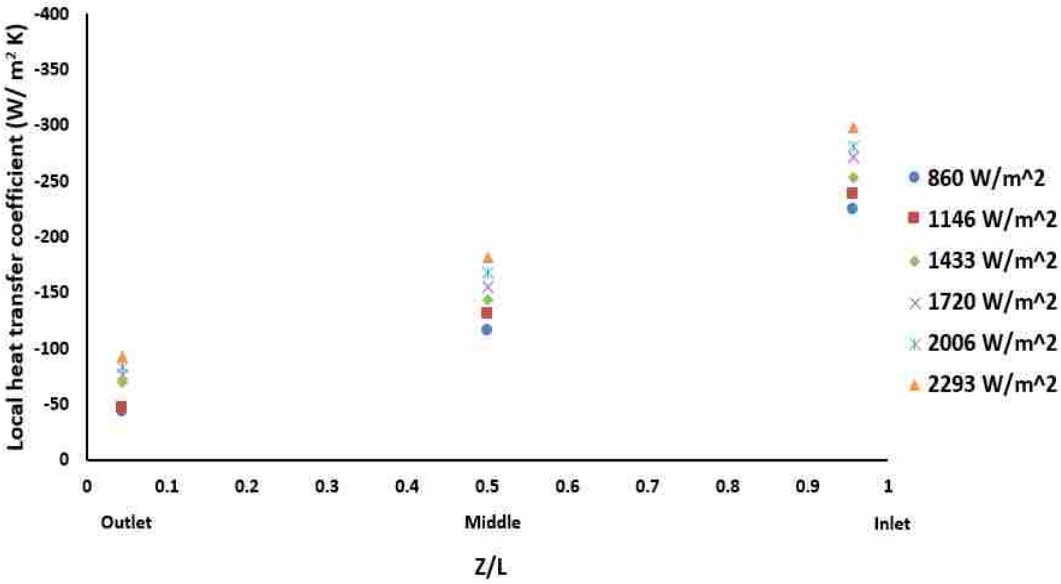

Fig. 25. Axial distribution of the local heat transfer coefficients along the downcomer channel

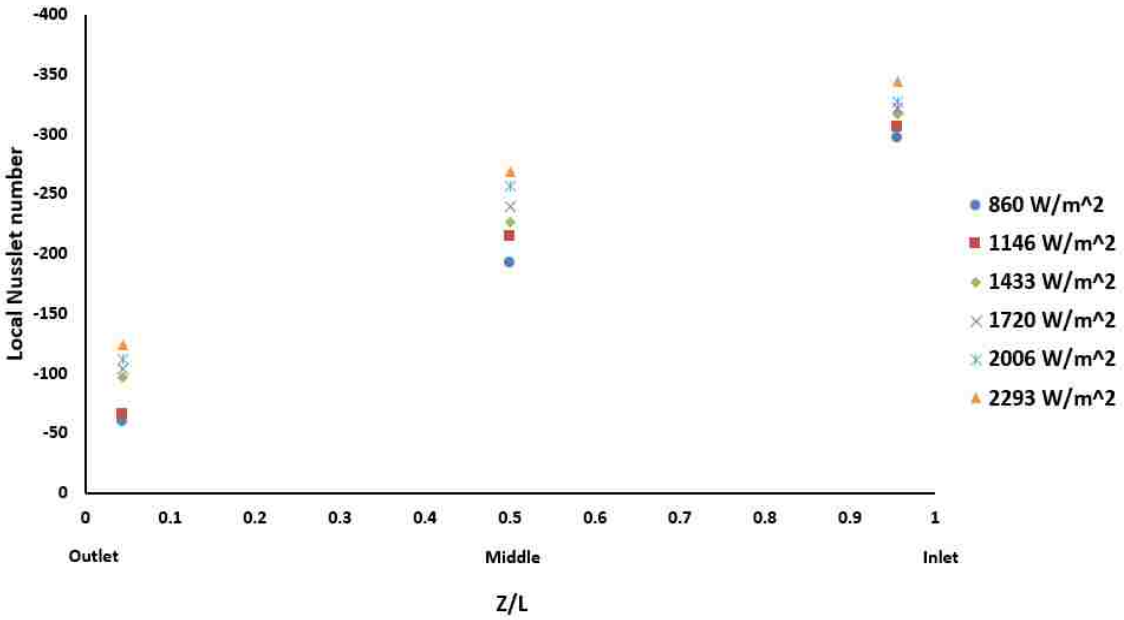

Fig. 26. Axial distribution of the local Nusselt number along the downcomer channel.

III. EXPERIMENTAL STUDY OF THE EFFECT OF HELIUM PRESSURE ON THE NATURAL CONVECTION HEAT TRANSFER IN A PRISMATIC DUAL-CHANNEL CIRCULATION LOOP

Ibrahim A. Said [1,3], Mahmoud M. Taha [1,3], S. Usman [2]*, M. H. Al-Dahhan [1,2]

[1] Multiphase Reactors Engineering and Applications Laboratory (mReal), Chemical and Biochemical Engineering Department, Missouri University of Science and Technology, Rolla, MO, 65409, USA

[2] Mining and Nuclear Engineering Department, Missouri University of Science and Technology, Rolla, MO, 65409-0170, USA

[3] Chemical Engineering Department, Faculty of Engineering, Alexandria University, Alexandria, Egypt

* *Corresponding author: usmans@mst.edu*

Abstract

The effects of helium pressure on the convection heat transfer coefficient and temperature fields (helium and wall surface temperatures) in a unique scaled-down dual-channel natural circulation loop with upper and lower plena have been investigated in this study. Natural convection is one of the passive safety systems of the prismatic very high-temperature reactors (VHTRs) during the accident scenarios. The operating helium pressure was varied from 413.47 to 689.12 kPa in the temperature range from 6 to 196 ^{o}C. Radial and axial measurements were carried out along the flow channels using a new sophisticated flush wall-mounted heat transfer coefficient probe in conjunction with the

radial adjuster for T-thermocouple that are integrated in a novel way to characterize natural convection heat transfer in terms of heat transfer coefficient, Nusselt number, helium temperature, and wall surface temperature. The obtained experimental results along the flow channels showed the dependence of natural convection on the system's pressure in which the Rayleigh number is proportional to the square of the helium pressure ($Ra \propto P^2$). Also, it was found that upon increasing the helium pressure from 413.47 to 689.12 kPa, the heat transfer coefficient and Nusselt number are increased by 30% and 35%, respectively. Moreover, the wall surface temperature along the downcomer and riser channels are decreased by 12.7% and 18% with increasing the helium pressure from 413.47 to 689.12 kPa, respectively.

Keywords: Helium pressure; natural circulation loop; prismatic very high-temperature reactors (VHTRs); accident scenarios; heat transfer coefficient probe

1. Introduction

Investigations of natural convection heat transfer and flow dynamics in different geometries and operating conditions have been the focus of many past and current studies by several authors. Natural convection has received significant attention from researchers due to its presence in nature and engineering applications. In nuclear reactors, natural convection is being implemented as an engineered feature to achieve passive safety [1,2]. Natural convection is one of the main passive safety phenomena in the prismatic very high-temperature reactors (VHTRs) cooled by gas helium for a safeguard under the loss of flow accidents (LOFA) [3]. In the event of the failure of the gas circulator, LOFA, the driving pressure drop force across the reactor core will decrease to zero. Subsequently, the natural circulation due to density differences will be established to remove the decay heat from the core. Also, during the LOFA scenario, the coolant flows direction is reversed, and there are two different possibilities for flow direction that may occur inside the flow channels in the core due to large temperature variation. For the heated sections of the core, the coolant would flow upward, while in the relatively cooled section, the coolant would flow downward, establishing the natural circulation loop due to buoyancy force. The coolant channels with upward flow act as riser channels, while the coolant channels with downward flow act as downcomer channels. Natural convection currents by helium plumes transport the decay heat from the reactor core to the reactor cavity cooling system, and it prevents the core from possible meltdown and localized hot spots. There are many parameters affecting the rate of natural convection heat transfer, and consideration of each in a representative geometry can enhance one's knowledge about the phenomenon. Most reactor safety analyses and related natural convection studies are

conducted using standard computational fluid dynamics (CFD) codes combined with heat transfer computations such as CFD-STAR-CCM+, and CFD-Fluent and thermal hydraulic codes such as RELAP5-3D that can provide crucial details of heat transfer data. There are extensive computational studies of natural circulation in the prismatic very high-temperature reactor (VHTRs) that have been reported in the open literature [1,3-8]. However, the thermal hydraulic codes used for these studies involve approximations in the obtained results because of the inexact nature of turbulence models that are used, assumptions used in the describing governing equations such as the Boussinesq approximation, nature of discretization required and so forth. Despite many numerical and experimental studies available on natural convection heat transfer in the open literature [9-21], little consideration is given to the effect of operating pressure variation on the flow field, heat transfer coefficient, and temperature profile [22-26]. Furthermore, the previous studies were carried out in simple geometries with limited measurement techniques and can not be extended for complex reactor geometries. Therefore, the Multiphase Reactors Engineering and Applications Laboratory (mReal) research team at Missouri S&T developed a unique scaled-down separate effect experimental facility of two flow channels[27]. The mReal research team developed a new integrated noninvasive heat flux sensors and radial temperature adjusters for the T-thermocouple sensor (1.6 mm in diameter) in a novel way to measure axially and radially heat transfer coefficient and the corresponding temperatures along the flow channels. Design features of the facility is discussed in details elsewhere[27]. Several experimental measurements were executed on the nature convection for a loop of two flow channels (riser and downcomer channels) with upper and lower plena under different helium pressures (413.47, 482.38, 551.29,

620.20, and 689.12 kPa). Therefore, the main objective of the current work is to experimentally investigate the phenomenon of the natural convection in terms of heat transfer coefficients, Nusselt number and temperature fields (gas and wall surface temperatures) at different operating pressures with helium as a working fluid using the newly developed facility and the novel techniques.

Under these operating conditions, the variation of natural convection coefficients and the axial and radial temperature fields along the riser and downcomer channels have been studied. The obtained knowledge and benchmarking data can be valuable for detailed validation of thermal hydraulic codes and CFD codes integrated with the heat transfer computations. Though this work only uses two channels for coolant flow, the study can be extended to multiple channels and different working fluid.

2. Experimental setup

The experimental setup is a scaled down separate effects facility fabricated using stainless steel alloy to handle high temperature and pressure. Figures 1-2 show a physical picture and schematic diagram of the experimental setup[27]. This setup is capable of simulating accident scenarios for thermal hydraulics phenomena in prismatic very high-temperature reactors (VHTRs). It consists of two plena (i.e., upper and lower plena) with two channels for coolant flow in the reactor core. The two channels mimic the upward and downward flows inside the reactor core in the case of loss of flow accidents (LOFA). In particular, the interest is to model pressurized conduction cooldown scenario (PCC). The inside diameter of the flow channels is kept constant at 16 mm, while the height of the channels was 1 m, representing five prismatic blocks. The upward flow in the riser channel,

for reactor core, is simulated by electrically heating the riser channel by four heavily insulated Duo-Tape electrical heaters (50.8 x 609.6 mm) with a maximum wattage capacity of 312 watts at 120 V. Each electrical heater is individually connected to a variable voltage regulator with a digital power reader to control the magnitude of wattage supplied to the riser channel. The downward flow in the downcomer channel is mimicked by executing cooling for the outer surface of the channel. A helical coil heat exchanger is implemented around the downcomer channel to cool the surface and initiate the downward flow. Also, the outer surface of the upper plenum is equipped with a cooling jacket to keep the outer surface temperature of the upper plenum at a constant value. An automatic chiller (Applied Thermal Control Ltd, K4 chiller) with temperature and pressure controllers has been used to provide chilled water at the desired temperature to the cooling jacket and helical coil heat exchanger for downcomer. The difference between the inlet and outlet of chilled water across the cooling jacket and heat exchanger always turns out to be less than 1.5 K. Hence; the constant wall surface temperature can be assumed as a thermal boundary condition for the downcomer channel and upper plenum. The lower plenum walls are maintained at adiabatic conditions by using thick ceramic fiber blanket. To reduce the heat losses to the environment, the whole setup is thermally insulated by a ceramic fiber blanket, as shown in Figure 1. Further detailed explanation of the experimental setup in conjunction with design considerations can be found elsewhere [27].

3. Measurement techniques

3.1 Radial temperature sensor adjuster

A radial temperature sensor adjuster for T-thermocouple has been designed and developed in-house to measure radial temperature variation of the coolant (helium) along the flow channels (riser and downcomer) for different axial locations. This radial temperature adjuster is used to adjust the radial location of the T-thermocouple sensor (1.6 mm in diameter with a time response of 4 seconds) along the flow channels (Figure 3). Also, Figure 4 shows a schematic diagram of the radial positions of the T-thermocouple sensor for a given axial location. Eight radial measurements of helium temperature with a step size of 1 mm have been performed. It is worth mentioning that the radial sensor adjuster is speficially designed and constructed for this application and can withstand high temperature and pressure up to 300 ^{o}C and 1.03 x 10^{6} Pa, respectively.

3.2 Noninvasive flush wall mounted heat transfer coefficient probe

A new noninvasive heat transfer coeficient probe has been designed, developed, tested, and implemented as an integrated part of the channels. The current probe consists of the micro-foil heat flux sensor ($6.35x10^{-3}$ m x $1.78x10^{-2}$ m x $8x10^{-5}$ m) from RDF Corporation (model no. 27036-1). This new fast-response sensor has been used to measure reliably the heat flux and surface temperature in single and multiphase flow systems [27,28] . By measuring simultaneously the local instantaneous heat flux between the surface of the sensor and the flowing fluid, the surface temperature of the sensor, and the flowing gas temperature, the heat transfer coefficient can be obtained. The measured instantaneous heat flux (q_i), surface temperature ($T_{s,i}$), and characteristic fluid

temperature ($T_{b,i}$) can be used as per Equations 1-2 to estimate the local instantaneous heat transfer coefficients (h_i) and the local time-averaged heat transfer coefficients (h_{avg}):

$$h_i = \frac{q_i}{(T_{s,i} - T_{b,i})} \quad (1)$$

$$h_{avg} = \frac{1}{N} \sum_{i=1}^{i=N} h_i \quad (2)$$

The sampling time is 40 seconds at sampling rate 50 Hz to collect 2000 data points in order to achieve a high stable value of the estimated heat transfer coefficients for the experimental conditions. The characteristic fluid temperature ($T_{b,i}$) for the riser channel is measured for a given axial location by averaging eight radial values of helium temperature ($T_{f\,i,j}$) with a step size of 1 mm (1/16 of the inside diameter):

$$T_{b,i} = \frac{1}{8} \sum_{j=1}^{j=8} T_{f\,i,j}. \quad (3)$$

For the downcomer channel, the characteristic fluid temperature ($T_{b,i}$) is the centerline's helium temperature. For the downcomer, there was only slight variation in the measured radial helium temperatures for any given axial location. Based on experiments that were conducted in the downcomer channel, only 2 K or less radial tempertaure variations were observed. Hence, centerline's helium temperature was used as the characteristic fluid temperature for the downcomer channel.

It is worth mentioning that the sophisticated heat flux sensor has the capability to detect the direction of heat transfer between the surface of foil sensor and the flowing fluid. Negative heat flux signals mean that heat transfers from the flowing fluid to the surface of foil sensor while positive heat flux signals imply that heat transfers from the surface of

foil sensor to the flowing fluid. The heat flux foil sensor is flush mounted on the inner surface of the flow channels using high-temperature glue. Hence, the micro-foil sensor is considered a noninvasive technique. Six non-dimensional axial locations along the riser channel (Y/H= 0.044, 0.279, 0.409, 0.591, 0.773, 0.956 (end effect)) and three non-dimensional axial locations along the downcomer channel (Y/H= 0.044, 0.5, 0.956) are used in the current work to simultaneously measure the heat flux and the surface temperature using the flush wall mounted heat transfer probe and the flowing gas radial temperature using the thermocouple adjuster. These positions are used to measure these parameters during steady-state conditions. One can remark that the number of axial locations in the downcomer channel is less than the riser channel due to low variation in the measured heat transfer coefficients and the flowing gas temperatures by performing experiments to assess such variations.

3.3 Data acquisition (DAQ) system

The data acquisition system of the national instrument terminal block (NI SCXI-1303), SCXI module, SCXI combination chassis with the controller, and chassis power card in conjunction with nine amplifiers and a personal computer were used for the data collection and reduction (Figure 5). The data acquisition and post-processing are executed using LabVIEW software and MATLAB. It is worth mentioning that the measured heat flux signals from the foil sensors, in the range of microvolts, need to be amplified before sending these to the data acquisition system (DAQ). Afterwards, the amplified signals of heat flux in conjunction with the signals of temperatures from the thermocouples are sampled for over 40 seconds at a sampling rate of 50 Hz. The

sampling rate of 50 Hz is selected based on our experiments with various sampling rates that showed no difference in the heat transfer coefficient. Also, collecting 2000 data points ensured achieving high stable values of the estimated heat transfer coefficients over the range of our experimental conditions.

4. Description of the experiemental work

Each experimental test starts by introducing dry helium into the present facility until the desired pressure is achieved. Five values of helium pressure are used as the main variable in the current study (413.47, 482.38, 551.29, 620.20, and 689.12 kPa). Then, the electrical heaters and chiller are simultaneously turned on and adjusted to the desired values. The water from the chiller simultaneously flows to the cooling jacket around the upper plenum and the helical coil heat exchanger around the downcomer channel. The outer surface temperatures for the upper plenum and downcomer channel are kept constant at 5 ^{o}C for all experimental runs[27]. An isoflux thermal condition is implemented for the riser channel at a constant value of 1720 W/m^2 for all experimental tests. After adjusting the desired values of the helium pressure, outer surface temperatures of the upper plenum and downcomer channel, and wattage supplied to the riser channel, the system is allowed to reach steady-state conditions. The thermal steady-state condition was achieved approximately within 3-4 hours depending on the experimental condition. The steady-state conditions were achieved when the local heat flux signals did not vary by more than 0.8 W/m2 within 30 minutes, and the temperature signals did not vary by more than 0.5 K within 30 minutes. Once the steady-states are achieved, the signals of the heat transfer coefficients at different axial locations along the riser and downcomer

channels are simultaneously measured with the radial and axial temperatures. To achieve highly accurate heat transfer results and to minimize the experimental error, each experimental run was repeated three times. The amplitude-domain method was used for the time series data analysis[29] to quantify the amplitude distribution in the measured signals. The results showed that the maximum standard deviations were 0.06 and 0.02 for heat transfer coefficients and temperature, respectively. This reveals that the measured parameters are close to the mean value with an acceptable experimental error.

5. Results and discussion

5.1 Pressure dependent of Rayleigh number

The Rayleigh number (Ra) is used as a common dimensionless value to describe natural convection [30]

$$\mathrm{Ra} = \frac{g \rho^2 \beta \Delta T D^3 C_p}{\mu k} \tag{4}$$

. The Ra can be rearranged in terms of pressure by substituting all density-dependent properties with $\rho = \frac{P}{R T}$ for ideal gas to yield

$$\mathrm{Ra} = \frac{g \beta \Delta T D^3 C_p}{k \mu T^2 R^2} P^2 = \mathrm{C}\, P^2 \tag{5}$$

where *C* is a substitute for all variables that fixed besides the pressure. To validate the assumption of helium (working fluid) as an ideal gas and hence the validity of Equation 5, the following analysis has been performed. The ideal gas properties can be classified into four categories depending on the operating pressure. These categories are dense,

dilute, rarefied, and Knudsen gas and can be defined based on the mean free path, λ , and the characteristic geometric length, L, as follows: [31]

Dense gas $\lambda \ll L$, $\lambda \approx$ d (6)

Dilute gas $\lambda \ll L$, $\lambda \gg$ d (7)

Rarefied gas $\lambda \approx L$ (8)

Knudsen gas $\lambda \gg$ L (9)

For the helium molecules, diameter (d) is 3.7 x 10^{-10} m. By using Eq. (10), the mean free path is easily obtainable [32]. The mean free path at different pressure and the corresponding Knudsen number (Kn)are shown in Tables 1-2 for the riser and downcomer channels, respectively. The Knudsen number (Kn) is the ratio of the mean free path of the geometric length.

$$\lambda = \frac{K_B \, T_f}{\sqrt{2} \, \pi \, d^2 \, P} \quad (10)$$

$$\text{Kn} = \frac{\lambda}{L} \quad (11)$$

It is clear from Tables 1-2 that over the given range of the operating pressure from 413.47 to 689.12 kPa for the riser and downcomer channels, the current experiment is located within the dilute gases range (Eq.7), where *C* is not a strong function of operating pressure [31,33,34]. Thus, the Rayleigh number is proportional to P^2, which confirms the assumption of helium as an ideal gas.

5.2 Flow and heat reversal close to the outlet of the riser channel (Y/H = 0.956)

` Heat and flow reversal may occur at the exit of the heated channel (riser) under operating conditions that are not clearly reported in the open literature. In the current study, the flow and heat reversal corresponds to the inflow of colder/denser working fluid (helium) from the upper plenum into the top section of the riser. Therefore, this reversed heat and flow should induce flow oscillation and consequently separation of the ascending boundary layer as reported by Bouia et al. [35]. Figure 6 shows a reversal in the direction of the heat transfer in terms of negative heat flux signals, from the flowing helium to the inner wall of the riser channel close to the exit of the riser (Y/H = 0.956). This observation is also reported by Barnes [36], in which Barnes observed that heat is transported from the flowing fluid to the inner wall at the final section of the heated section. It is worth mentioning that the other heat flux signals, from Y/H = 0.044 to Y/H = 0.773, give positive signals, which confirms that there is no reversal in the direction of heat. Furthermore, figure 6 shows that the magnitude of reversed heat fluxes increases as the operating pressure decreases due to an increase in the intensity of co-circulation with decreasing pressure. Also, a central peaking for radial helium temperature is observed close to the exit (Y/H = 0.956) for all experimental conditions, as shown in Fig. 7. The central peaking of the radial helium temperature is evidence of the flow and heat reversal, which is consistent with the observed negative signals for the heat fluxes close to the exit (Y/H = 0.956).

5.3 Wall surface temperature distribution along the riser channel

The wall surface temperature distributions are shown in Fig. 8. The axial distribution of the surface temperature with the dimensionless channel length (Y/H) for different operating pressures (413.47, 482.38, 551.29, 620.20, and 689.12 kPa) exhibits the following trend: the value of the wall surface temperature gradually increases from the channel entrance (Y/H = 0.044) until a certain limit to reach a maximum value at Y/H = 0.773, beyond which it begins to decrease. This phenomenon can be explained as follows: at the entrance of the riser channel, the surface temperature gradually increases until the boundary layer fills the channel. From the entrance of the channel to the maximum value, the helium inside the channel is heated by convection currents from the inner surface of the channel while it is flowing through the riser channel from the leading edge (Y/H = 0.044), which makes the helium temperature increase with the axial distance until a maximum value at Y/H = 0.773. A reduction in the wall surface temperature is observed after Y/H = 0.773, as shown in Fig. 8. The dip in the wall surface temperature after Y/H = 0.773 could be attributed to a large expansion ratio between the riser channel and upper plenum. Also, this reduction could be attributed to the flow and heat reversal as well as a cold inflow of denser helium inside the top section of the riser from the upper plenum, and in turn, a reduction in the wall surface temperature is observed close to the exit (Y/H = 0.956). This trend is similar to that found in the open literature[13,14,16,37]. It is worth mentioning that the wall surface temperature in the riser channel is decreased by 18% for the operating pressure increase from 413.47 to 689.12 kPa.

5.4 Radial distribution of helium temperature along the riser channel

Figures 9 -13 show the radial variation of the helium temperatures along the riser channel for different axial locations under operating pressures ranging from 413.47 to 689.12 kPa. Very similar trends for the radial temperature are obtained for all experimental conditions. Three main radial profiles could emerge from Figures 9-13 as follows:

A) Developing radial profile from Y/H = 0.044 to Y/H < 0.591.

B) Flattened radial profile at $0.591 \leq$ Y/H ≤ 0.773. At $0.591 \leq$ Y/H ≤ 0.773, the helium flow is slow and unable to remove large amounts of thermal energy. Hence, the bulk temperature of helium equals to a value approximately equaling the inner wall surface temperature as shown in Figures 9-13.

C) Reversed radial profile close to the exit of the riser (Y/H $\geq$ 0.956). At Y/H $\geq$ 0.956, the direction of the heat transfer is reversed. For the revered profile, the buoyancy force has no more contribution to the helium velocity.

The flattened and reversed radial profiles have significant effects on the dynamic performance of the natural convection in terms of buoyancy force. The exact axial location of the heat transfer reversal requires higher resolution of the axial data collection between $0.773 <$Y/H <0.956.

5.5 Axial distribution of the local heat transfer coefficient (*h*) and Nusselt number (Nu_D) along the riser channel

Local values of heat transfer coefficients are shown in Figure 14. To meaningfully compare the current finings with any similar future computations or experimental studies in the literature, a plot of $Nu_D = \frac{h_{avg} D}{k}$ is shown in figure 15. Use of Nu_D will enable comparison with other geometries and fluids. As shown in Figures 14-15, Nu_D and *h* decrease with the increase of dimensionless axial distance (Y/H) from the lower end of the riser (Y/H = 0.044) until a minimum value at Y/H = 0.279, then it starts to increase until Y/H = 0.591. One can remark a reduction in the Nu_D and h after Y/H=0.591. This behavior of *h* and Nu_D can be explained if Figure 16 is considered. Figure 16 is a schematic diagram which has been used to visualize the effect of operating pressure on the Nu_D and *h*. It is worth mentioning that the variation of *h* along the riser channel length is similar to the variation of Nu_D. At the entrance of the riser channel, point (A), the cold helium is drawn into the lower end of the riser channel, causing a higher heat transfer coefficient (h) and consequently a higher Nusselt number (Nu_D). From point (A) to point (B), the boundary layers grow up, causing an increase of the temperature distribution and consequently a reduction of the Nu_D and *h*. This makes the Nu_D and *h* decrease with the axial distance (Y/H) until a point (B) where the minimum h and Nu_D are attained. Through line (BCD), the values of Nu_D and *h* increase due to the laminarization effect in the wall region (buoyancy effect) and also due to the upstream

axial conduction in the solid wall preheating the helium in the hydrodynamics developing section [27]. Beyond point (D), one would expect Nu_D and *h* to continue increasing with the constant heat flux condition as represented by (DE), but a reduction in the values of Nu_D and h is observed, represented by (DF). This reduction could be attributed to an extension of the end effect of the riser channel. Also, it is clear from Figures 14-15 that the natural convection intensity in terms of Nu_D and *h* is suppressed by decreasing the pressure. This could be attributed to the fact that Ra is directly proportional to the square of the operating pressure as addressed in the section 5.1 of *Pressure dependent of Rayleigh Number.* Furthermore, with increasing the operating pressure, the molecular movement and subsequent collision increase and cause an increase in convective heat transfer.

5.6 Axial distribution of wall surface temperature and centerline's helium temperature along the downcomer channel

Our initial assessment experiments in the downcomer channel showed no significant statistical radial variations of helium temperature for given axial location. Hence, inner wall surface temperature and centerline's helium temperature are only reported in the downcomer channel. Figures 17-18 show that the axial variation of the inner wall surface temperature and centerline' helium temperature at three different axial locations (Y/H) for different levels of operating pressure ranging from 413.47 to 689.12 kPa using helium: close the inlet (Y/H = 0.956), in the middle (Y/H = 0.5), and close to the exit (Y/H = 0.044). With increasing the operating pressure from 413.47 to 689.12

kPa, the helium centerline, and channel wall temperatures are decreased by 15.5 and 12.7 % respectively. It is also clear from Figures 17-18 that the local difference between the centerline helium temperature and wall surface temperature for any given axial location (Y/H) is small due to the large volume of the upper plenum in comparison of the volume of downcomer channel as reported by Said et al.[27]. Also, a general trend of gradual decrease in both temperatures is observed along the channel from the inlet (Y/H=0.956) to the outlet (Y/H = 0.044). An end effect is observed close to the outlet of the downcomer channel in terms of an increase in temperature due to co-circulation of helium at the outlet of downcomer channel, as well as conductive heat transfer between two channels close to the exit of the downcomer channel.

5.7 Axial distribution of local heat transfer coefficient (*h*) and Nusselt number (Nu_D) along the downcomer channel

Figures 19-20 show the variation of heat transfer coefficient (*h*) and Nusselt number (Nu_D) along the downcomer channel for three axial positions (Y/H) under different levels of operating pressure: close the inlet (Y/H = 0.956), in the middle (Y/H = 0.5), and close to the exit (Y/H = 0.044). The negative values of Nu_D and *h* in Figures 19-20 represent a negative direction for heat transfer from the flowing helium to the inner wall, while the positive values of Nu_D and *h* correspond to a positive direction for heat transfer from the inner wall to the flowing helium. For all experimental conditions, for the downcomer channel, the direction of heat transfer is observed to be from to the helium flow to the inner wall of the downcomer channel for Y/H = 0.956 and Y/H = 0.5, while a reversal in

the direction of heat transfer with positive values close to the exit (Y/H = 0.044) are observed for pressure values greater than 413.47 kPa due to end effects in terms of co-circulation. One can remark that the values of Nu_D and *h* are increased with increasing the operating pressure. Also, it is observed that the local Nusselt number (Nu_D) and heat transfer coefficient (*h*) for a given operating pressure that the local Nu_D and *h* decrease from the leading entrance of the downcomer channel (Y/H = 0.956) to the outlet (Y/H = 0.044). This decreasing rate of the local Nu_D and *h* is evidence of the decreasing flow in the downcomer channel and establishment of the natural circulation.

6. Remarks

Natural convection heat transfer along the flow channels in a unique dual-channel circulation loop has been experimentally studied at various helium pressures. In the current study, a new noninvasive heat transfer coefficient probe and radial adjuster T-thermocouples were successffuly developed, tested, and employed to experimentally characterize the plenum-to-plenum (P2P) heat transfer and associated temperature fields (helium and wall surface temperatures) during natural convection in VHTRs for various helium pressures. The key findings from the present study are summarized as follows:

- The Rayleigh number (Ra) is proportional to the square of the operating pressure (Ra α P^2).
- The steady-state temperatures, inner wall surface, and helium temperatures are lower at high helium pressure, which means lower heat transfer resistance.

- Inner wall surface temperatures in the riser channel and downcomer channel decrease by 18% and 12.7%, respectively with increasing the helium pressure from 413.47 to 689.12 kPa.
- There is no significant change between the centerline's helium and the wall surface temperatures along the downcomer for given conditions due to the large volume of the upper plenum which acts as a shroud to coming helium plumes from the riser channel.
- A central peak in the helium temperature is observed close to the exit of the riser channel due to co-circulation and conjugate heat transfer.
- Heat transfer by convection along the channels is found to increase by increasing the helium pressure, which means lower heat transfer resistance. By increasing the helium pressure, the mass flow rate increases because of increase in the density difference in the circulation loop.
- The heat transfer coefficient and Nusselt number are increased by 30% and 35% with increasing the system's pressure from 413.47 to 689.12 kPa, respectively.

Acknowledgment

The authors acknowledge the financial support provided by the U.S. Department of Energy-Nuclear Energy Research Initiative (DOE-NERI) Project (NEUP 13-4953 (DENE0000744)) for the 4th generation nuclear energy, which made this work possible.

Nomenclature

Symbols

C	constant
C_p	heat capacity of helium (J/ kg.K)
d	helium molecules diameter (9.8 x 10^{-11} ,m)
D	inside diameter of the flow channel (m)
g	acceleration gravity (m/s^2)
h_{avg}	time-averaged local heat transfer coefficient ($W/m^2.K$)
h_i	local instantaneous heat transfer coefficient ($W/m^2.K$)
k	thermal conductivity of helium (W/m.K)
K_B	Boltzmann constant (1.38×10^{-23} J/K)
Kn	Knudsen constant
L	characteristic geometric length (m)
N	number of data points
Nu_D	Nusselt number, dimensionless, $\frac{h_{avg} D}{k}$
P	operating pressure (Pa)
q_i	local instantaneous heat flux (W/m^2)
R	universal gas constant (J/Kmol K)
Ra	Rayleigh number, dimensionless
T_s	channel inner surface temperature (K)
T_b	characteristic helium temperature (K)

T_f	radial temperature (K)
Y/H	dimensionless axial position

Greek letters

β	volumetric expansion coefficient of helium (1/K)
μ	dynamic viscosity of the helium (kg.m/s)
ρ	density of helium (kg/m^3)
λ	mean free path (m)

Subscript

i	axial position
j	radial position

References

1. Aldridge RJ. *Scaling Study of the Depressurized Conduction Cooldown Event in the High Temperature Test Facility Using RELAP5-3D/ATHENA*. Oregon State University: Department of Nuclear Engineering and Radiation Health Physics, Oregon State University; 2013.

2. Castañeda JA. *Scaling analysis of the OSU high temperature test facility during a pressurized conduction cooldown event using RELAP5-3D*: Nuclear Engineering, Oregon State University; 2014.

3. Tung Y-H, Ferng Y-M, Johnson RW, Chieng C-C. Study of natural circulation in a VHTR after a LOFA using differentturbulence models. *Nuclear Engineering and Design.* 2013;263:206-217.

4. Haque H, Feltes W, Brinkman G. Thermal response of a modular high temperature reactor during passive cooldown under pressurized and depressurizedconditions. *Nucl Eng Des.* 2006;236:475-484.

5. Simoneau JP, Champigny J, Mays B, Lommers L. Three-dimensional sim-ulation of the coupled convective, conductive and radiative heat transfer duringdecay heat removal in an HTR. *Nucl Eng Des.* 2007;237:1923–1937.

6. Tung YH, Johnson, R.W.,. CFD Calculations of Natural Circulation in a HighTemperature Gas Reactor Following Pressurized Circulator Shutdown. ASME,IMECE, IMECE 2011-64259.; 2011.

7. Tung YH, Johnson, R.W., Chieng, C.C., Ferng, Y.M.,. Modeling Strategies toCompute Natural Circulation using CFD in a VHTR after a LOFA. ASME, IMECE,IMECE 2012-93007.; 2012.

8. Tung Y-H, Ferng Y-M, Johnson RW, Chieng C-C. Transient LOFA computations for a VHTR using one-twelfth core flow models. *Nucl Eng Des.* 2016;301:89-100.

9. Misale M. Experimental study on the influence of power steps on the thermohydraulic behavior of a natural circulation loop. *Int J Heat and Mass Transfer.* 2016;99:782-791.

10. Vijayan PK, Sharma M, Saha D. Steady state and stability characteristics of a single-phase natural circulation in a rectangular loop with different heater and cooler orientations. *Experimental Thermal and Fluid Science.* 2007;31:925-945.

11. S.K. Mousavian M. Misale, F. D'Auria, M.A. Salehi. Transient and Stability Analysis in Single-Phase Natural Circulation. *Annals of Nuclear Energy.* 2004;31:1177-1198.

12. Vijayan PK, Nayak AK, Pilkhwal DS, Saha D, Raj VV. Effect of loop diameter on the stability of a single-phase natural circulation loop. *Nureth 5.* 1992:261-267.

13. Al-Arabi M, Khamis M, Abd-ul-Aziz M. Heat Transfer by Natural Convection from the In side Surface of a Uniformly Heated Vertical Tube. *Int J Heat and Mass Transfer.* 1991;34:1019-1025.

14. Mohammed HA, Salaman YK. Heat transfer by natural convection from a uniformly heated vertical circular pipe with different entry restriction configuration. *Energy Conversion and Management.* 2007;48:2244-2253.

15. Salman YK, Mohammed HA. Free convection heat transfer with different sections lengths placed at the exit of vertical circular tube subjected to a constant heat flux. *Al-Khwarizmi Engineering Journal.* 2007;3(3):31-52.

16. Mohammed HA, Salman YK. Laminar air flow free convection heat transfer inside a vertical circular pipe with different inlet configuration. *Thermal Science.* 2007;11(1):43-63.

17. M. Misale PG, J.C. Passos , G. Ghisi de Bitencourt. Experiments in a single-phase natural circulation mini-loop. *Experimental Thermal and Fluid Science.* 2007;31:1111-1120.

18. P.K. Vijayan MS, D. Saha,. Steady state and stability characteristics of single-phase natural circulation in a rectangular loop with different heater and cooler orientations. *Experimental Thermal and Fluid Science.* 2007;31:925–945.

19. Misale M. Overview on single-phase natural circulation loops. Proc. of the Intl. Conf. on Advances In Mechanical And Automation Engineering – MAE 2014; 2014.

20. Mustafa Z. Ghani YKS. Natural convection heat transfer in inclined open annulus passage heated from two sides. *International Journal of mechanical engineering and technology.* 2014;5(11):76-91.

21. Welander P. On the oscillatory instability of a differentially heated fluid loop. *Journal of Fluid Mechanic.* 1979;29(1):17-30.

22. Mehrabian MA. Effect of pressure on free convection heat transfer from a horizontal cylinder at constant wall temperature. *ENGINEERING MODELLING.* 2003;16:55-61.

23. Langebach J, Senin S, Karcher C. Influence of Varying Pressure on Natural Convection and Radiation Heat Transfer in an Enclosure. *Proc Appl Math Mech.* 2005;5:575-576.

24. Miraj M, Alim MA, Andallah LS. Effects of pressure work and radiation on natural convection flow around a sphere with heat generation. *International Communications in Heat and Mass Transfer.* 2011;38:911-916.

25. HOSSEINI R, SAIDI M. Experimental Study of Air Pressure Effects on Natural Convection From a Horizontal Cylinder. *Heat Transfer Engineering.* 2012;33(10):878-884.

26. V A, Vaidyab AM, Vijayanb PK. Effect of Pressure on Steady State and Heat Transfer Characteristics in Supercritical CO2 Natural Circulation Loop. *Procedia Engineering.* 2015;127:636-644.

27. Said IA, Taha MM, Usman S, Wood BG, Al-Dahhan MH. Investigation of natural convection heat transfer in a unique scaled-down dual-channel facility. *AIChE Journal.* 2017;63(1):387-396.

28. Rahman S. Abdulmohsin MA-D. Characteristics of Convective Heat Transport in a Packed Pebble-Bed Reactor Using Novel Non-Invasive Heat Transfer Probe. *Nuclear Engineering and Design.* 2015;284:143.152.

29. Sklar B. *Digital communications fundamentals and applications.* Second ed. Prentice Hall: Prentice Hall; 2001.

30. Incropera FP, Dewitt DP. *Fundamentals of heat and mass transfer.* 5 th ed. New York, USA: John Wiley & Sons Inc.; 2003.

31. Jan Langebach SS, and Christian Karcher. Influence of Varying Pressure on Natural Convection and Radiation Heat Transfer in an Enclosure. *PAMM · Proc Appl Math Mech.* 2005;5:575–576.

32. Chambers A, Fitch, R. K., and Halliday, B. S.,. *Basic Vacuum Technology.* 2nd ed. ed. Bristol,UK: IOP Publishing Ltd.,; 1998.

33. L. Bergmann CS. *Lehrbuch der Experimentalphysik - Bd. 5 Vielteilchensysteme.* Berlin: de Gruyter; 1992.

34. H. D. Baehr KS. *Die thermodynamischen Eigenschaften der Luft.* Berlin: Springer Verlag; 1961.

35. Sanvicente E, Giroux-Julein S, Menezo C, Bouia H. Trnasitional natural convection flow and heat transfer in an open channel. *International Journal of Thermal Sciences.* 2013;63:87-104.

36. Barnes JF. *An experimental investigation on heat transfer from the inside surface of a hot smooth tube to air, helium, and carbon dioxide.* Ministry of Aviation;1961.

37. Lau GE, Timchenko V, Menezo C, et al. Numerical and Experimental Investigation of Unsteady Natural Convection in a Vertical Open-Ended Channel. *Computational Thermal Sciences: An International Journal.* 2012;4(5):443–456.

List of tables

List of figures

Table 1. Variation of the mean free path (λ) and Knudsen number (Kn) with the operating pressure for riser channel

P (kPa)	**λ(m)**	**Kn (dimensionless)**
413.47	3.10945E-07	1.9434E-05
482.38	2.60918E-07	1.63074E-05
551.29	2.2391E-07	1.39943E-05
620.20	1.95296E-07	1.2206E-05
689.12	1.73118E-07	1.08198E-05

Table 2. Variation of the mean free path (λ) and Knudsen number (*Kn*) with the operating pressure for downcomer channel

P (kPa)	**λ(m)**	**Kn (dimensionless)**
413.47	2.20231E-07	1.37644E-05
482.38	1.88613E-07	1.17883E-05
551.29	1.64864E-07	1.0304E-05
620.20	1.46387E-07	9.14921E-06
689.12	1.31572E-07	8.22324E-06

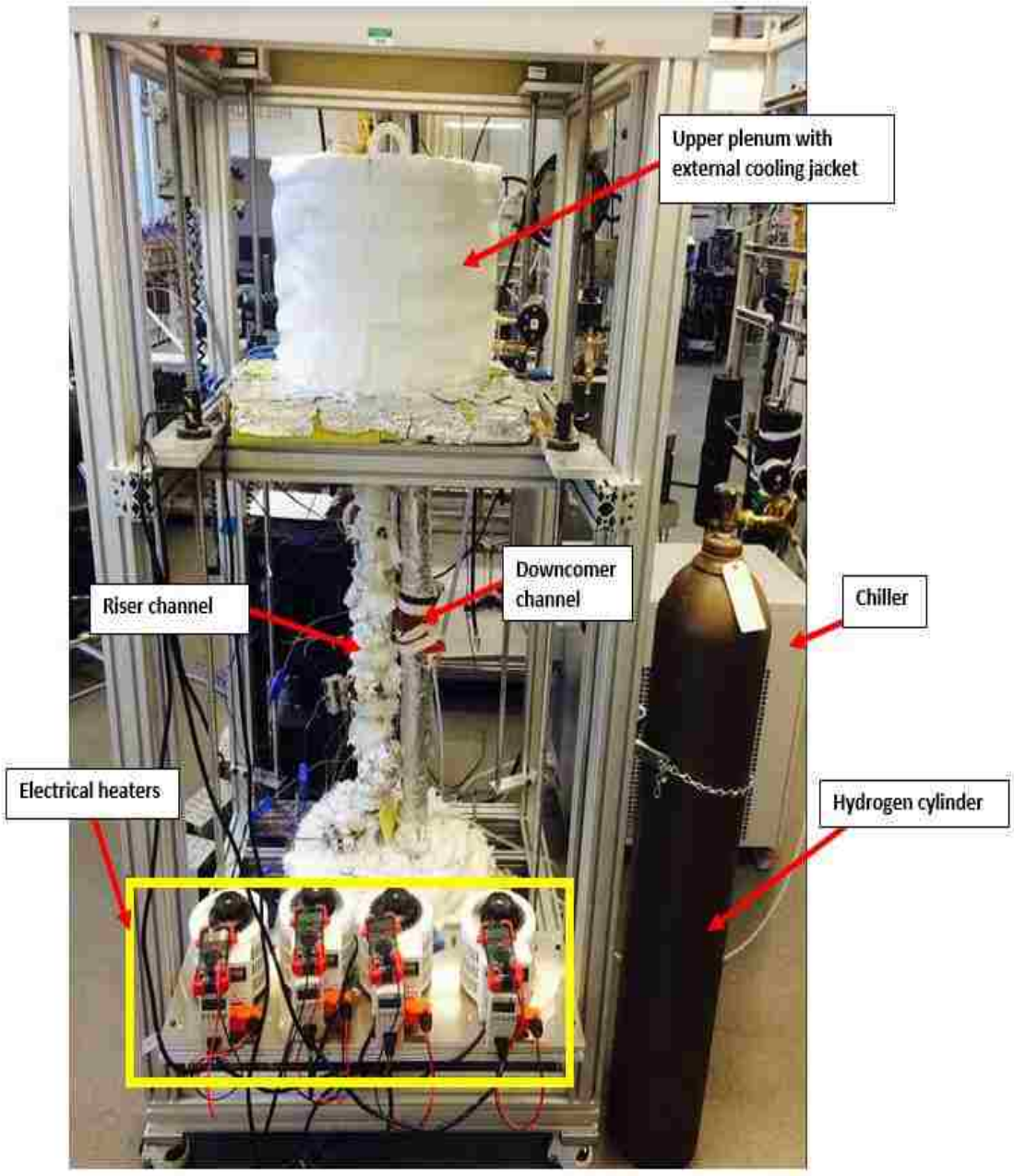

Figure 1. Physical picture of the unique scaled-down dual-channel circulation loop facility.

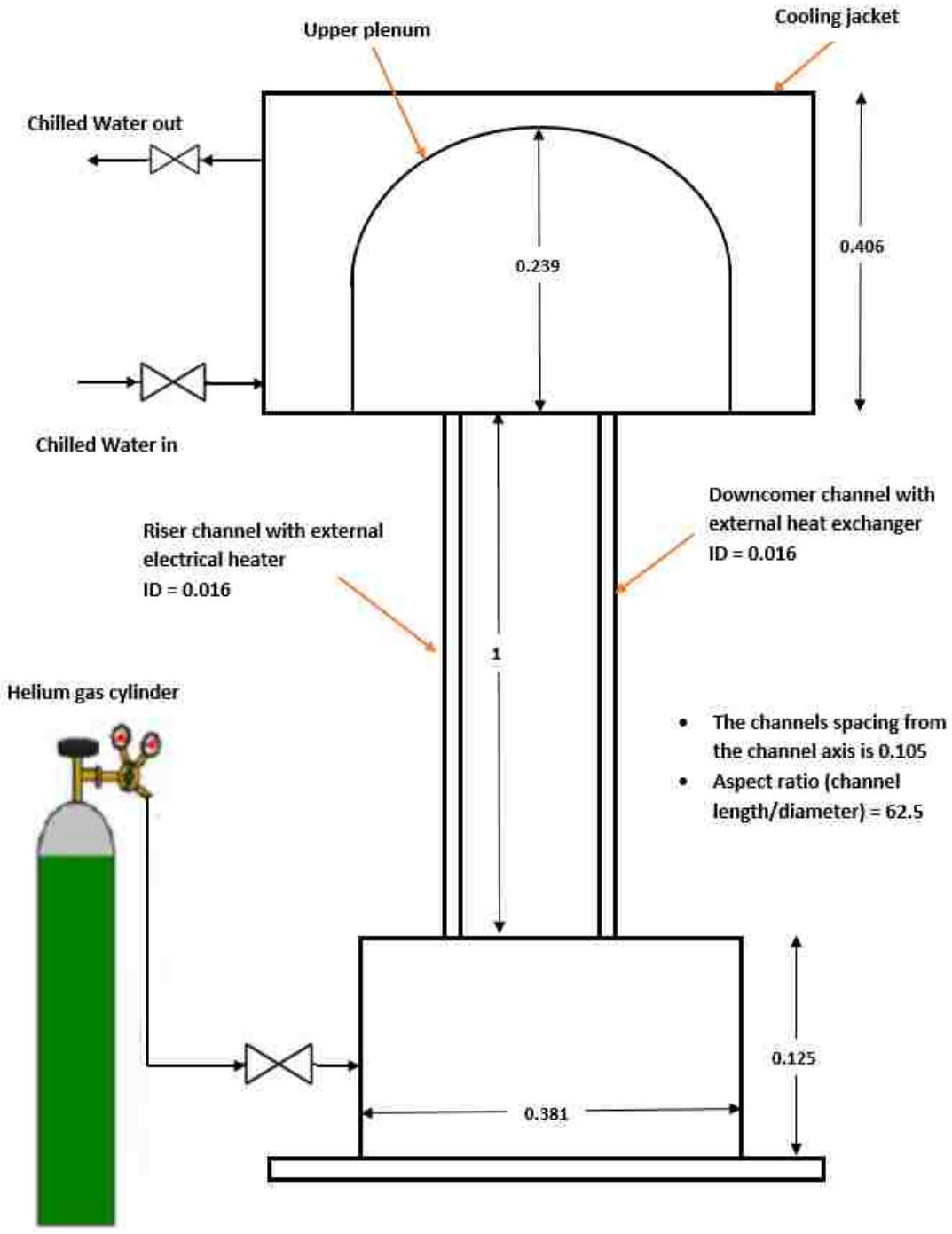

Figure 2. Schematic diagram of the unique scaled-down dual-channel circulation loop facility (all dimensions in m).

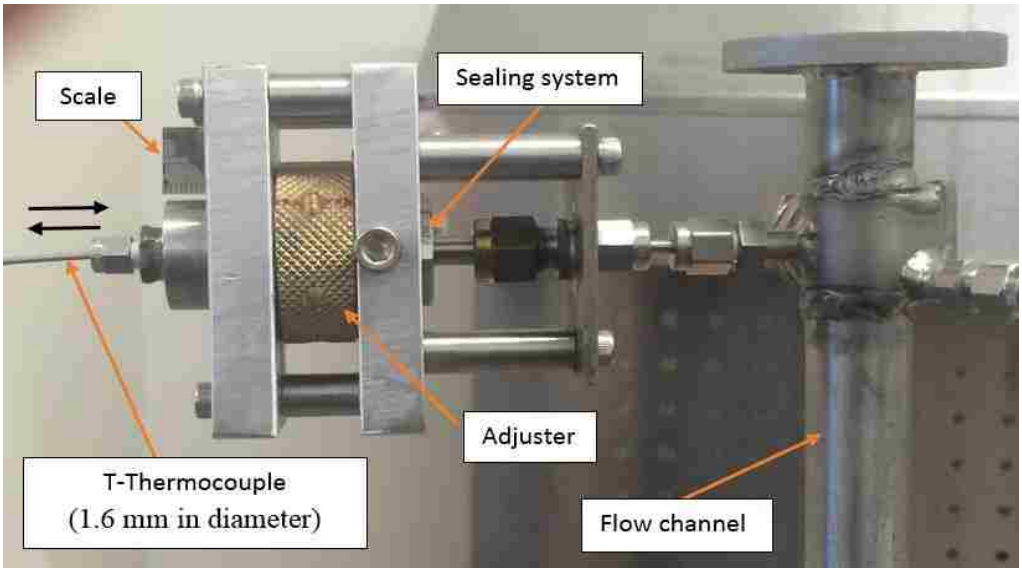

Figure 3. Physical picture for the radial thermocouple adjuster.

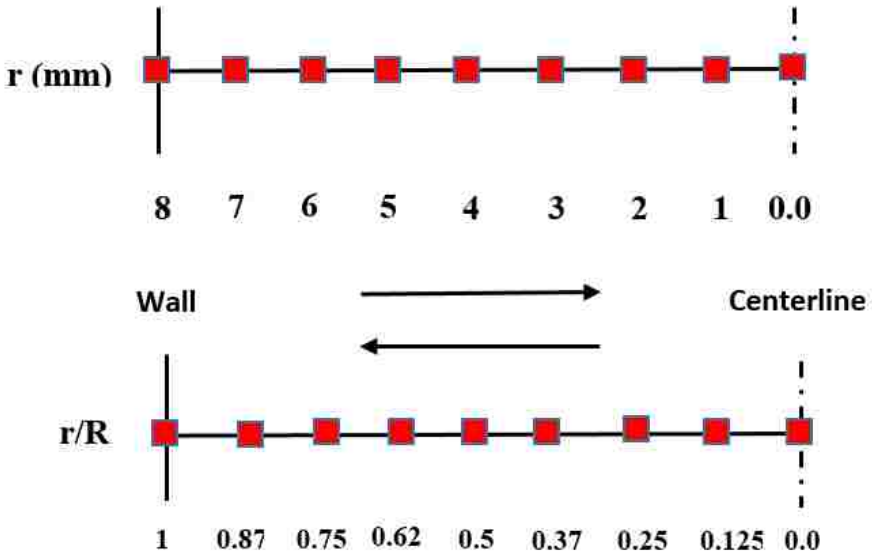

Figure 4. Radial position of the T-thermocouple sensor (1.6 mm in diameter).

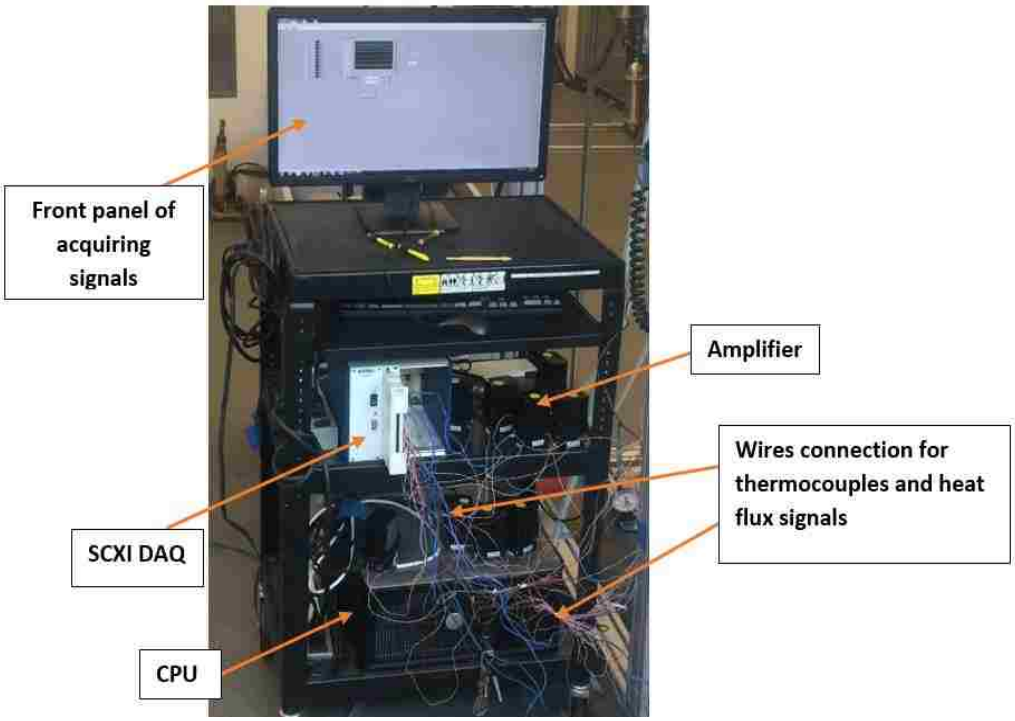

Figure 5. Physical picture for the data acquisition station.

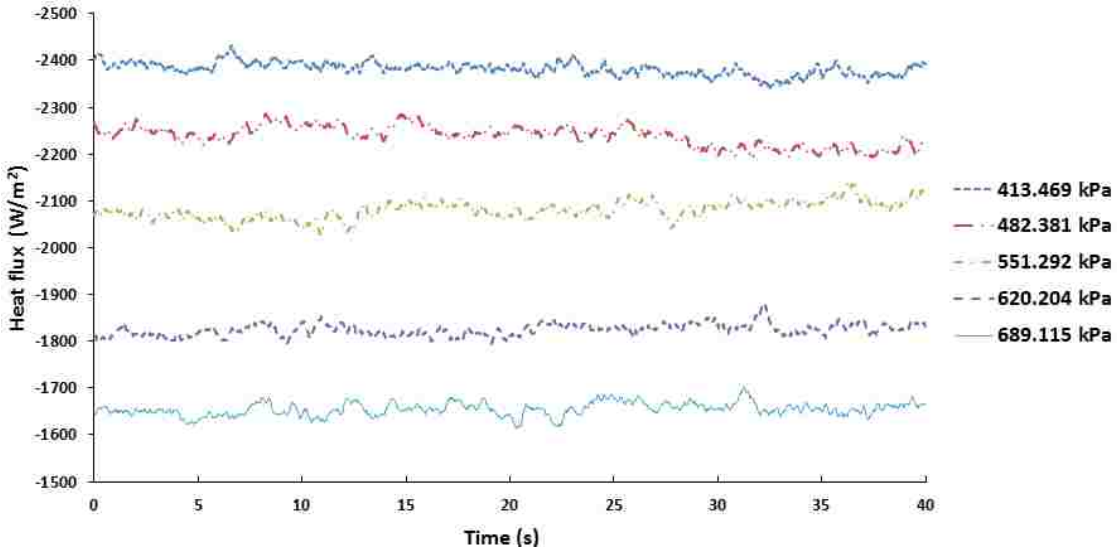

Figure 6. Raw heat flux signals close to the exit of the riser channel (Y/H = 0.956).

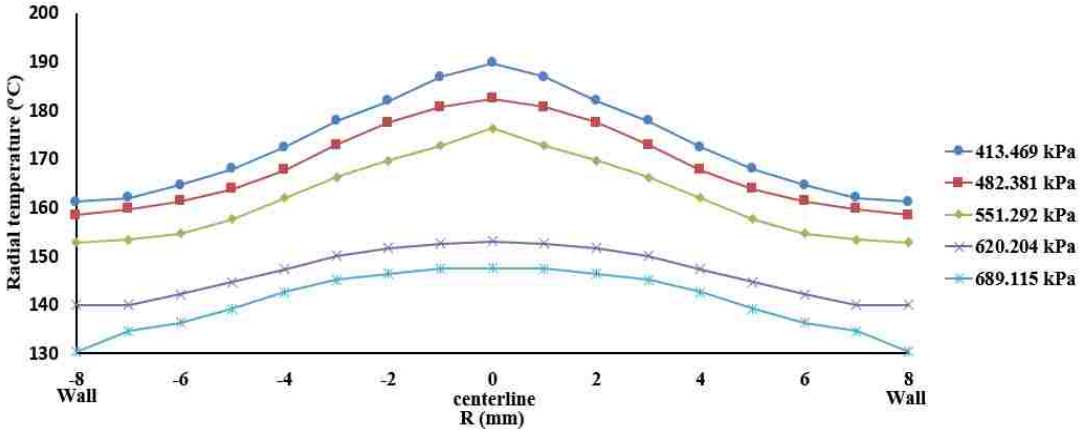

Figure 7. Radial distribution of the helium temperature close to the exit (Y/H = 0.956)

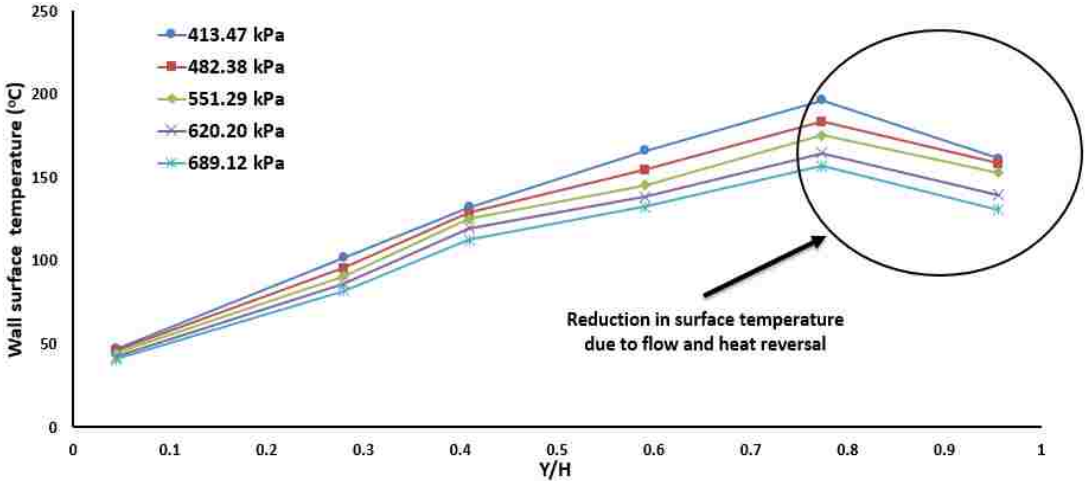

Figure 8. Axial distribution of the wall surface temperature along the riser channel

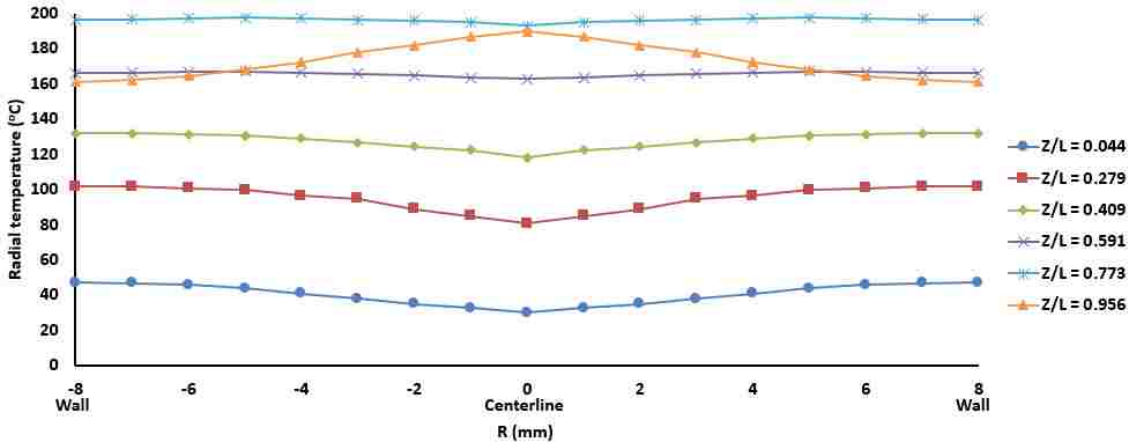

Figure 9. Radial distribution of the helium temperature at 413.47 kPa for various axial locations

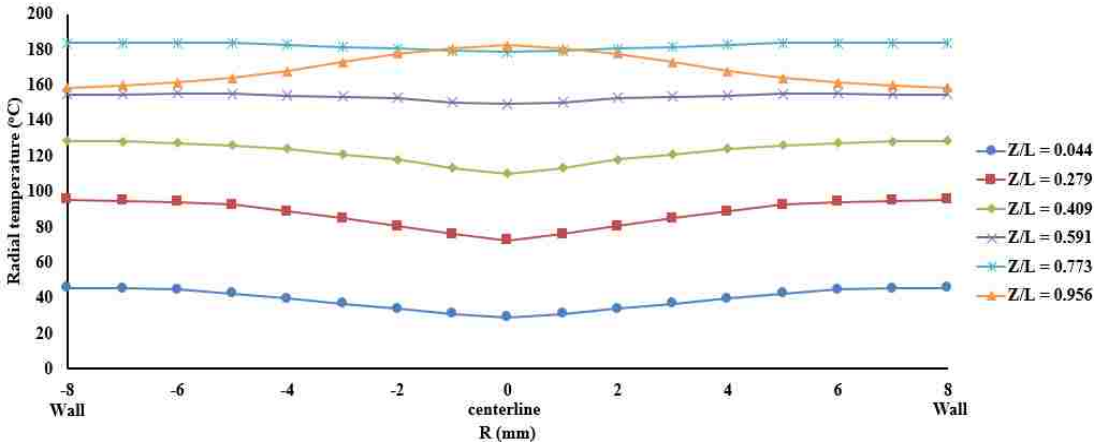

Figure 10. Radial distribution of the helium temperature at 482.38 kPa for various axial locations

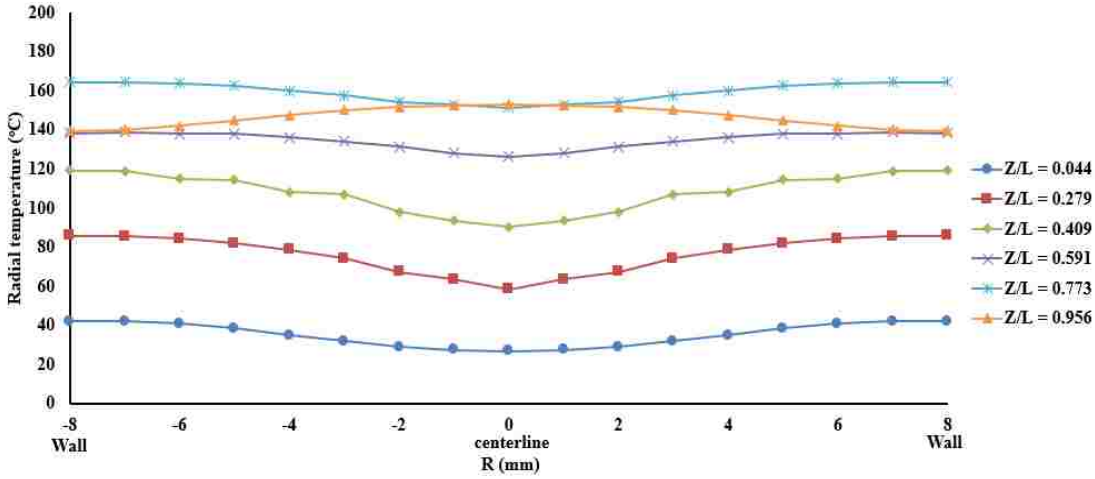

Figure 11. Radial distribution of the helium temperature at 551.29 kPa for various axial locations

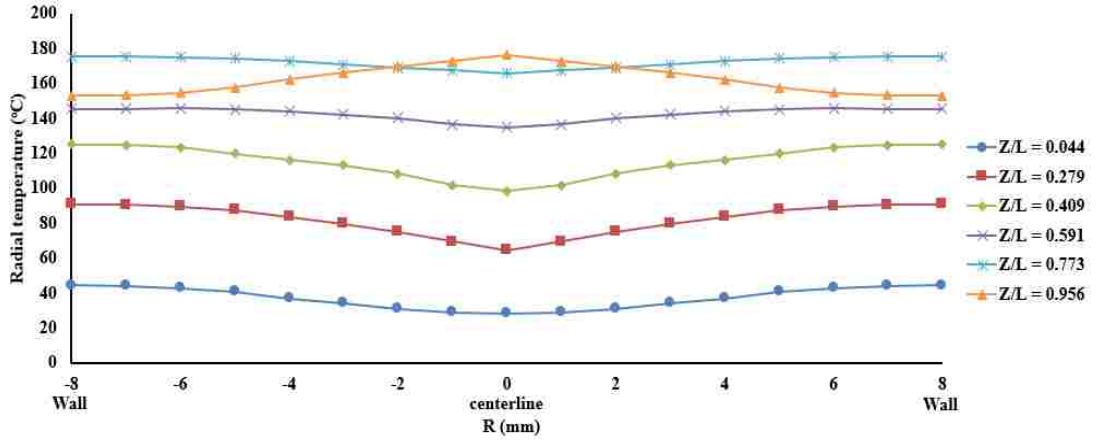

Figure 12. Radial distribution of the helium temperature at 620.20 kPa for various axial locations

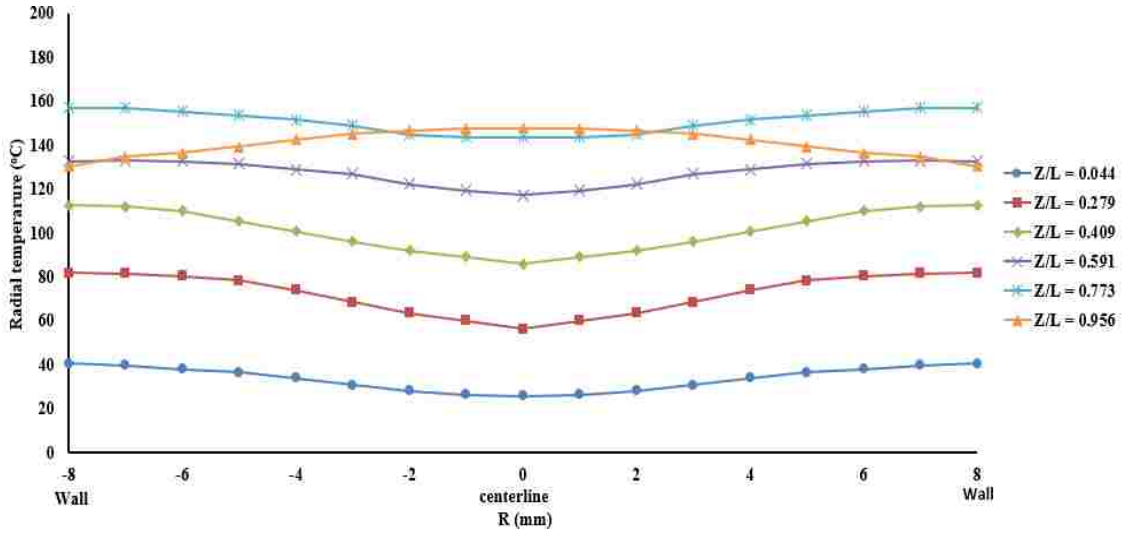

Figure 13. Radial distribution of the helium temperature at 689.12 kPa for various axial locations

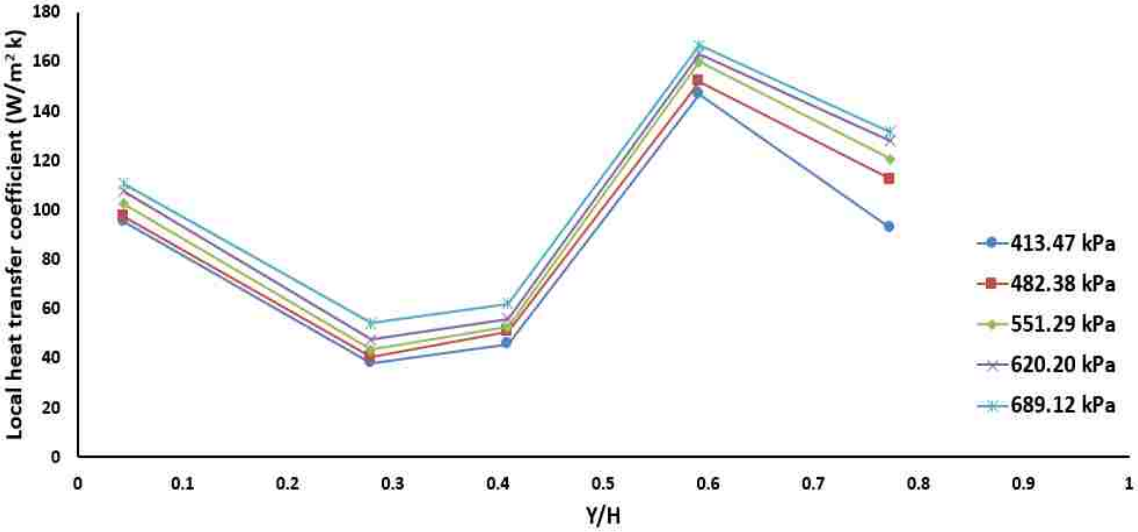

Figure 14. Axial distribution of the local heat transfer coefficient along the riser channel

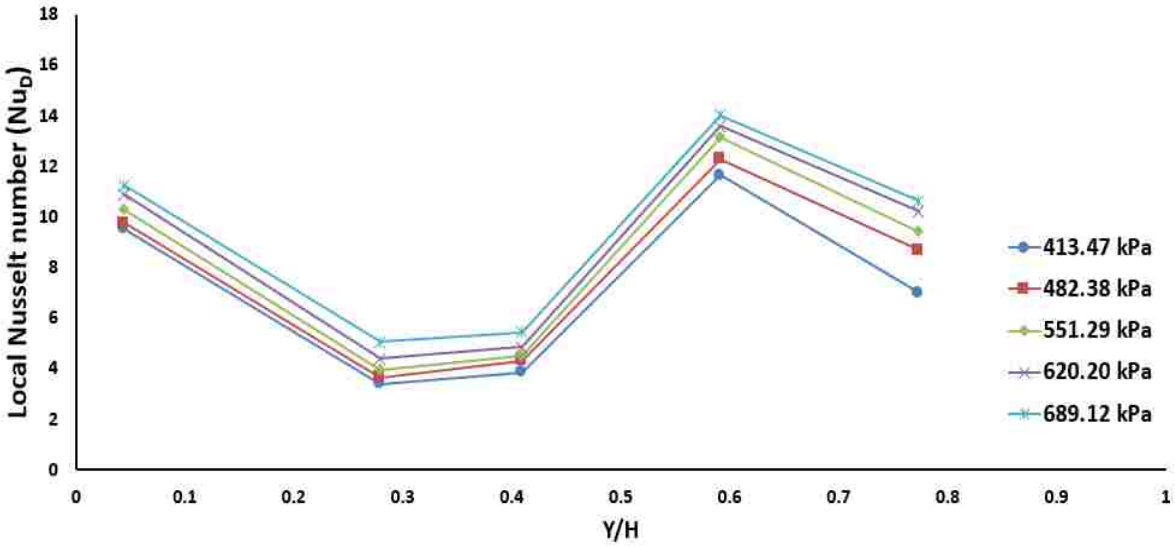

Figure 15. Axial distribution of the local Nusselt number along the riser channel

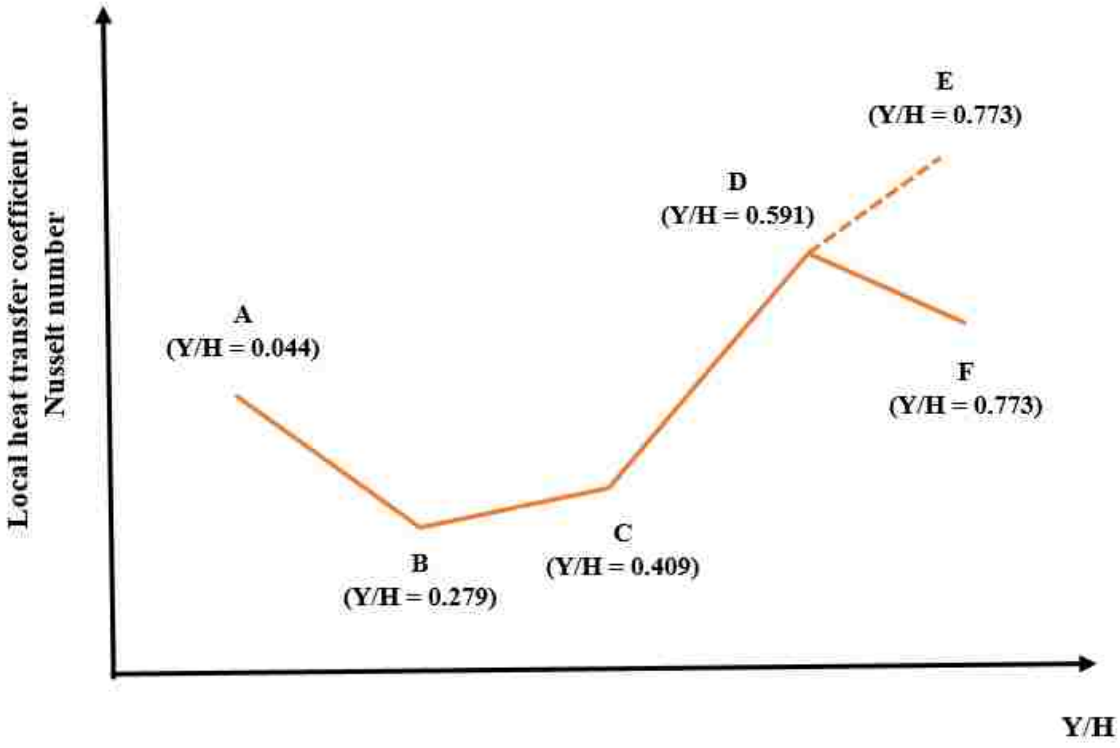

Figure 16. Variation of the local heat transfer coefficient or Nusselt number versus the axial distance along the riser channel.

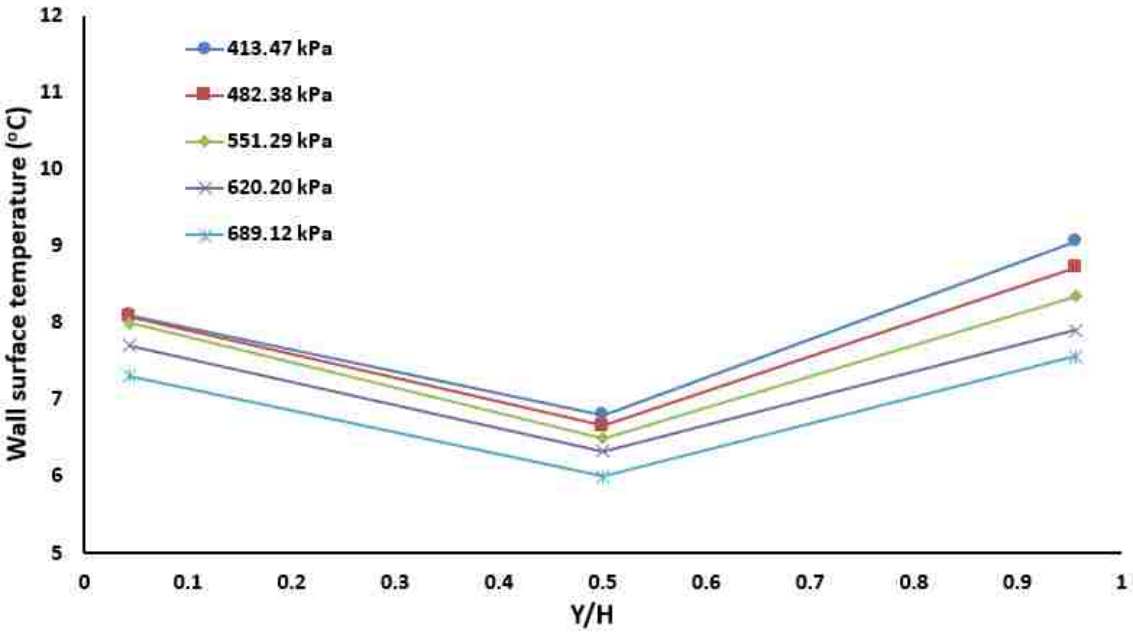

Figure 17. Axial distribution of wall surface temperature along the downcomer channel

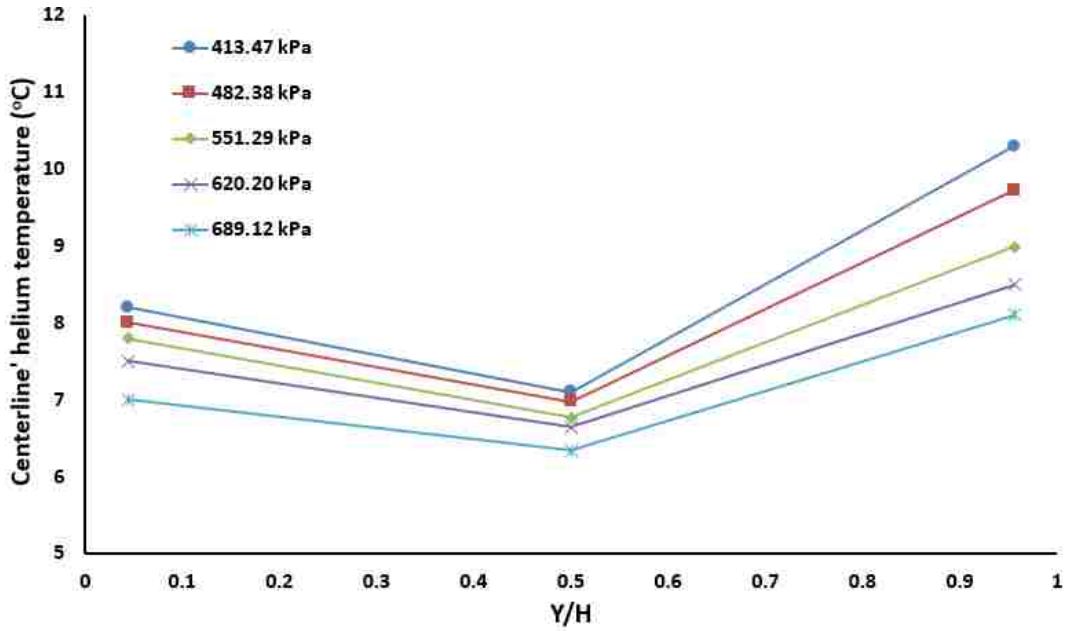

Figure 18. Axial distribution of the centerline' helium temperature along the downcomer channel

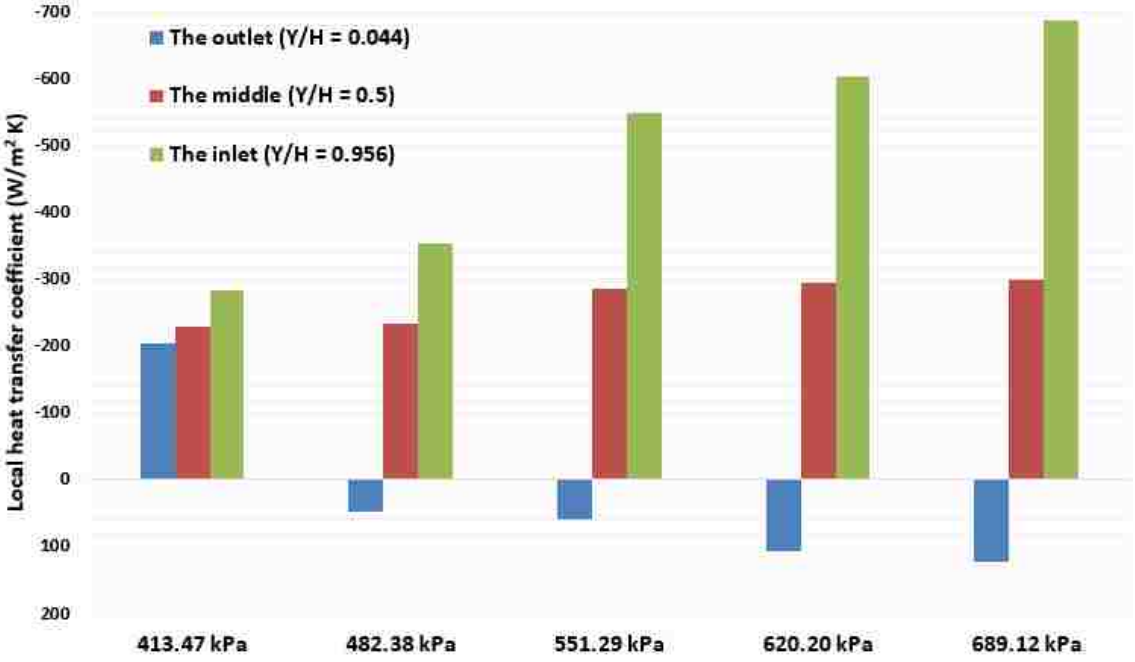

Figure 19. Distribution of the local heat transfer coefficient (*h*) along the downcomer channel

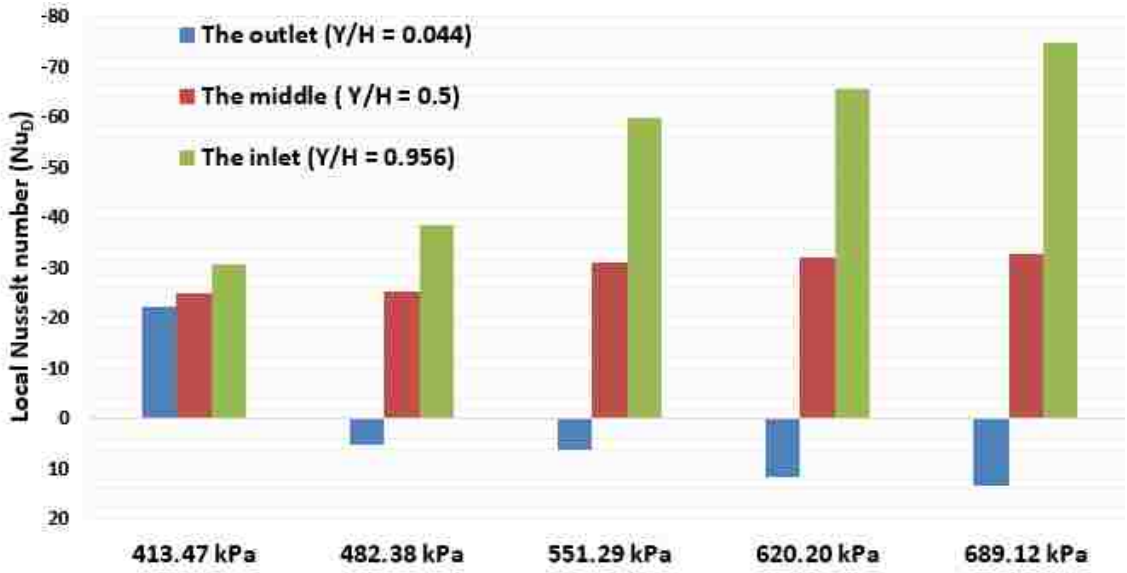

Figure 20. Distribution of the local Nusselt number (Nu_D) along the downcomer channel

IV. AXIAL DISPERSION AND MIXING OF COOLANT GAS WITHIN A SEPARATE-EFFECT PRISMATIC MODULAR REACTOR

Ibrahim A. Said [1,3], Mahmoud M. Taha [1,3], Vineet Alexander [1], Shoaib Usman [2], Muthanna H. Al-Dahhan [1,2]*

[1] Multiphase Reactors Engineering and Applications Laboratory (mReal), Chemical and Biochemical Engineering Department, Missouri University of Science and Technology, Rolla, MO, 65409, USA

[2] Mining and Nuclear Engineering Department, Missouri University of Science and Technology, Rolla, MO, 65409-0170, USA

[3] Chemical Engineering Department, Faculty of Engineering, Alexandria University, Alexandria, Egypt

* *Corresponding author: aldahhanm@mst.edu*

Abstract

Multiphase Reactors Engineering and Applications Laboratory (mReal) research team performed, for the first time, gas phase dispersion experiments in a separate-effect cold-flow experimental setup for the coolant flow within heated channels (riser channels) of the prismatic modular reactor core under accident scenario using sophisticated gaseous tracer technique. The current separate-effect experimental setup was designed and developed in light of local velocity measurements obtained experimentally by using the hot wire anemometry (HWA) in a previous experimental study carried out at mReal for the same operating conditions. The current measurements consist of pulse-response of gas tracer (helium) that is flowing through the mimicked riser channel (separate-effect setup) using air as a carrier in conjunction with integral convolution method to account the extra dispersion within the sampling lines and analytical system. The dispersion of the

gas phase within the separate-effect riser channel was described using one-dimensional axial dispersion model (1D-ADM). In the current study, the axial dispersion coefficient (D) and Peclet number (N_{Pe}) of the coolant gas phase and their residence time distribution (RTD) within the developed representative separate-effect channel were measured and quantified. Effect of heating intensities in terms of heat fluxes on the coolant gas dispersion along core riser channels were mimicked in the current study by a certain range of volumetric air flow rate ranging from 0.0015 to 0.0034 m^3/s which corresponding to heating intensity range from 200 to 1400 W/m^2. Results confirm that a reduction in the response curve spreads in terms of residence time distribution (RTD) is achieved by increasing the volumetric air velocity (representing heating intensity). Also, the experimental results reveal a reduction in values of axial dispersion coefficient (D) (an increase of Peclet number (N_{Pe})) with increasing the air volumetric flow rate (heating intensity). This could be attributed to an increase of the eddy diffusivity of mass. The current quantification of axial gas dispersion along the coolant channel will be used to advance the present knowledge of the safety features of the prismatic modular reactor under accident scenario

Keywords:

Prismatic modular reactor; gaseous tracer technique; axial dispersion coefficient (D); Peclet number (N_{Pe})

Introduction

The prismatic modular reactor (PMR) is a promising candidate of the next generation nuclear plants (NGNPs). One of the prismatic modular reactor (PMR) advantages is its capability to passively remove the decay heat from the reactor core through natural circulation under the loss of flow accidents (LOFA) scenario (Tung et al. 2013). In the scenario of the loss of flow accident (LOFA), the natural circulation, due to large temperature variations and consequently density differences, is initiated to remove the decay heat from the reactor core. Furthermore, during the LOFA event, the direction of the coolant flows within the reactor core is reversed, and there are two different possibilities for the direction of the flow may occur inside the coolant flow channels due to large densities variations. For the heated portions of the reactor core, the gas coolant flows upward, while in the relatively cooled portions (lower temperature) the gas coolant flows downward establishing the natural circulation. The gas coolant channels with downward flow act as downcomer channels, while the coolant channels with upward flow act as riser channels. A description and more details regarding the prismatic modular reactor under accident scenario is given by Said et al. (2017). The efficiency of the natural circulation as a safety feature of the prismatic modular reactor is dependent upon how the gas coolant removes the decay heat from the reactor core. Therefore, to reliably simulate the thermal hydraulic phenomena within the reactor core, the gas-coolant heat transfer and dynamics need to be characterized by a representative geometry. In the open literature, there are few studies performed on the flow field in the prismatic modular reactor under the natural circulation using computational fluid dynamics (CFD) (Haque et al. 2006; Simoneau et al. 2007; Tung and Johnson 2011; Aldridge 2013; Tung et al. 2013;

Tung et al. 2014; Tung et al. 2016). Furthermore, there are unique experimental studies that were performed in the Multiphase Reactors Engineering and Applications Laboratory (mReal) at Missouri S&T, Rolla that are directed to understand the heat transfer and coolant dynamics within a dual-channel circulation loop under high pressure and temperature (Said et al. 2017; Said et al. Under review 2017; Said et al. 2017 under review; Taha et al. 2017 under review; Taha et al. 2017 under submission). The mReal research team implemented sophisticated measurement techniques, including hot wire anemometry (HWA), radial temperature T-thermocouple adjuster, and heat transfer coefficient probe to experimentally measure and analysis local coolant velocities, temperature fields (coolant and inner wall temperatures), and local heat transfer coefficients along the flow channels under different operating conditions. Findings from these studies at mReal fill the gap in the literature in terms of providing a unique benchmark data of heat transfer in conjunction with gaseous dynamics within a representative geometry of prismatic modular reactor (PMR), which can be implemented for verification and validation (V&V) the computational fluid dynamics (CFD) codes combined with heat transfer computations such as CFD-STAR-CCM+, and CFD-Fluent and thermal hydraulic codes such as RELAP5-3D. It is worth mentioning there is a critical need to tie the findings at mReal with the gas coolant dispersion and mixing along the coolant channels to understand the thermal hydraulic of the PMR under accident scenario. To the authors acknowledge, there are no reported studies in the open literature related to quantifying and understanding the gas coolant dispersion along the flow channels of the prismatic modular reactor (PMR) under an accident or normal scenarios. The only available experimental studies in the open literature are oriented to empty tubes

under different operating and design conditions (Wen and Fan 1975). Unfortunately, these studies are carried out in non-representative geometries and operating conditions that cannot be extended to the prismatic modular reactor under LOFA scenario. In the current study, sophisticated gaseous tracer (GT) technique, for the first time, has been developed and implemnted to accurately characterize and quantify the gas dispersion (both molecular diffusion and turbulent mixing) and identify the degree of mixing along the flow channels. Implementation of the gas dispersion and mixing measurements using the gaseous tracer technique within the dual-channel circulation loop of Said et al. at mReal (Said et al. 2017) is technically challenging and will not produce reliable benchmark data due to temperature limitations and other difficulties as discussed in the next section of the *experimental work*. Hence, the measured axial local gas coolant velocities with the use of hot wire anemometry (HWA) along the riser channel of the dual-channel circulation loop under different heating intensities (200 to 1400 W/m^2) (Moharam 2017 under submission) were used to design and develop the current separate-effect test section which mimics the riser channel of the dual-channel circulation loop at mReal under atmospheric cold flow conditions. This is executed by matching the axial local gas coolant velocities between the riser channel in the dual-channel circulation loop, which is designed at mReal with reference to high-temperature test facility at Oregon State University (Castañeda 2014; Said et al. 2017) and the current separate-effect test section for atmospheric air condition. This is achieved by adjusting the cross sectional area of the test section as well as the input volumetric air flow rate to the test section to get similarity in terms of local air velocity between the separate effect test section and the dual-channel circulation loop. The current study provides high temporal resolutions and

spatial benchmarking data in terms of axial dispersion coefficients for safe, efficient design, and operation of the PMR under accident scenarios.

Experimental work

Gas dispersion and mixing challenges

Multiphase Reactors Engineering and Applications Laboratory (mReal) research team at Missouri S&T designed and constructed a high pressure and temperature dual-channel facility, mimicking prismatic modular reactor (PMR), for natural circulation passive safety system heat transfer and gas dynamics investigations (Said et al. 2017). Implementation of the gas dispersion measurements using the gaseous tracer technique in this facility is technically challenging and will not produce reliable measurements in terms of residence time distributions (RTD). These difficulties arise from the following: 1) temperature limitations (the thermal conductivity detector component of the gaseous tracer technique cannot withstand temperature exceeds 40°C), 2) recirculation of the gas tracer within the dual-channel at mReal (the dual-channel facility is a closed system under high pressure and temperature, and there is a great opportunity for the gas tracer to reciruclate that will affect the measured signals repeatability), and 3) vacuum pumping components of gaseous tracer technique would affect naturally-driven flow within the dual-channel facility.

New approach of the experimental setup

A separate effect cold-flow convergent channel was designed and developed for gas dispersion investigations mimicking naturally-driven upward flow within the riser

coolant channel of the dual-channel facility. Therefore, this separate-effects convergent channel was designed with matching the axial local velocity measurements of the riser channel of the dual-channel facility which is operated under different heating intensities (200, 600, 1000, and 1400 W/m^2) by implementing hot wire anemometry (HWA) measurement technique (Moharam 2017 under submission). Each heating intensity in the dual-channel circulation loop facility for the riser channel is represented by adjusted air volumetric flow rate (0.0015, 0.0024, 0.0032, and 0.0034 which are corresponding to 200, 600, 1000, and 1400 W/m^2, respectively) that is forced to flow through this developed convergent channel. In other words, naturally driven flow inside the dual-channel facility for the riser channel was matched by controlling forced flow through the convergent channel. Afterward, the convergent channel dimensions were calculated by using the previously reported axial air gas mean velocities and controlled volumetric flow rates. Table 1 shows actual velocities of the air as a coolant within the riser channel of the dual-channel circulation loop (from HWA measurements), and the matched one through the developed converged channel (cold flow conditions). Figure 1 shows a schematic diagram of the separate-effect convergent channel that is used for the current experiments. The convergent channel is divided into three regions: A) lower mixing region (lower plenum) which is modeled as ideal continuous stirred tank reactor (CSTR) to provide the inlet tracer concentration to the one-dimensional axial dispersion model (1D-ADM) as explained in the section of *convolution and regression methods*, (B) upper mixing region (upper plenum) which is designed and developed for mimicking channel end effects (Said et al. 2017) as well as uniform sampling, and (C) core channel which mimics the riser channel without end effects. Preliminary experiments in terms of

residence time distribution (RTD) were performed to check the uniformity of mixing in the lower and upper plena (A&B). The sampling of the gas tracer for the preliminary experiments was done at different radial positions as: r/R = 1 (center of the convergent channel), r/R = 0.5, and r/R = 0.0 (near the wall surface of the convergent channel). Figure 2 of the preliminary experiments for the upper plenum at different sampling radial positions (0.0034 m^3/s) shows that there were no significant differences in the measured signals of the gas tracer under the same operating conditions. This finding confirms that well-mixed conditions were achieved through lower and upper plena (A&B).

Gaseous tracer technique

The gaseous tracer (GT) is an advanced technique used to accurately measure the residence time distribution (RTD) in a complex flow structure of single and multiphase flow systems by injecting pulse or step change gas tracer and then monitoring its concentration at the exit (Han and Al-Dahhan 2005; Han 2007; Abdulmohsin and Al-Dahhan 2016). The measured RTD can be utilized to characterize and quantify the gas dispersion (which includes the contribution of both molecular diffusion and turbulent mixing) and identify the degree of mixing in the system. The well-designed gaseous tracer measurement technique that was developed by (Han 2007) in conjunction with the needed methodology of integral convolution to obtain a direct measurement of the gas dispersion through the test channel has been adopted in the current work. Schematic diagram and physical picture of the gaseous tracer technique configuration with the current convergent channel are shown in Figures 3 and 4, respectively. As shown in Figures 3 and 4, the gaseous tracer unit consists of a gas analyzer, gas vacuum pump, and

PC with data acquisition system (DAQ). The gas analyzer is a GOW-MAC 20 series binary analyzer which contains a flowing reference thermal conductivity detector (TCD), held at room temperature. A GOW-MAC 59-300 vacuum pump was used to draw the gas sample out of the test channel and pass to the TCD. The outlet of the convergent channel is connected to the sample line of the TCD, where the outlet pulse response is recorded. The response from the TCD was amplified, converted to digital signals, and recorded as time series data at a sampling frequency of 10 Hz that can be adjusted as well. Common difficulties involved in the gaseous tracer technique are non-ideal injections and extra dispersion in the sampling and analysis system, which may cause significant measurement errors if they are not accounted. Due to the extra dispersion caused by the sampling and analytical components, responses measured by the gas analyzer do not exactly represent the actual tracer response. To take account of the extra dispersion effects in the sampling and analytical system, a convolution or deconvolution method needs to be applied (Levenspiel 1972). These two methods both yield a fair comparison between experimental measurements and reactor model predictions, either by adding the extra dispersion to the model predictions (convolution) or by removing the extra dispersion from the measurements of the whole system (deconvolution). However, due to its numerical instability, the deconvolution method is difficult to apply and is not widely used in chemical engineering research (Mills and Duduković 1989). On the other hand, the convolution method had not been employed in gas dispersion studies till 1990 (Wachi and Nojima 1990; Shetty et al. 1992; Kantak et al. 1995). Before that, the systems were assumed to have ideal tracer input and an ideal sampling and analytical system, which are not the actual cases. In the current study, the convolution integral method is implemented

to quantify the extra dispersion in the in the lower and upper plena along with the extra dispersion exists because of the sampling and analytical system. To estimate the extra dispersion in the lower and upper plena as well as the sampling and analytical system, three ports for injection (I-1, I-2, and I-3) and one port for sampling (S-1) were designed and developed along the convergent channel as shown in Figures 3 and 4. The gas tracer (helium) introduced through a solenoid valve controlled by a digital timer, the injecting time was set to be 0.5 s as one shot, and the pulses were precisely started at the set time. Gas samples were continuously withdrawn to the gas analyzer through thin nylon tubes (1.6 mm inner diameter) under vacuum generated by the pump connected to the exit of the analytical instrument. Using the designed injection and sampling ports, for each air volumetric flow rate conditions, three measurements were obtained as shown in Table 2.

Analysis and processing of the gas tracer signals

In this study, averaged resident time results were obtained from three replications of each experimental. Figure 5 shows a sample of the measured output signals for three experimental runs for an average volumetric flow rate of 0.0032 m^3/s for measurement–1 (I1-S). It is worth mentioning that the reproducibility of all the current measurements was within ± 1.5 %. The measured signals for all experimental tests in terms of helium concentration (mV) are normalized by the minimum (C_{min}) and maximum (C_{max}) concentration values to achieve a common scale for all signals from zero to one. It is worthwhile to mention here that normalizing of the output tracer signal is an important step for qualitative comparison for the dispersion of different sections signals within the system. The normalized value of the output tracer signal in terms of dimensionless

response (C_{normal}) can be estimated as follows (Han 2007; Abdulmohsin and Al-Dahhan 2016):

$$C_{normal} = \frac{c_i - c_{min}}{c_{max} - c_{min}} \quad (1)$$

For all measurements, minimum values for output tracer signals are zero as shown in Figure 5. Hence, we can rewrite Equation 1 to become as follows:

$$C_{normal} = \frac{c_i}{c_{max}} \quad (2)$$

Figure 6 shows normalized signals for the gas tracer under different injection positions corresponding to Table 2. It is remarkable that there is no significant difference between measurement-1 (I1-S) and measurement-2 (I2-S). Table 3 shows the mean residence time (t_m) as a first moment of the RTD and variance (σ^2) as a second moment of the RTD for the three measurements (I1-S, I2-S, and I3-S) for selected operating conditions (0.0032 m^3/s and 0.0034 m^3/s) just for illustration. The mean residence time (t_m) and the variance (σ^2) are defined as follows:

Mean residence time (t_m)

It is the average value of the response time (t), or it is the mean age of the gas tracer within the test section. Mean is the first moment of the RTD function. The mean (t_m) is given by (Levenspiel 1972):

$$\sigma^2 = \frac{\int_0^\infty t_i c_i \, dt}{\int_0^\infty c_i \, dt} \quad (3)$$

or we can rewrite it in a discrete form as follows:

$$t_m = \frac{\sum t_i c_i}{\sum c_i} \quad (4)$$

Variance (σ^2)

It is a measure of the gas tracer response about the mean (t_m) and has units of (s^2). The magnitude of the variance depends on the degree of the dispersion within the system, the greater value of variance, the higher degree of dispersion in the system and hence, the more response curve spreads and vice versa. The variance is given by the following equation (Levenspiel 1972):

$$\sigma^2 = \frac{\int_0^\infty t_i^2 c_i \, dt}{\int_0^\infty c_i \, dt} - t_m^2 \qquad (5)$$

or we can rewrite it in a discrete form

$$\sigma^2 = \frac{\sum t_i^2 c_i}{\sum c_i} - t_m^2 \qquad (6)$$

Variance and mean residence time results confirm that as the volumetric air flow rate (heating intensity) increases, the mean residence time and variance decrease. In other words, there is a reduction in the response curve spreads which is achieved by increasing the volumetric air velocity and consequently the heating intensity.

Convolution and regression methods

The main objective of integral convolution and regression methods is to properly extract the response or residence time distribution (RTD) of the test section separately from the whole system, which includes sampling lines from the system to the thermal conductivity detector (TCD) as well as external volumes of upper and lower plena. The upper and lower plena were assumed to follow an ideal continuous stirred tank reactor (CSTR) model, while the test section (channel core) was assumed to be one-dimensional

axial dispersion model (1D-ADM). It is worth mentioning that these assumptions were validated by the experimentally measured signals of the gas tracer as shown in the next sections.

Description of the gas dispersion and mixing within the lower plenum using a CSTR model

An ideal CSTR model was used to assess the gas tracer mixing within the lower plenum (figures 3 and 4) to get the input gas tracer concentration (C_{in}) to the one-dimensional axial dispersion model (ID-ADM). Figure 7 shows the sequence of the integral convolution and regression to obtain the CSTR parameter (τ_s) in conjunction with the input concentration (C_{in}) to the 1D-ADM. For the ideal CSTR model the concentration of the gas tracer throughout the reactor is identical to the concentration in the effluent stream. A non-reactive mass balance on the gas tracer for pulse injection at time t = 0 into the ideal CSTR model gives for time greater than zero

($t > 0$) (Levenspiel 1972; Fogler 1999; Abdulmohsin and Al-Dahhan 2016)

Gas tracer in – Gas tracer out = Accumulation (7)

$$0.0 - C_i \upsilon = V \frac{dC_i}{dt} \quad (8)$$

By separating the variables and integration with $C_i = C_{max}$ at t = 0 and normalizing the concentration yields

$$C_i = C_{max}\, e^{-\frac{t}{\tau_s}} \quad (9)$$

$$C_{in} = \frac{c_i}{c_{max}} = e^{-\frac{t}{\tau_s}} \quad (10)$$

where C_{in} is a dimensionless form for the theoretical lower plenum tracer output signal, which is the input to the ID-ADM for the test section, *t* is the instant time, and τ_g is the residence time within the lower plenum for the CSTR model. It is worth mentioning that the τ_g of the CSTR model was estimated by the regression analysis using the measured gas tracer signal in terms of residence time distribution at the lower plenum outlet. Measuremnt-2 (I2-S) "$C(2)$" was used as the same input to the lower plenum to convolute the lower plenum as an ideal CSTR to predict the input tracer concentration ($C_{in}^{*}(t)$) to the 1D-ADM (Levenspiel 1972; Han 2007; Abdulmohsin and Al-Dahhan 2016)

$$C_{in}^{*}(t) = \int_0^t C_{in}(t').C(2)(t-t')\,dt' \qquad (11)$$

More details regarding the convolution method can be found elsewhere (Levenspiel 1972; Han 2007; Abdulmohsin and Al-Dahhan 2016). The convoluted output, $C_{in}^{*}(t)$, of the ideal CSTR prediction was compared with the measured response of the measurement-1 (I1–S) "$C(1)$". Then, the parameter τ_g was estimated by minimizing the averaged squared error between the convoluted prediction from CSTR ideal model ($C_{in}^{*}(t)$) and the experimental measured value $C(1)$ from measurement-1 (I1–S) as follows: (Han 2007; Abdulmohsin and Al-Dahhan 2016):

$$\text{Error} = \frac{1}{n}\sum_{j=1}^{n}[C_{in}^{*}(t_j) - C(1)(t_j)]^2 \qquad (12)$$

Figures 9-11 show a good agreement between the predicted $C_{in}^{*}(t)$ and measured values from experiment-1 "$C(1)$", in which the average squared errors were found between

$1.2x10^{-3}$ and $4.7x10^{-3}$ for volumetric air flowrate ranging from 0.0015 to 0.0034 m^3/s. This indicates that the gas mixing within the lower plenum can be modeled as an ideal CSTR model for all experimental conditions. Thus, the calculated C_{in} from the ideal CSTR model in the lower plenum in conjunction with the fitted parameter τ_g was used as an input tracer concentration to the test section, in which the 1D-ADM is based on a known input tracer concentration.

Estimation of the gas dispersion within the test section using the axial dispersion model

The one-dimensional axial dispersion model (ID–ADM) is used to describe the gas tracer dispersion within the test section. In this model, there is an axial dispersion of the gas tracer, which is governed by analogy to Fick's law of diffusion. Every element of the system is transported by molecular and convective diffusions at a rate equal to "D A$\frac{dC}{dZ}$" in conjunction with bulk flow "UAC". Where D is the effective dispersion coefficient within the system (m^2/s), A is the cross sectional area (m^2), U is the superficial velocity (m/s), and $\frac{dC}{dZ}$ is the concentration gradient of the tracer ($mole/m^4$). A non-reactive mole balance on the gas tracer over a short length ΔZ of the test section in absence of radial variations yields (Levenspiel 1972; Han 2007; Abdulmohsin and Al-Dahhan 2016)

$$D\frac{\partial^2 c}{\partial z^2} - U\frac{\partial c}{\partial z} = \frac{\partial c}{\partial \tau} \qquad (13)$$

The gas tracer concentration in the mole balance equation (Equation 15) can be rewritten in a dimensionless form as follows:

$$D\frac{\partial^2 c_{out}}{\partial x^2} - U\frac{\partial c_{out}}{\partial x} = \frac{\partial c_{out}}{\partial t} \quad (14)$$

where,

$$c_{out} = \frac{c}{c_{max}} \quad (15)$$

Once initial and boundary conditions defined, the solution of Equation 14 will yield the effluent tracer concentration (C_{out}).

Closed-closed Danckwerts boundary conditions (Danckwerts 1953) were used in this study. An assumption is established for no radial variations of the tracer concentration or dispersion either downstream (Z = 0.0) or upstream (Z = L) of the test section. However, between the downstream and upstream we have axial dispersion. The corresponding boundary conditions are as follows:

At Z = 0.0 (downstream)

$$U\,C - D\frac{dC}{dZ} = U\,C_{in} \quad (16)$$

The tracer concentration within Equation 16 can be rewritten in a dimensionless form as follow:

$$U\,C_{out} - D\frac{dC_{out}}{dZ} = U\,C_{input} \quad (17)$$

where,

$$c_{out} = \frac{c}{c_{max}} \quad (18)$$

$$C_{in} = \frac{c_{input}}{c_{max}} \quad (19)$$

At Z = L (upstream)

$\frac{dC}{dZ}$ = 0.0 (20)

where C_{in} is estimated by Equation 10 with the fitted parameter of $\boldsymbol{\tau_s}$ as shown in Figure 7. The initial condition is given by

t = 0.0, C = 0.0 (21)

Figure 12 shows the sequence of the integral convolution and regression analysis schematically to obtain the parameter "D" of the 1D-ADM. Using C_{in} from Equation 10 as the input tracer concentration to 1D-ADM to yield an output profile C_{out}, which is then convoluted by C(3) from measurement–3 (Table 2) (Levenspiel 1972) to produce the convoluted prediction (C^*_{out})

$$C^*_{out}(t) = \int_0^t C_{out}(t').C(3)(t-t').dt' \quad (22)$$

Then the convoluted 1D-ADM prediction,C^*_{out}, was compared against the measured response of the measurement–1 "$C(1)$" of the whole system. Then, the dispersion coefficient parameter, D, was estimated by minimizing the averaged squared error between the convoluted prediction from 1D-ADM ($C^*_{OUT}(t)$) and the experimental measured value $C(1)$ from measurement-1 as follows (Levenspiel 1972; Han 2007; Abdulmohsin and Al-Dahhan 2016):

Error $=\frac{1}{n}\sum_{j=1}^{n}[C^*_{OUT}(t_j) - C(1)(t_j)]^2$ (23)

Figures 13-16 show a good model fit of C^*_{OUT} and C(1) for selected operating conditions. The averaged squared error calculated by Equation (23) was in the range of 6.8×10^{-3} ~ 22.24×10^{-3}.

The axial dispersion coefficient (D) is used to determine the dispersive Peclet number (N_{Pe}) which represents the ratio of the rate of transport by convection to the rate of transport by dispersion as follows:

$$N_{Pe} = \frac{V d}{D} \quad (24)$$

The value of N_{Pe} is used to quantify the degree to which the axial dispersion affects the performance of the separate-effect test section. A high value of the N_{Pe} corresponds to a slightly dispersed system.

Effect of the volumetric air flow rate (corresponding to heating intensity) on the gas phase axial dispersion coefficient (D) along the riser channel

The qualitative effect of the volumetric air flow rate on the axial dispersion coefficient (D) can be illustrated by noting that, as the dispersion coefficient (D) varies from 0 to ∞, the system behavior changes from ideal plug flow to perfect mixing. As shown in Figure 17, D values decrease with increasing the volumetric air flow rate (increasing heating intensity). This behavior can be explained by the classical approach of turbulent mass transfer (Wen and Fan 1975). The reduction in the values of axial dispersion coefficient (D) was evidently influenced by increasing the value of the eddy diffusivity of mass as turbulence was generated. A similar effect has been reported by Taylor (1954), Keyes (1955), and Aris (1956) for empty tube under turbulent conditions. Besides, the Peclet number (N_{Pe}) was calculated and shown in Figure 18. The values of

N_{Pe} increase apparently with increasing the volumetric air flow rate (heating intensity), indicating a reduction in the rate of dispersion (Wen and Fan 1975).

Remarks

Gaseous dispersion experiments were conducted, for the first time, in a mimicked cold-flow separate-effect riser channel of the prismatic modular reactor using advanced gaseous tracer technique. The current separate-effect facility was designed and developed considering measured local velocities in a previous study under same operating conditions along the riser channel of the dual-channel circulation loop at mReal (Said et al. 2017). Experiments were conducted using helium as a tracer within the air as a carrier under atmospheric conditions. The gas axial dispersion coefficient (D) and the Peclet number (N_{Pe}) have been measured and quantified under the different volumetric air flow rates of 0.0015, 0.0024, 0.0032, and 0.0034 m^3/s which are corresponding to the heating intensity of 200, 600, 1000, and 1400 w/m^2, respectively. The key findings are summarized as follows:

- The dispersion and mixing in the sampling lines and analytical system are a significant source of errors in the measured residence time distribution (RTD) and consequently values of D and N_{Pe}. Hence, the integral convolution method is implemented to account the extra dispersion and provide accurate gaseous dispersion measurements.
- The results confirmed that a reduction in the residence time distribution (RTD) is achieved by increasing the volumetric air velocity (increasing heating intensity).

- The results showed that the axial dispersion coefficients (D) decrease with increasing the volumetric air flow rate. This could be attributed to an increase in the value of eddy diffusivity of mass as turbulence is generated.
- The values of the Peclet number (N_{Pe}) are found to be increased with increasing the heating intensity (as represented by volumetric air flow rate).
- The current study provides insight on the gas phase dispersion within the riser channel of the prismatic modular reactor (PMR) under accident scenario using advanced gaseous tracer technique.
- The measured gas phase axial dispersion coefficients (D) and Peclet number (N_{Pe}) of the coolant gas flow in the riser channel are useful for efficient operation and safe design of the prismatic modular reactor (PMR).

Acknowledgment

The authors acknowledge the financial support provided by the U.S. Department of Energy-Nuclear Energy Research Initiative (DOE-NERI) Project (NEUP 13-4953 (DENE0000744)) for the 4th generation nuclear energy, which made this work possible.

Notation

c	concentration of the tracer in the gas phase, mol/m^3
c_{min}	minimum concentration of the tracer in the gas phase, mol/m^3
c_{max}	maximum concentration of the tracer in the gas phase, mol/m^3
c_{inj}	concentration of the injection tracer, mol/m^3

C_{in}	dimensionless tracer concentration in the gas phase at the lower plenum outlet
C_{in}*	dimensionless convoluted tracer concentration in the gas at the lower plenum outlet
C_{out}	dimensionless tracer concentration in the gas phase at the test section outlet
C_{out*}	dimensionless convoluted tracer concentration in the gas at the test section outlet
C_{normal}	normalized value of the output tracer signal (dimensionless)
D	effective axial dispersion coefficient of the gas phase, m^2/s
L	length of the separate-effect test section, m
d	inlet inside diameter of the separate effect test section, m
n	total number of experimental data points
N_{Pe}	dispersive Peclet number (V d/D), dimensionless
U	superficial gas velocity, (m/s)
t	time, s
t_m	mean residence time of the bed, s
Z	axial distance along the test section, m
Z/L	non-dimensional length, dimensionless
υ	volumetric air flow rate, m^3/s
σ^2	variance, s^2
τ_g	CSTR parameter, s

References

Abdulmohsin, R. S. and M. H. Al-Dahhan (2016). "Axial dispersion and mixing phenomena of the gas phase in a packed pebble-bed reactor." Annals of Nuclear Energy 88: 100-111.

Aldridge, R. J. (2013). Scaling study of the depressurized conduction cooldown event in the high temperature test facility using RELAP5-3D/ATHENA.

Aris, R. (1956). On the dispersion of a solute in a fluid flowing through a tube. Proceedings of the Royal Society of London A: mathematical, physical and engineering sciences, The Royal Society.

Castañeda, J. A. (2014). Scaling Analysis of the OSU High Temperature Test Facility during a Pressurized Conduction Cooldown Event using RELAP5-3D. M.Sc, Oregon State University.

Danckwerts, P. (1953). "Continuous flow systems: distribution of residence times." Chemical engineering science 2(1): 1-13.

Fogler, H. S. (1999). Elements of chemical reaction engineering.

Han, L. (2007). Hydrodynamics, back-mixing, and mass transfer in a slurry bubble column reactor for Fischer-Tropsch alternative fuels. Ph.D., Washington University.

Han, L. and M. Al-Dahhan (2005). Axial dispersion of gas phase in slurry bubble column reactor. 2005 AIChE Annual Meeting, October.

Haque, H., W. Feltes and G. Brinkmann (2006). "Thermal response of a modular high temperature reactor during passive cooldown under pressurized and depressurized conditions." Nuclear Engineering and Design 236(5–6): 475-484.

Kantak, M., R. Hesketh and B. Kelkar (1995). "Effect of gas and liquid properties on gas phase dispersion in bubble columns." The Chemical Engineering Journal and The Biochemical Engineering Journal 59(2): 91-100.

Keyes, J. J. (1955). "Diffusional film characteristics in turbulent flow: Dynamic response method." AIChE Journal 1(3): 305-311.

Levenspiel, O. (1972). Chemical reaction engineering, John Wiley % Sons.

Mills, P. and M. Duduković (1989). "Convolution and deconvolution of nonideal tracer response data with application to three-phase packed-beds." Computers & chemical engineering 13(8): 881-898.

Moharam, M. T. (2017) (under submission). Experimental Investigation of Natural Circulation in Separate-and-Mixed Effects Test Facility mimicking Prismatic Modular Reactor (PMR) Core. Ph.D., Missouri University of Science and Technology.

Said, I. A., M. M. Taha, Rizwan-Uddin, U. Shoaib and M. H. Al-Dahhan (2017) (under review). "Experimental study of the effect of helium pressure on the natural convection heat transfer in prismatic dual-channel circulation loop." International Journal of Thermal Sciences.

Said, I. A., M. M. Taha, U. Shoaib and M. H. Al-Dahhan (2017) (under review). "Experimental investigation of the helium natural circulation heat transfer in two channels facility using varying riser channel heat fluxes." Experimental Thermal and Fluid Sciences.

Said, I. A., M. M. Taha, U. Shoaib, B. G. Woods and M. H. Al-Dahhan (2017). "Investigation of Natural Convection Heat Transfer in a Unique Scaled-Down Dual-Channel Facility." AICHE Journal 63(1): 387-396.

Shetty, S. A., M. Kantak and B. Kelkar (1992). "Gas-phase back mixing in bubble-column reactors." AIChE Journal 38(7): 1013-1026.

Simoneau, J.-P., J. Champigny, B. Mays and L. Lommers (2007). "Three-dimensional simulation of the coupled convective, conductive, and radiative heat transfer during decay heat removal in an HTR." Nuclear Engineering and Design 237(15): 1923-1937.

Taha, M. M., I. A. Said, U. Shoaib and M. H. Al-Dahhan (Under review). "Investigation of natural circulation in a separate effects facility of two channels representing prismatic modular reactors (PMRs) core." International Journal of Thermal Sciences.

Taha, M. M., I. A. Said, U. Shoaib, B. G. Woods and M. H. Al-Dahhan (Under submission). "Design and development of an experimental test facility with a representative geometry of prismatic block modular reactor core." Nuclear Engineering and Design.

Taylor, G. (1954). The dispersion of matter in turbulent flow through a pipe. Proceedings of the Royal Society of London A: Mathematical, Physical and Engineering Sciences, The Royal Society.

Tung, Y.-H., Y.-M. Ferng, R. W. Johnson, and C.-C. Chieng (2016). "Transient LOFA computations for a VHTR using one-twelfth core flow models." Nuclear Engineering and Design 301: 89-100.

Tung, Y.-H., R. W. Johnson, Y.-M. Ferng and C.-C. Chieng (2014). "Modeling strategies to compute natural circulation using CFD in a VHTR after a LOFA." Nuclear Engineering and Design 275: 80-90.

Tung, Y. H., Y. M. Ferng, R. W. Johnson and C. C. Chieng (2013). "Study of natural circulation in a VHTR after a LOFA using different turbulence models." Nuclear Engineering and Design 263: 206-217.

Tung, Y. H. and R. W. Johnson (2011). CFD calculations of natural circulation in a high temperature gas reactor following pressurized circulator shutdown. ASME 2011 International Mechanical Engineering Congress and Exposition, IMECE 2011.

Wachi, S. and Y. Nojima (1990). "Gas-phase dispersion in bubble columns." Chemical engineering science 45(4): 901-905.

Wen, C.-Y. and L.-t. Fan (1975). Models for flow systems and chemical reactors, M. Dekker.

Table 1. Values of the air velocity within the riser channel of the dual-channel facility and the convergent channel (separate-effect test section).

Heating intensity (W/m^2)	Non-dimensional length (Z/L)	Velocity in the dual-channel facility (hot flow system) (m/s)	Velocity in the convergent channel – separate effect test section (cold flow system) (m/s)
200	0.178	0.7264	0.7514
	0.436	1.0333	1.0400
	0.546	1.0941	1.1040
	0.729	1.1634	1.1741
	0.867	1.3157	1.3359
600	0.178	1.3696	1.2524
	0.436	1.6673	1.7334
	0.546	1.7765	1.8401
	0.729	1.7964	1.9569
	0.867	1.8596	2.2265
1000	0.178	1.6479	1.5029
	0.436	2.2599	2.0801
	0.546	2.3773	2.2081
	0.729	2.4192	2.3482
	0.867	2.1659	2.6718
1400	0.178	1.8175	1.7533
	0.436	2.3937	2.4268
	0.546	2.5720	2.5761
	0.729	2.6985	2.7396
	0.867	2.2898	3.1171

Table 2. The designed three measurements for the gaseous tracer technique.

Measurement	Tracer injection	Tracer detection	Tracer signal	Dispersion zones
Measurement–1 (I1-S)	I1	S	C (1)	Sampling lines+ measurement system + lower plenum + test section + upper plenum
Measurement–2 (I2-S)	I2	S	C (2)	Sampling lines + measurement system + test section + upper plenum
Measurement–3 (I3-S)	I3	S	C (3)	Sampling lines + measurement system + upper plenum

Table 3. Mean residence time (t_m) and variance (σ^2) for the three measurements (I1-S, I2-S, and I3-S) for selected two volumetric air flowrates.

Volumetric air flow rate: 0.0032 m^3/s (corresponding to heat flux of 1000 W/m^2)		
Measurement	Mean Residence time (t_m), s	Variance (σ^2), s^2
Measurement–1 (I1-S)	13.06	9.95
Measurement–2 (I2-S)	12.81	8.81
Measurement–3 (I3-S)	12.505	8.02
Volumetric air flow rate: 0.0034 m3/s (corresponding to heat flux of 1400 W/m^2)		
Measurement	Mean Residence time (t_m), s	Variance (σ^2), s^2
Measurement–1 (I1-S)	12.87	8.08
Measurement–2 (I2-S)	12.77	8.42
Measurement–3 (I3-S)	12.43	7.478

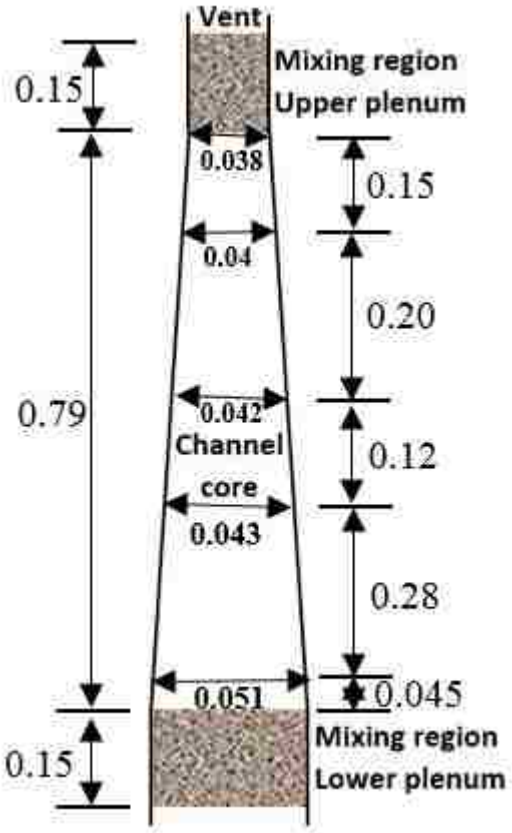

Figure 1. Schematic diagram for the separate effects convergent channel

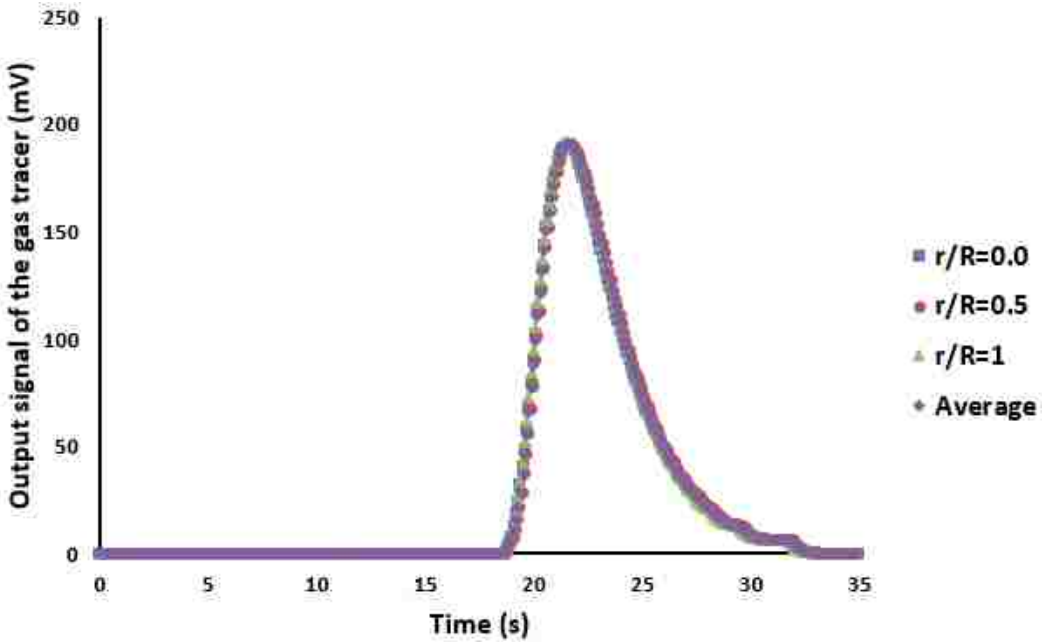

Figure 2. Residence time distribution (RTD) of the upper plenum for different sampling radial positions at volumetric air flow rate of 0.0034 m^3/s for measurement–1 (I1-S)

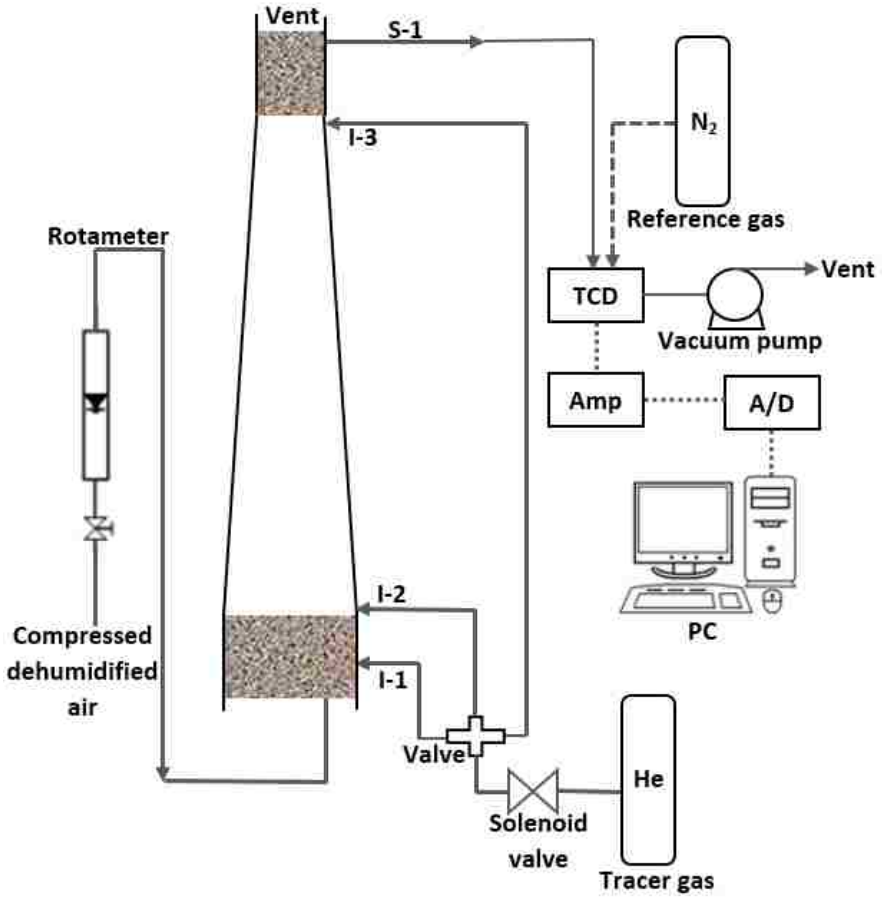

Figure 3. Schematic diagram of the convergent channel in conjunction with gaseous tracer technique.

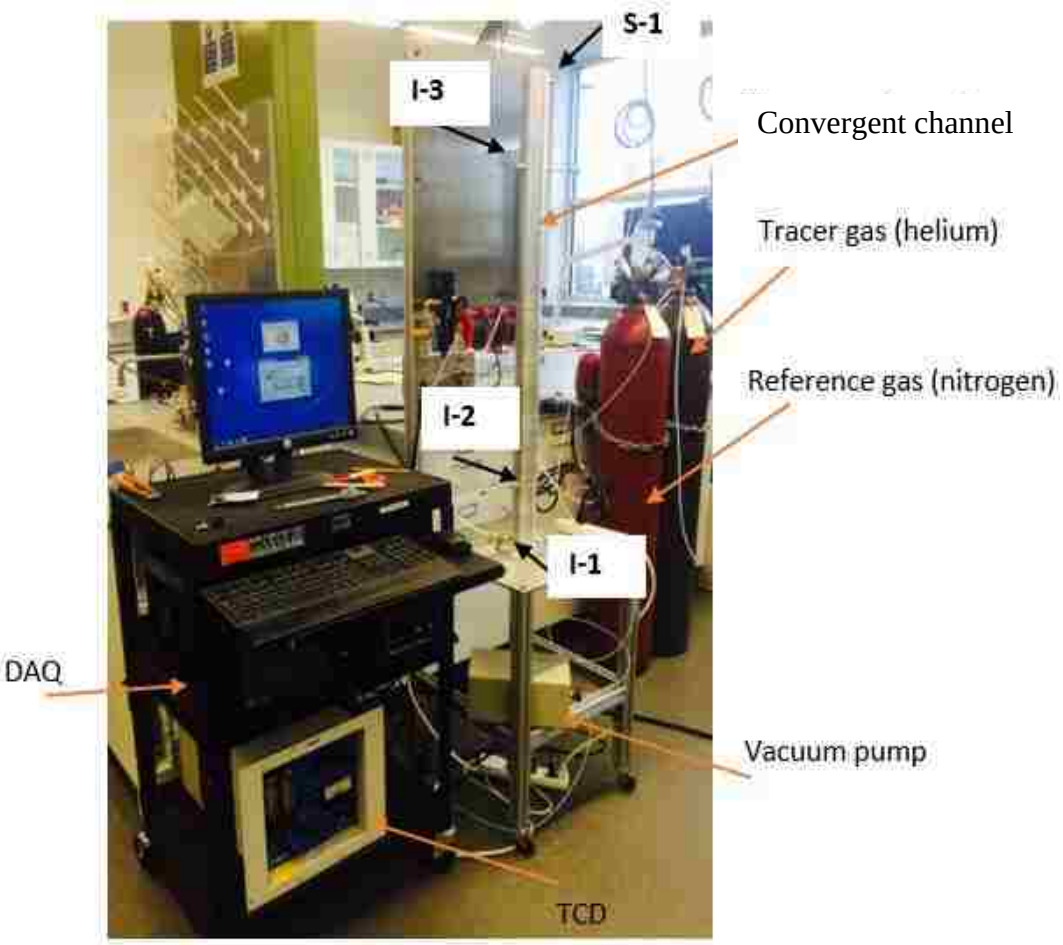

Figure 4. Physical picture for the convergent channel in conjunction with gaseous tracer technique.

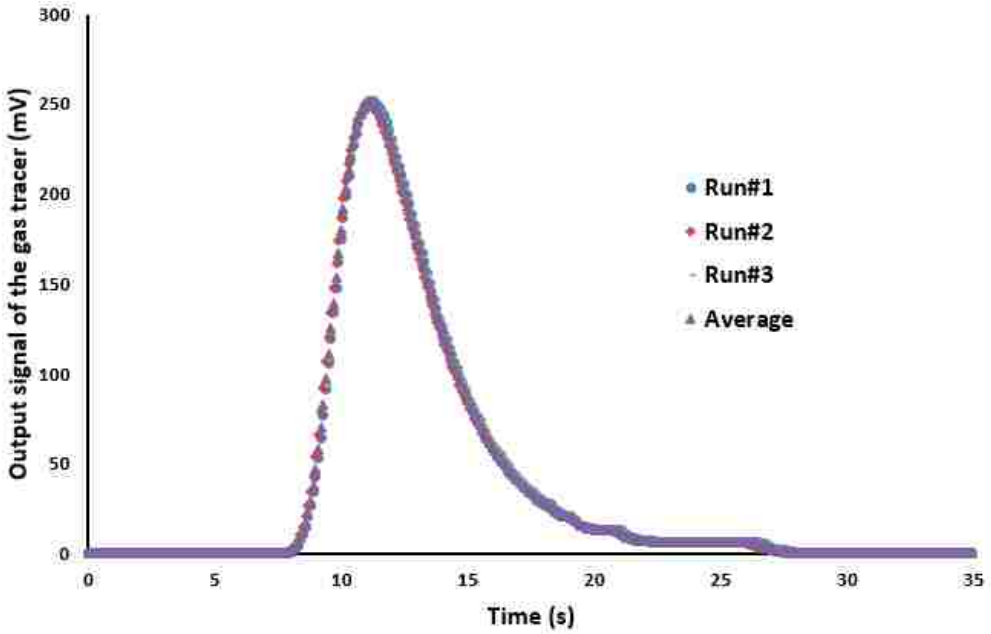

Figure 5. Raw signals for the three experimental runs for average volumetric air flow rate of 0.0032 m^3/s for measurement of I1-S.

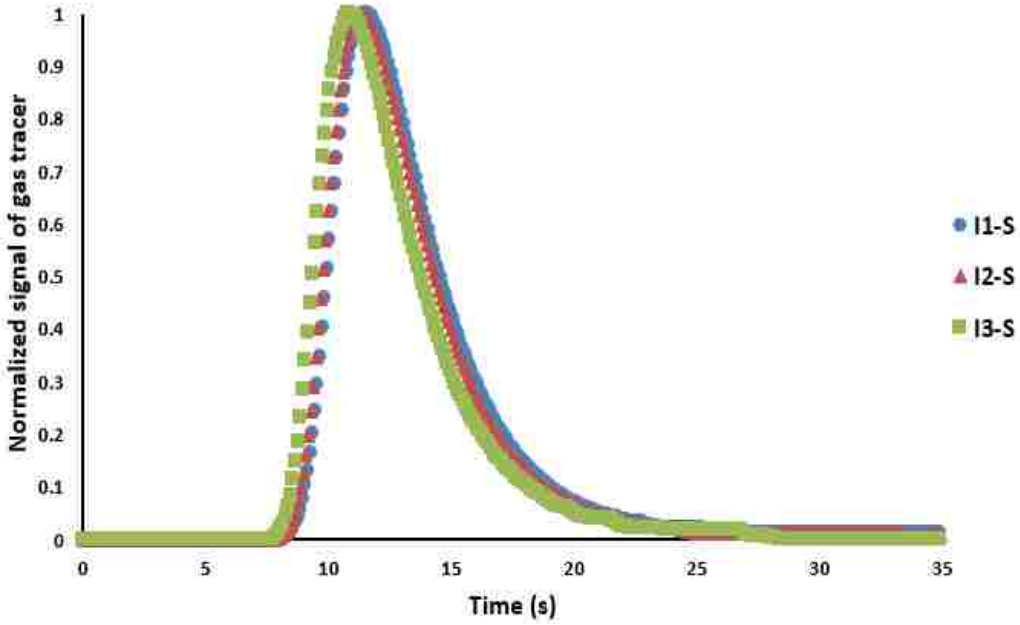

Figure 6. Residence time distribution (RTD) of the gas tracer for the three different measurements at average volumetric air flow rate of 0.0015 m3/s.

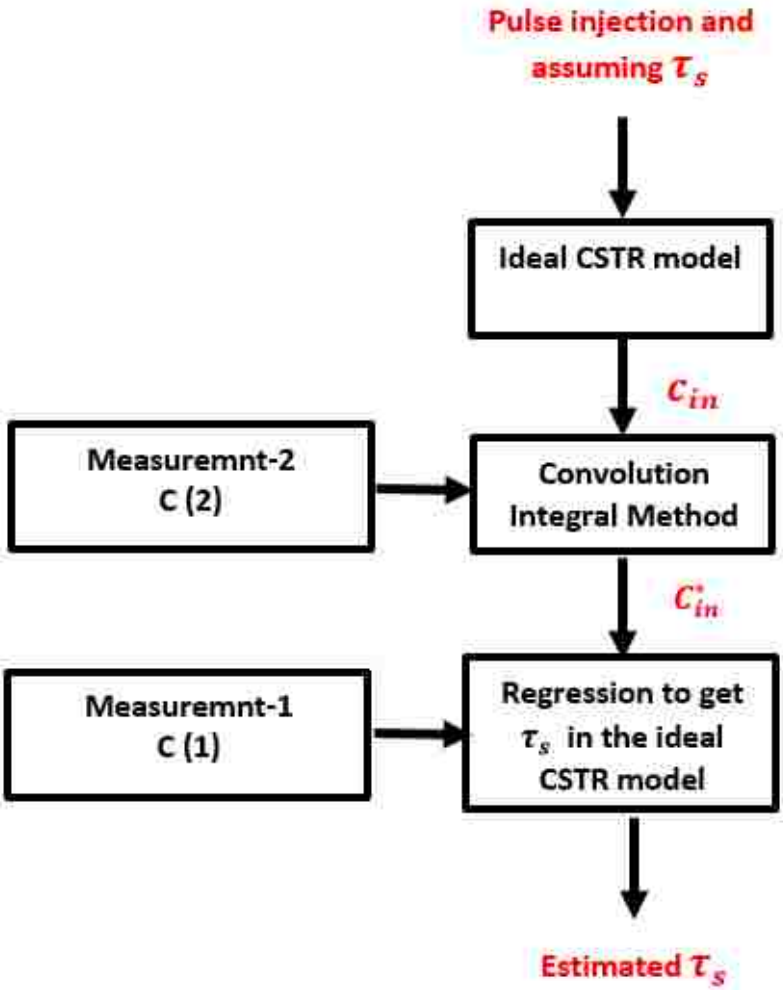

Figure 7. Diagram of the convolution and regression (model fit) of the tracer responses curves to get the CSTR parameter (τ_s) and the inlet concentration to the ADM (c_{in}).

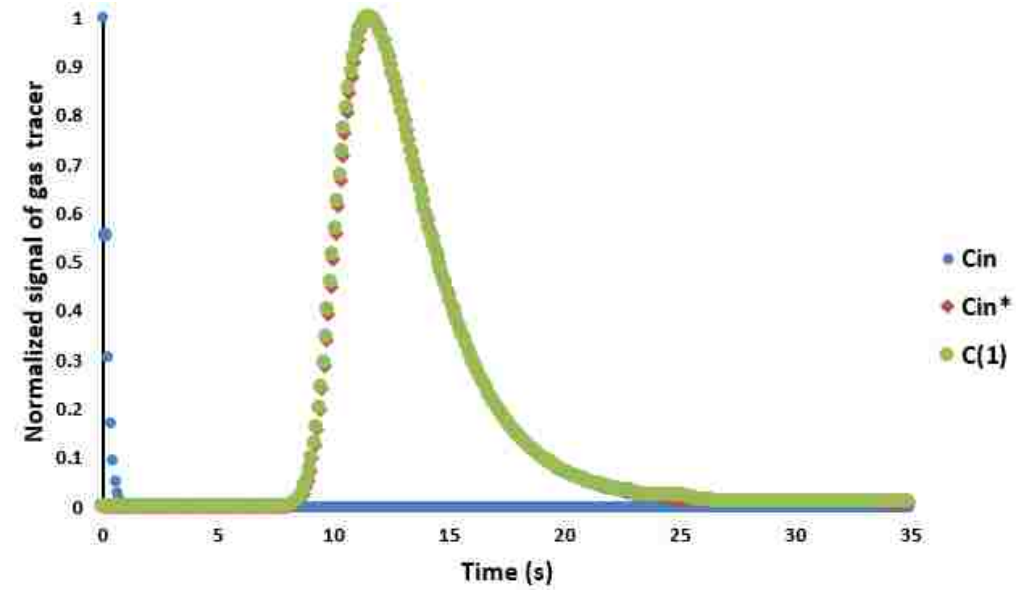

Figure 8. Responses of the normalized gas tracer signal for the lower plenum with CSTR model fit for 0.0015 m^3/s.

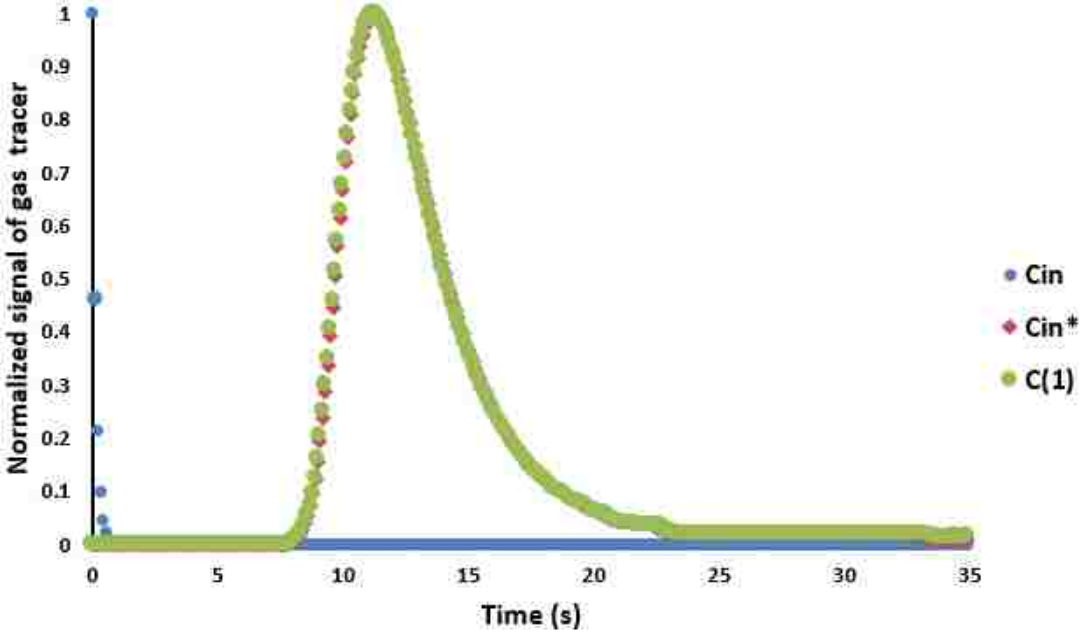

Figure 9. Responses of the normalized gas tracer signal for the lower plenum with CSTR model fit for 0.0024 m^3/s.

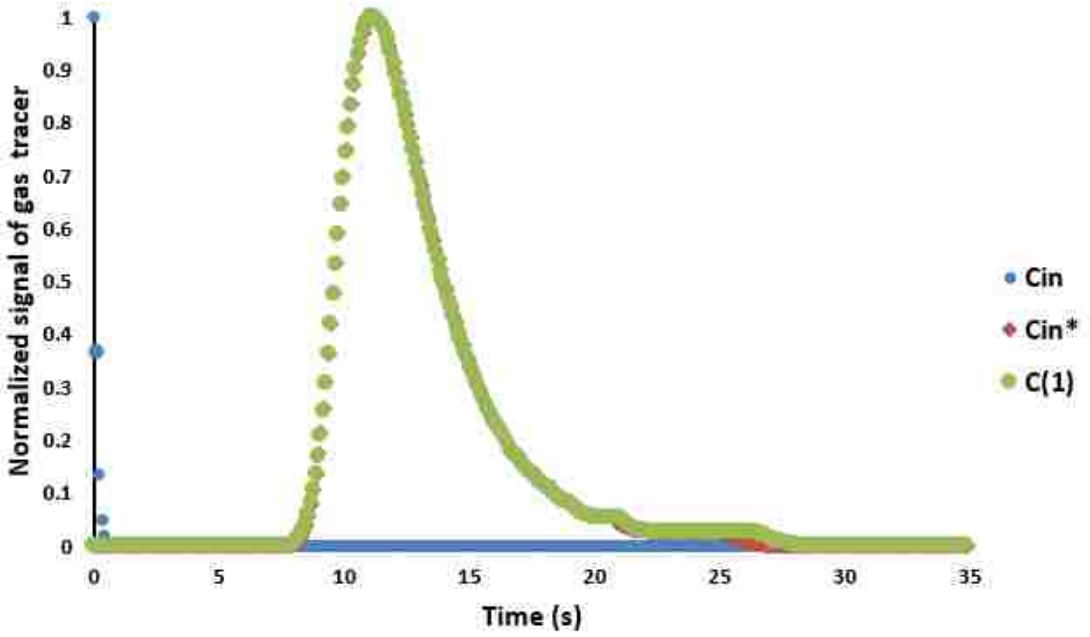

Figure 10. Responses of the normalized gas tracer signal for the lower plenum with CSTR model fit for 0.0032 m^3/s.

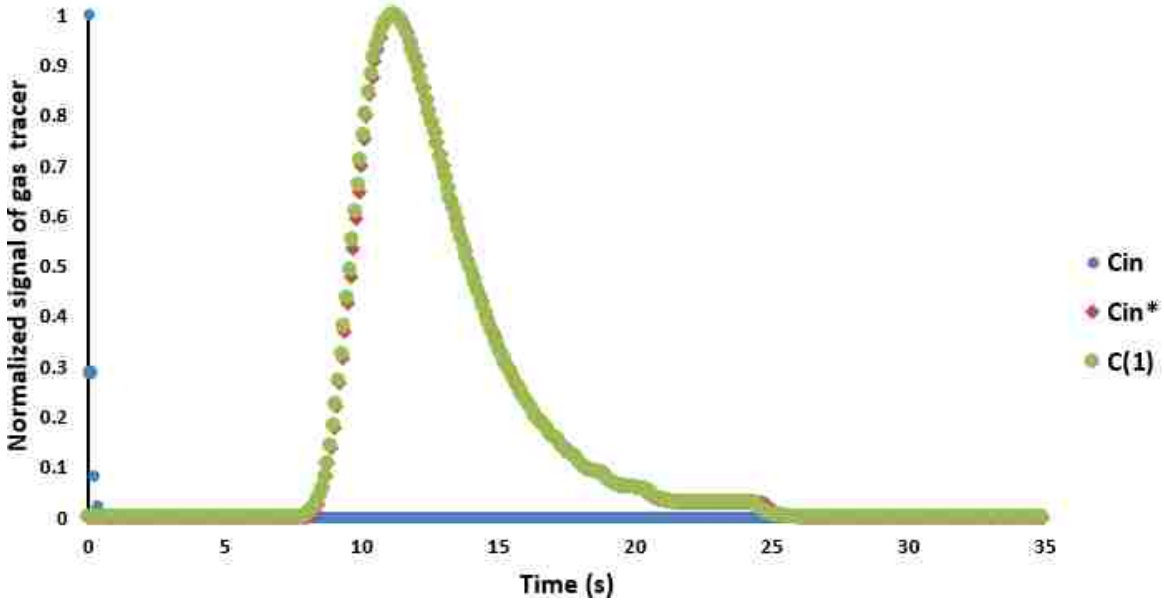

Figure 11. Responses of the normalized gas tracer signal for the lower plenum with CSTR model fit for 0.0034 m^3/s.

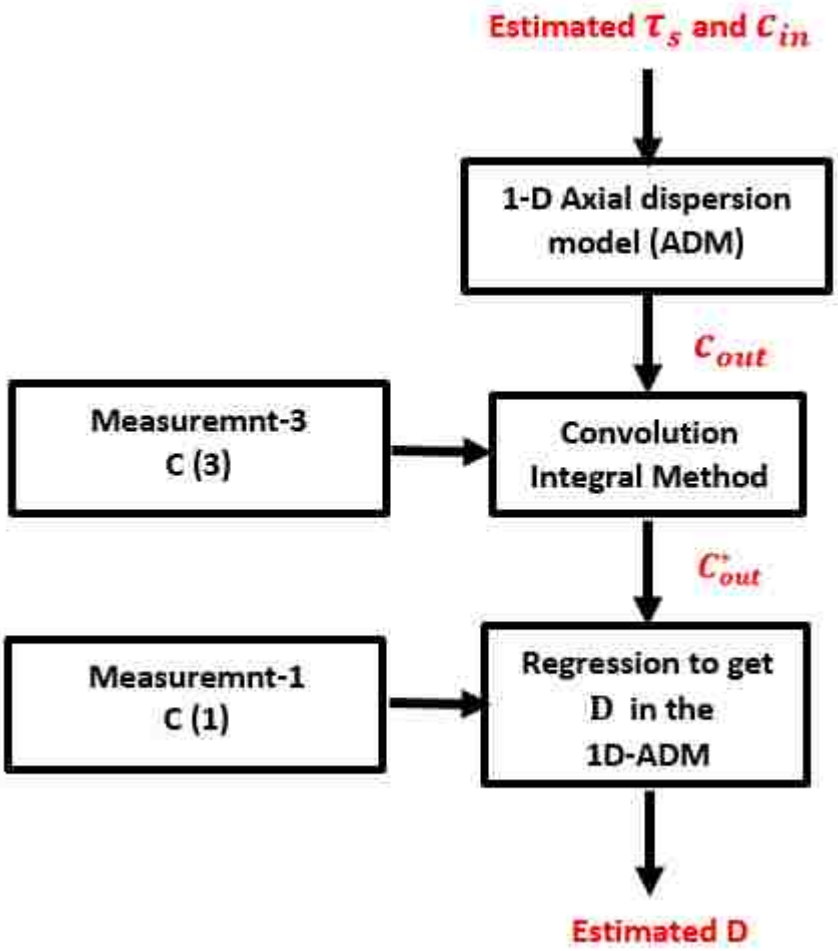

Figure 12. Diagram of the convolution and regression (model fits) for the gas tracer responses curves to get the dispersion coefficient (D) for the core channel.

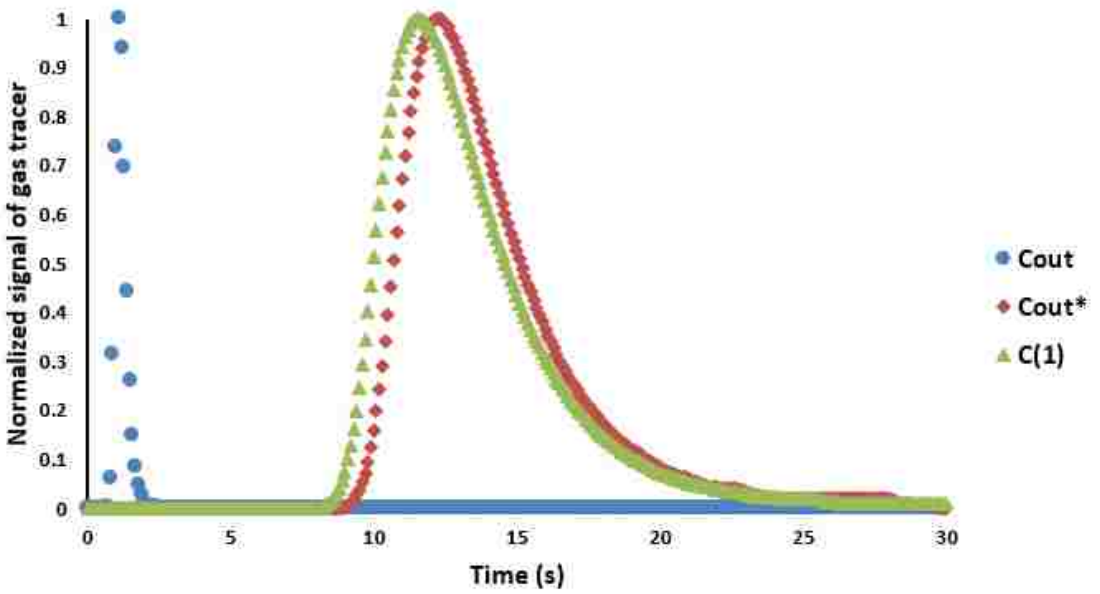

Figure 13. Responses of the normalized gas tracer signal for the core channel outlet with 1D–ADM fit for 0.0015 m^3/s.

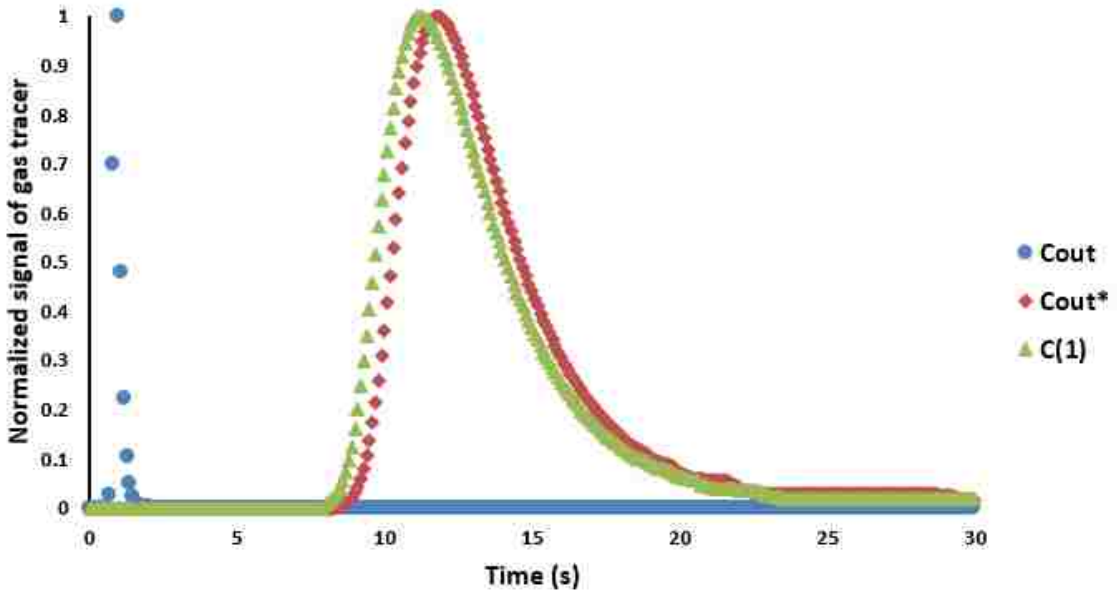

Figure 14. Responses of the normalized gas tracer signal for the core channel outlet with 1D–ADM fit for 0.0024 m^3/s.

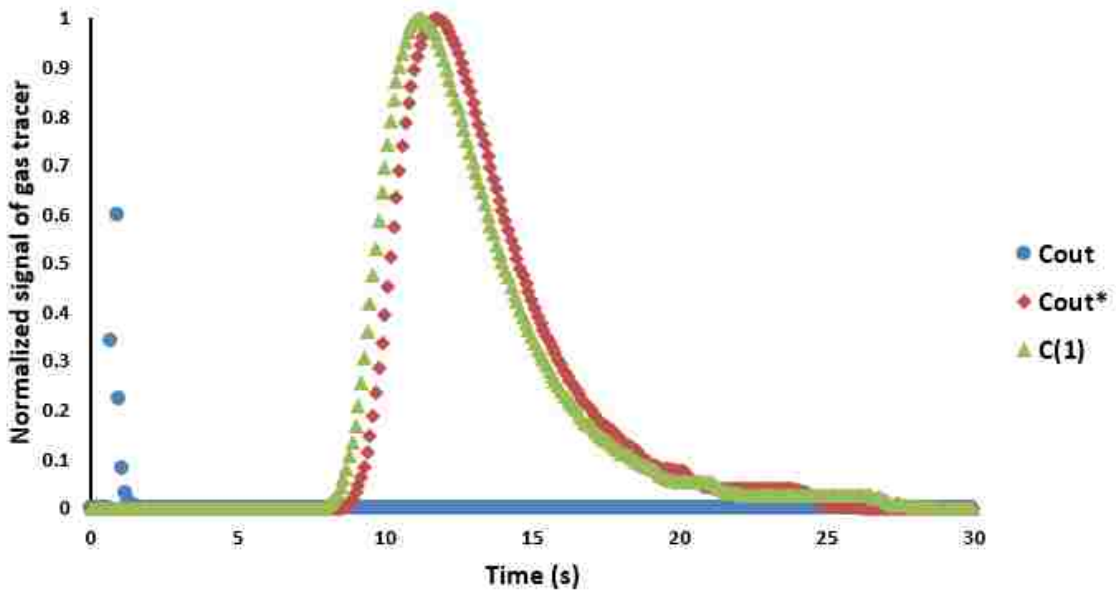

Figure 15. Responses of the normalized gas tracer signal for the core channel outlet with 1D–ADM fit for 0.0032 m^3/s.

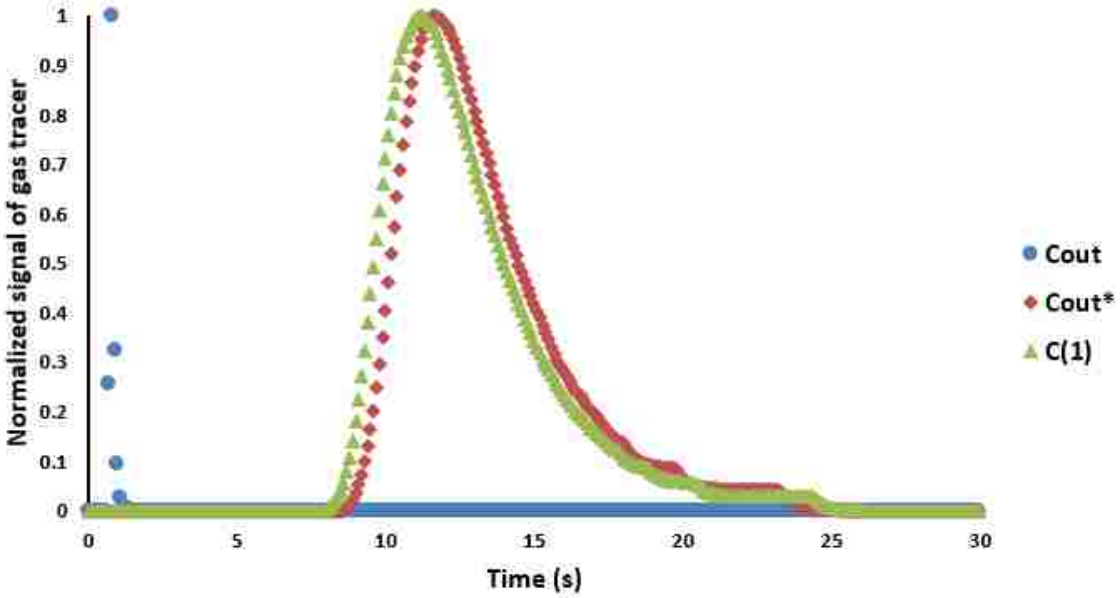

Figure 16. Responses of the normalized gas tracer signal for the core channel outlet with 1D–ADM fit for 0.0034 m^3/s.

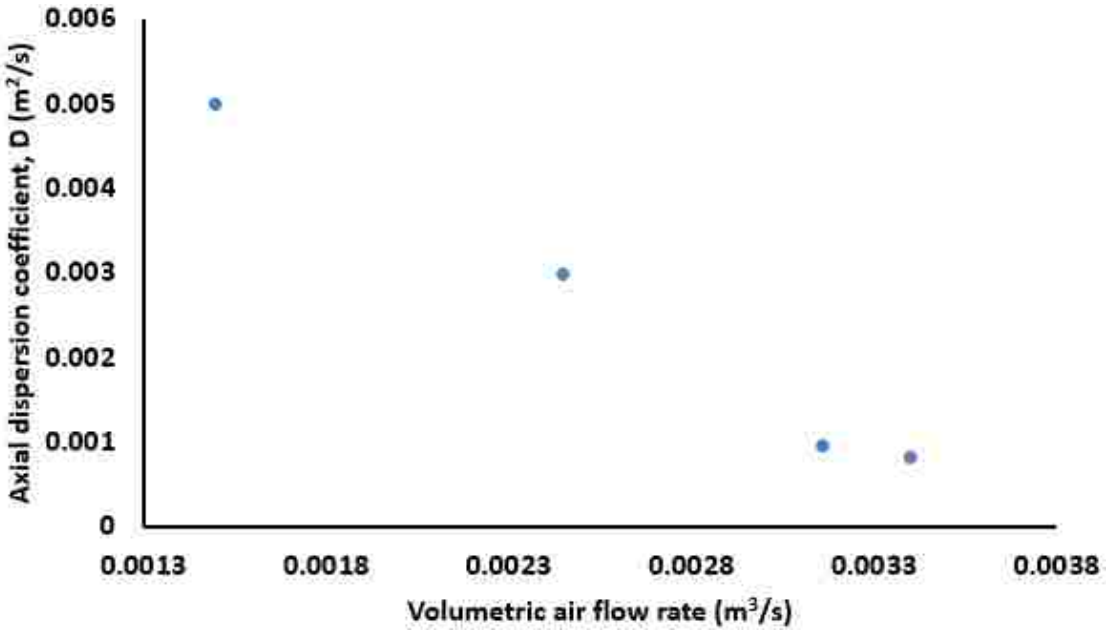

Figure 17. Effect of the volumetric air flow rate (heating intensity) on the gas phase axial dispersion coefficient (D).

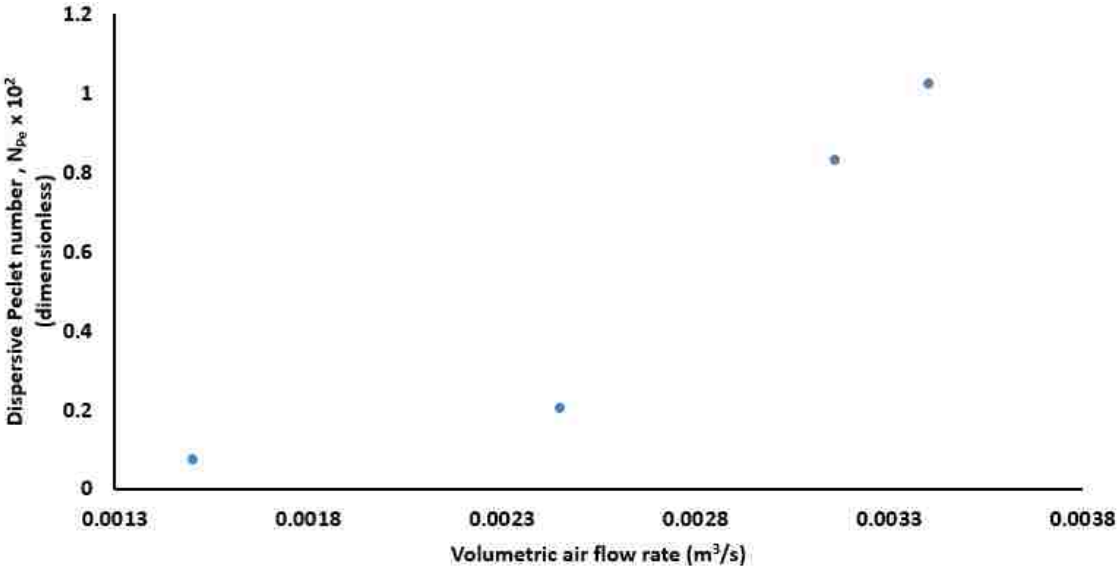

Figure 18. Effect of the volumetric air flow rate (heating intensity) on the gas phase Peclet number (N_{Pe}).

SECTION

2. RECOMMENDATIONS

The current study provides high-resolution and fidelity benchmark data on heat transfer data and gaseous dynamics for the prismatic very high temperature reactor under accident scenarios. The benchmark data, includes local heat fluxes, local heat transfer coefficients, Nusselt numbers, axial and radial temperatures, axial dispersion coefficients, and Peclet numbers along the flow channels under different operating conditions.

While the current information provides more insight into the thermal hydraulic of prismatic very high temperature reactor, especially for the accident scenario of natural convection, the full potential of the current study initiative can only be executed by carrying out the following recommendations:

- Extending the current study of two flow channels into multi-flow channels with use of the same sophisticated measurement techniques. The current dual-channel facility is designed and developed to accommodate multichannel as well as annular space between the reactor core and the outer vessel.
- Investigation the heat transfer and gaseous dynamics within the upper plenum and identifying the thermal stresses on the inner surface of the upper plenum as well as the velocity vectors under different intensities of natural circulation.
- Implementing the results reported in the current work to verify and validate heat transfer computations and correlations that are integrated with CFD simulations

- Investigation can be also carried out on different working fluids, including nitrogen and argon.
- Implementation of gaseous tracer technique can be extended to different intensities of natural convection using different separate-effect facility.

VITA

Ibrahim Ahmed Said Abdallah was born in Kuwait in January 1987 but he is an Egyptian. he received his B.S. degree and first M.S. degree in Chemical Engineering from Alexandria University, Egypt in 2009 and 2013, respectively. He was ranked out the first of the students in the class and received honors with distinction. He served as an Instructor and Researcher at Alexandria University from January 2010 to January 2014. Ibrahim joined the research group of Prof. Muthanna Al-Dahhan in January 2014 at Missouri University of Science and Technology in Rolla, MO, USA to pursue his Ph.D. degree in chemical engineering. In December 2015, he received his second M.S. degree in chemical engineering from Missouri University of science and technology. During his Ph.D. studies, Ibrahim worked on a challenging project of investigation the natural convection heat transfer and gaseous dynamics of the prismatic very high temperature reactor under accident scenarios using advanced sophisticated measurement techniques. This work has been supported by U.S. Department of Energy (DOE). He mentored more than ten undergraduate students during his Ph.D. studies. He is also served as Director of Communications and Department Representative within the Council of the Graduate Students (CGS) at Missouri University of Science and Technology. He is served as a lecturer within the Chemical and Biochemical Engineering Department at Missouri S&T. Ibrahim received his Ph.D. degree in Chemical Engineering from Missouri University of Science and Technology in December 2017.